CRANFIELD UNIVERSITY

DIMITRIOS LOUVROS

INVESTIGATION OF THE RELIABILITY DETERIORATION OF AGEING MARINE STRUCTURES

SCHOOL OF ENGINEERING

MSc by research

Thesis submitted for the Degree of Master of Science
Academic Year: 2012-2013

Supervisors: Prof. Feargal Brennan, Dr Athanasios Kolios

September 2013

CRANFIELD UNIVERSITY

SCHOOL OF ENGINEERING
MSc by Research

Thesis submitted for the Degree of Master of Science
Academic Year: 2012-2013

Academic Year 2012-2013

DIMITRIOS LOUVROS

Investigation of the reliability deterioration of ageing marine structures

Supervisors: Prof. Feargal Brennan, Dr Athanasios Kolios
September 2013

ABSTRACT

In the present work, an investigation of the fatigue life benefits emerging from fillet weld geometries optimization has been carried out.

At first, an introduction to ageing mechanisms, corrosion and especially fatigue, acting on operating marine structures has been made. Residual stresses at weld toes, stress modes, and types, geometrical factors (weld angle, toe radius, leg length), welding techniques selected, post-welding treatment and plate's material are some of the principal factors affecting the fatigue life of a fillet weld joint.

Especially, the accuracy of various approaches in fatigue life estimation of specific geometries under pre-set types and levels of stress is studied. It is evident so far that even the notch stress concept is the most accurate method based on S-N curves, the Fracture Mechanics approach can offer more accurate solutions of a crack development through the material. Towards this, a literature review on crack evolution aspects in welded and non-welded plates under bending and tension was performed; substantial parameters were determined and finally implemented in the LEFM model which was used for the simulation purposes of Chapter 6.

As far as the crack aspect ratio evolution is concerned, an extensive reference is available in literature since many researchers have investigated its contribution to the determination of geometrical paths, commonly known as "Preferred Propagation Paths". Their significance is related with our ability to determine accurate SIF solutions leading to precise fatigue life estimations.

A typical fillet weld joint 2-D model has been developed in CAE Abaqus software and a Finite Element Analysis of subject T-profile has been carried out. Through this analysis, the fillet weld angle, the weld leg length, the weld toe curvature radio ρ and the carrying load plate thickness are examined for their impacts on the maximum surface stress. Finally, a number of stress mitigating measures are proposed and their effects are analyzed.

Undoubtedly, the notch stress concept today is gradually gaining more and more acceptance among other fatigue analysis practices, hence the need for an estimation of the actual surface stresses along fillet weld toes, has become imperative. Towards this, different 2-D geometries are tested against stress concentration factors developed at weld toes, which are calculated on the basis of maximum in-plane principal stresses over nominal stresses in mode I pure bending and pure tension respectively. Moreover, validation with corresponding results from literature is provided. Finally, three different concepts for reducing the maximum surface stresses are presented. The first one proposes grinding of the weld toe area and formulation of an artificial U-notch or a part- circular profile. The second one applies to non-penetrating welds and assumes the existence of a root gap of a specific geometry which is related to the fatigue life and stress concentration factor of the fillet weld joint. Last but not least, the relatively recent concept of the variable radius notch is discussed, even though it is applicable mostly to notched bodies, not weld joints.

Afterwards, a Linear Elastic Fracture Mechanics analysis of reference 2D fillet weld model is demonstrated. A number of geometrical parameters considered at previous stage for their impact on surface Stress Concentration levels at the weld toe region, have been correlated to fatigue life benefits in terms of increased number of stress cycles till failure.

An extensive analysis of 9 different T-butt weld joint geometries has been provided in order to investigate how positively a possible SCF reduction can affect the fatigue life of a weld joint. Essential geometric variations (weld angle, length, toe radius, root slot) were considered in the 2D model. All calculated benefits both in pure bending and pure tension cases have been reported accordingly.

Based on a linear interpolation of the points scatter (SCF, N-cycles) both in banding and tension, it was observed that a surface stress mitigation of 1% could lead to 1,33 up to 2,5% fatigue life benefit in the range of SCF=2 – 2,5. It is evident so far that the geometrical optimization of a weld joint in respect of notch stress mitigation can be a powerful tool both in shipbuilding and

maintenance practice in the future. However, technically wise their application may incur high initial costs of improved tools of welding and post welding treatment and robots even though it would consist a cost effective solution in a medium/long term basis.

Finally, the above process is followed by a reliability analysis of the most critical geometrical parameters affecting the fatigue life of a fillet weld joint. Reliability assessment results concerning medium, high and low cycle fatigue are provided and a comparative analysis of each factor's impact on fatigue life has been carried out.

Keywords:

Linear Elastic Fracture Mechanics, stress intensity factor, structural reliability, fillet weld joint, fatigue life

ACKNOWLEDGEMENTS

In every aspect of our life, the quality of our relationships, cooperation and communication with people is a measure of our happiness and love. Words sometimes are not enough to describe our feelings for people dedicated to offering their lives to other people and especially students.

Professionalism, excellent teaching competency and willingness are only a few virtues of my supervisor Dr. Athanasios Kolios. Not only does he deserve my deep respect and gratitude for his remarkable insight, and clear opinion on research topics, but also for his multilateral qualification, and diligence.

On the other hand, Prof. F. Brennan's excellent approach to all students, his politeness, vigorous and thorough spirit are only a few representative aspects of his personality, very impressive and inspiring to me and all students that had the honor to get in close contact and consult him in their life.

Under their supervision, every student can be engaged smoothly and properly in the demanding field of research and proceed to their domain with confidence and eagerness. For any attempt towards the demanding and beautiful task of engineering research, a collaborative environment and constructive communication with experienced and wise people is a prerequisite.

Many and kind regards should also be addressed to my colleagues in Centrofin Management Inc. for their valuable guidance and support in various topics of this work. Especially my deep gratitude should be addressed to Mr. Ioannis Pantos, Technical Manager, whose deep knowledge and long experience in naval architecture and marine technology were eagerly shared to me in every instance.

Many thanks go also to all my friends and especially Dr. Anastasia Vasileiou, Ph.D.c Michail Makrodimitris and Ph.D.c. Alexandros Kitselis for their continuous support, useful suggestions and love.

Finally, my deep gratitude should be addressed to my parents for their unpretentious love and patience at all times. For their invaluable support and assistance in every difficulty and their wise advices at several critical circumstances of my life have always been plentifully provided to me.

TABLE OF CONTENTS

LIST OF FIGURES

(*) Figures 2-2, 2-3, 2-5 and 2-6 represent actual shipbuilding and supervision cases and they are kindly provided by the responsible person for the purposes of this report.

LIST OF TABLES

LIST OF EQUATIONS

LIST OF ABBREVIATIONS

VLCC	Very Large Crude oil Carrier
IACS	International Association of Classification Societies
CSR	Common Structural Rules
AWS	American Welding Society
SCF	Stress Concentration Factor
IMO	International Maritime Organization
RBD	Risk Based Design
GBS	Goal Based Standards
RBI	Risk Based Inspection
SOLAS	Safety Of Life At Sea (convention)
RBA	Risk Based Approval
GTST	Goal Tree Success Tree
TEU	Twenty feet Equivalent Units (Containerships capacity unit)
FEU	Forty feet Equivalent Units (Containerships capacity unit)
QRA	Quantitative Risk Analysis
PSPC	Performance Standard for Protective Coatings
POD	Probability Of Detection
DNV	Det Norske Veritas
SAFEDOR	Design, Operation and Regulation for Safety (conference)
LEFM	Linear Elastic Fracture Mechanics
EPFM	Elastic Plastic Fracture Mechanics
SIF	Stress Intensity Factor
CADC	Crack Aspect Development Curves
CTOD	Crack Tip Opening Displacement
FEA	Finite Element Analysis
BEM	Boundary Element Method
PPP	Preferred Propagation Path

1 INTRODUCTION

Marine design and construction during past decades has been a field of intensive investigation and analysis aiming at cost effective, ergonomic and safer constructions operating in adverse seas and environments.

Higher tensile steels, improvements in risk analysis of vessels and offshore constructions from design stage, advances in welding techniques for critical hull weldments such as vessels' erection joints and state of the art non-destructive testing methods contributed to this recent expand of the worldwide fleet and offshore oil platforms, accompanied by a substantial reduction of accidents at sea relatively to this global deadweight tonnage booming.

Notwithstanding, various challenges remain and in order to be adequately addressed, a new framework has to be introduced. Goal Based Standards, establishing a new design code based on broadly acceptable risk criteria, are aiming at the relatively new concept of Risk Based Ship Design and Approval in maritime community. Towards this, various IACS structural rules [65] have to be improved and redefined in several cases like Residual Stresses, Structural Redundancy, Human factor, Design transparency, Recycling, Survey and Maintenance.

Obtaining reliable marine constructions whilst reducing their lifecycle cost is believed to be effected by developing criteria which through an improved ship specific risk analysis will meet satisfactorily the initially stipulated targets. On the other hand, targets themselves should also be redefined, expressed in reliability terms and be aligned with the needs and tolerances of all concerned parties: from owner and onboard operators to society and environment as well.

Modern shipyards complying with IACS Common Structural Rules, produce vessels which meet above prescriptive rules for scantlings, geometrical constraints, safety construction considerations etc. Nowadays, the transition to performance-based design seems inevitable. A major difference is that design criteria are oriented directly to structure performance, avoiding over or under-estimations of scantlings. Through detailed risk and reliability analysis on every

component and the whole structure in terms of degradation and ageing due to fatigue and corrosion, external or internal loading uncertainties, maintenance and inspection risk, manufacturing and material uncertainties, onboard human activity and error, cargo operations history (loading, discharging) and other factors affecting the structure, we can obtain a robust design and apply fit-to-purpose safety margins to each component corresponding to pre-set minimum standards, emerging also from probabilistic studies on existing structures.

It is evident so far, that every structure should be evaluated for its reliability both in design stage and periodically during operation in order to establish a rational risk based maintenance scheme. Non-uniform degradation rates at various areas of a structure should be taken into consideration. Besides, analysis of corrosion rates at areas of geometric discontinuities is under investigation by various institutes and organizations. The difference of two initially “similar” structures after a period of continuous operation can be substantial, inducing the need of a risk based inspection and maintenance scheme able to detect timely any substantial crack or deformation. Hence, not only an in depth analysis of the deterioration mechanisms but also a probabilistic analysis of modern ships structures correspond to the risk based design philosophy.

Investigation towards marine structures fatigue life improvement has been carried out and developed initially in aircraft/ aerospace and nuclear industries but also in marine sector due to unpredicted failures of several structures caused by design stresses not exceeding the maximum yield point of the material.

From design stage, the fatigue capacity of a structure can be optimized by considering new weldment geometries, efficient structure arrangements including sophisticated crack paths, shot-pinning and formulation of crack arresting points of high residual stress, optimum materials and welding techniques etc.

Fatigue shielding of vessels is a challenge due to the extent of weldments, restricted time at erection stage in dockyards and extreme costs for refinement

of weld geometries, detection and smoothing of undercuts, continuous and safe monitoring of welding conditions etc.

As regards the root cause, it is commonly accepted from various analyses of fatigue cracks that weldments due to initial microseizures, porosity or material inclusions will initiate and propagate cracks at the most stress affected area. Stresses much lower than material's yield point, can induce micro-crack initiations. Since such phenomena are always present in welding materials, fatigue design should rather emphasize on crack propagation stage.

A representative type of weld joint consisting a critical part of every contemporary vessel and offshore platform is the T-butt weld joint (or fillet weld joint) further investigated in present work in respect of fatigue life expectancy and improvement. Traditionally, fillet weld joints would be avoided in construction whenever alternative means of joining were deemed as more practicable, safer and cost effective. Nonetheless, fillet weld joints combining the advantages of a light structure, high flexibilility in geometrical design and cost savings due to reduced fabrication time and effort, have become nowadays the most commonly used joints in contemporary ship construction. Hence, any attempt towards a more reliable construction should include a reliability analysis of each component in respect of stress mitigation, crack propagation rate control and fatigue induced crack initiation time and other factors.

In the present work, the stress mitigating effect of geometrical optimization is examined and relative fatigue life benefits are compared between several thousands of randomly selected geometries, for obtaining the contribution and effect of each geometric factor on fatigue life distribution. Above results can be introduced afterwards in a global reliability assessment of marine structures and used as predictive tools in design and hull inspection schemes, for reducing the probability of hull failure or crack detection (POD) respectively.

2 DESIGN & INSPECTION AGAINST AGEING

2.1 An overview of the ship structure

A ship hull consists mainly of the following components [100]:

a) Plate-stiffener combinations,

b) Panels of plating,

c) Frameworks,

d) Fittings.

Above components are then combined to form sub-structure components, categorized as follows [34]:

1. Bottom structure
2. Shell plating and framing
3. Bulkheads and pillars
4. Decks, hatches and superstructures
5. Fore and aft end structures

Numerous configurations of the above sub-structures are combined in ship hulls, depending on their type, capacity (deadweight, TEU/FEU etc.) and last but not least, the wave profile and weather conditions the vessel will be subjected to, according to her mode of operation and operational environment. A typical Very Large Crude Carrier (VLCC) midship section and the relevant nomenclature are illustrated in Figure 2-1.

The bottom structure along with the shell framing and deck plating, forms the backbone or the girder of a ship and is critical for the overall ship strength. Many DNV casualty reports refer to such critical areas [28], [29]. Particularly in modern ships with length exceeding 120m, the hull is longitudinally framed, the transverse framing being preferred in smaller ships. The stresses that a ship is subjected to are transferred from the external structure to the main hull stiffening components, where elastic deflections occur and even plastic deformations which absorb a part of the energy that is transferred to the

structure. However, since the ship is not fixed to a solid floor, a significant amount of energy is converted to acceleration. The fore end structure is also carefully designed against the wave impact and ice (for ice breakers) and the aft end against vibrations and thrust stresses that the water through the propeller returns to the support structure of the main engine bearings.

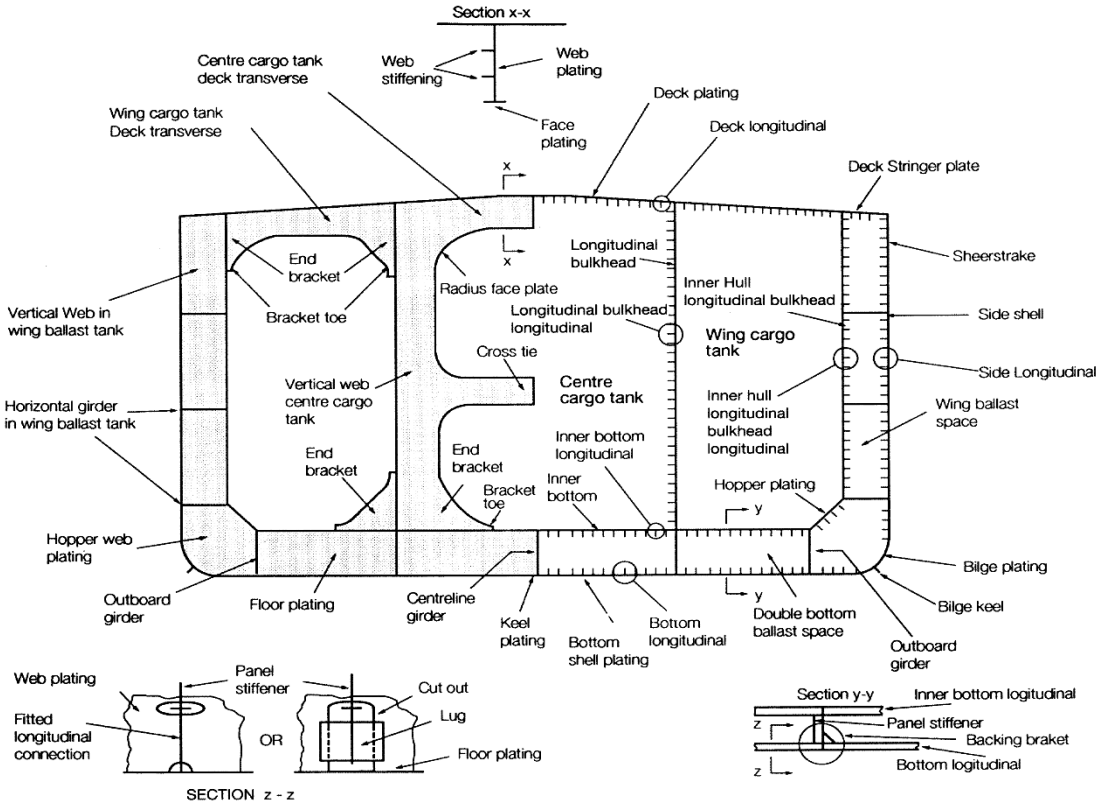

Figure 2-1 Typical VLCC midship section nomenclature

Finally, bulkheads have a significant contribution to the ship hull integrity, especially in larger ships, as Figures 2-2 and 2-3 from a Suezmax tanker block erection depict.

2.2 Critical ship hull components

Depending on the structural arrangement of a ship, critical ship hull areas [111] are the *"locations that due to stress concentration, alignment/ discontinuity and corrosion, a higher probability of failure is evident, in comparison to the*

surrounding structures". Hence, ship structure components, as described in §2.1, become critical when located to such areas.

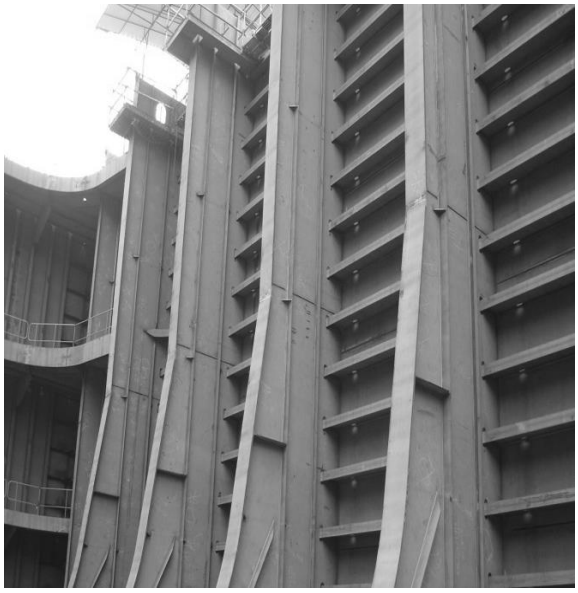

Figure 2-2 Suezmax Tanker longitudinal Bulkhead

Figure 2-3 Ship hull erection in dry-dock

For a typical double hull oil tanker, the susceptible to stress concentration and misalignment midship areas are depicted in Figure 2-4, while table 2-1 provides a number of prone to fatigue failure locations.

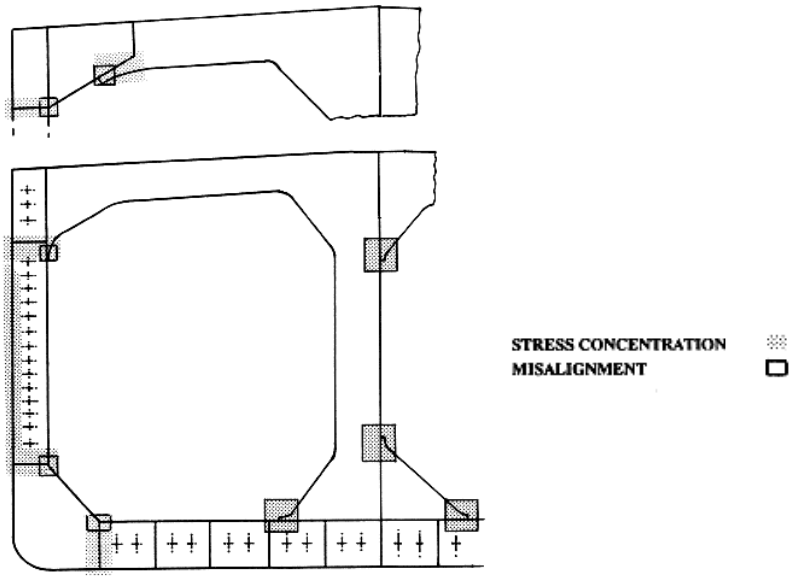

Figure 2-4 Critical areas in a double hull tanker midship section

1	Connection of hopper plate to inner bottom
2	Connection of hopper plate to inner hull longitudinal bulkhead
3	Gusset plate in line with inner bottom
4	Connection of topside tank plating to deck and inner hull
5	Connection of longitudinals to transverse bulkheads / webs
6	Connection of longitudinals to watertight/ ordinary floors
7	Panels of bottom girders in way of bilge wells
8	Connection of horizontal stringers to transverse web frames and side horizontal stringers
9	Connection of longitudinals to horizontal stringers
10	Corrugated bulkhead connection to deck and inner bottom

Table 2-1 Critical areas of double hull oil tankers

2.3 The ageing effect

The main ship hull degradation or ageing mechanisms are fatigue, corrosion and structural deformations and defects such as buckling. Particularly:

1. Fatigue failures are caused by alternating/ pulsating cyclical stresses which individually would not be sufficient to cause failure. In contrary, they initiate cracks which can become significant structural failures. They represent the most common cause of cracking in large tanker structures. Especially, the side shell and its connections with stiffeners are the most susceptible to fatigue areas, due to the combined actions of the three ship loading mechanisms and horizontal bending. A typical fatigue detail (Table 2-1 - case 1, Figure 2-4), is illustrated in Figure 2-5.

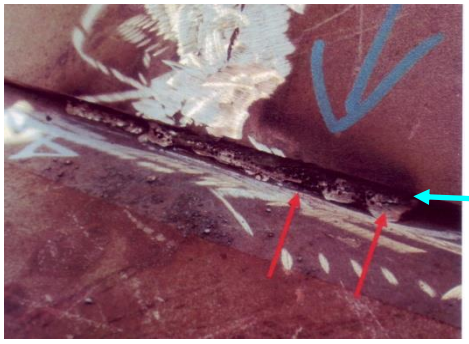

Figure 2-5 Fatigue crack at lower knuckle point – Hopper plate

Figure 2-6 Lower knuckle point

2. Corrosion can reduce significantly the strength of a ship structure, the effects on structural integrity depending mainly on the coating condition, the anodes condition and replenishment and the local environmental conditions (high temperatures, high salt density of water, microbes etc). Indicative types of corrosion are the general, pitting, grooving and weld metal corrosion. Implementation of corrosion additions to structural design is therefore imperative.

3. Structural defects such as buckling, weld defects and fractures, contribute also to the ageing of a ship or offshore structure. Permanent buckling

is usually the combined result of overloading, along with a considerable reduction of the cross section areas due to corrosion. Fractures usually initiate at latent defects in welding, at notches or weld undercutting in way of stress concentrations. Unfortunately, their detection by an optical inspection is usually a challenge, due to the existing coatings and poor lighting in these areas. However, a number of modern ultrasonic techniques and other inspection tools under investigation may facilitate this process in the future.

Further to the above mechanisms, the ageing of a ship and offshore structure depends on cargo handling related issues and proper crew training that can ensure safe cargo operations and proper navigation. Especially for bulk carriers, the former is highly related with significant deformations in cargo tanks.

Finally, it should be noted that dealing with ageing, as a cumulative quantity of structural deformations is a demanding task [51] that should be carefully approached. This is related with our potential ignorance of the precise strength capacity of an old structure which has been subjected to a number of modifications or uneven degradations (i.e. corrosion) and therefore any major repair and refitting work, if not done properly, could lead to unexpected accidents.

To an extent, defects will always be present in ship and offshore structures. Any attempt to mitigate the risk of a potential life loss or catastrophic event in the future will fail if uncertainties are not carefully considered and quantified [90] through risk and reliability analyses (Quantitative Risk Analysis- QRA). Uncertainties in structures modeling and capacity, marine and operation environments, and fabrication defects (misalignments, welding defects) should be taken into account. Although the embedded risk of defect inherent structures is minimized by risk based design, the importance of an effective ship inspection and repair strategy is always crucial to controlling the crack propagation and cross section diminution rates.

2.4 Condition assessment of ship structures

2.4.1 The optimal inspection strategy

The condition assessment of ship structures is carried out by classification societies, port authorities, flag states, cargo owners, ship owners and other parties. Most important rules that apply to this process are Common Structural Rules (CSR), Performance Standard for Protective Coatings (PSPC) and Goal Based Standards (GBS). In parallel to Risk Based Inspection (RBI) applied mostly in offshore structures condition assessment, the ship hull inspection regime is related to the philosophy of POD (Probability of Detection- see [44], [59]), relating the difficulties imposed by human or environmental factors to the defects/cracks detection during inspection.

The main concepts are the following:

1. Focusing on the most prone to failure areas of the structure
2. Consideration of the previous inspections data
3. Statement of quantitative acceptance criteria
4. Application of structural condition monitoring techniques
5. Use of data management tools and trace history

Combining the above concepts and retaining in parallel a balance between reliability and economy, is a substantial step towards an optimal inspection and maintenance strategy, as Figure 2-7 depicts. The green line implies the repair and unexpected cost from retaining the structure at a specific level of reliability.

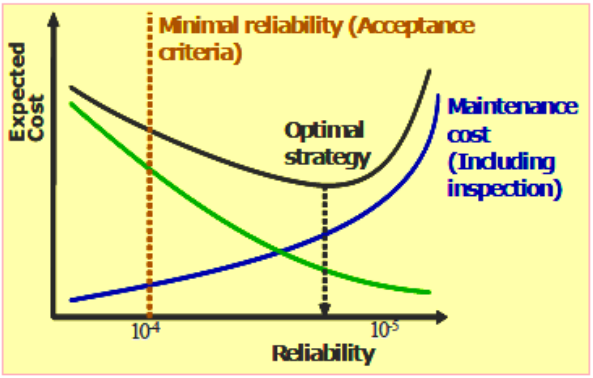

Figure 2-7 The optimal inspection and maintenance strategy

The optimal strategy is derived by considering a reliability value, where the sum of the maintenance and unexpected cost due to damages is minimized [50].

2.4.2 Ship hull condition monitoring

A variety of ship hull condition monitoring techniques [86] has been developed further to the traditional on-spot visual inspection or inspection through cameras. Such corrosion/crack detection techniques include:

- *Guided Wave Ultrasonic Testing* for pitting corrosion and weld defects detection
- *Acoustic Emission Technologies* against cracking and coating degradation)
- *Fiber Optic Sensors* which are inflammable and indicated for use in tanker applications
- *Magnetic Particle Inspection*
- *Alternative Current Field Measurement* providing detection and sizing information

Another important category is the coating condition monitoring, which involves on the spot inspections, electrical current procedures, camera vision systems, infrared thermograph measurements and paint deterioration systems.

Finally, the structural condition monitoring systems are fitted with strain gauges integrated with ship motion, pressure and/or fiber optic sensors. These systems offer real-time displaying of the hull stresses, ship motions, wave impact pressure and accumulated fatigue damage. Main challenges however remain, such as the effective data processing, adoption of fatigue damage sensors and acoustic emission technologies etc.

3 FATIGUE LIFE & FRACTURE MECHANICS

3.1 Fundamentals of fatigue

3.1.1 Definition and properties

Fatigue in materials science, represents a progressive and localized structural damage that occurs when a material is subjected to cyclic loading.

Under alternating or pulsating loading of nominal tensile stress limit or even lower than the material's yield point, microcrack initiation and propagation may lead to total collapse of a structure. Fatigue damage is the effect of combined and concurrent action of tensile stress, plastic strain and cyclic stress.

In brief, fatigue will start from initiation of a crack (surface microcracks are usually the most critical especially in bending), which under some critical load conditions will propagate to an extent –critical size– that the weakened part cannot carry the exerted loads. At the end, a brittle fracture or plastic collapse may occur to the remaining cross section.

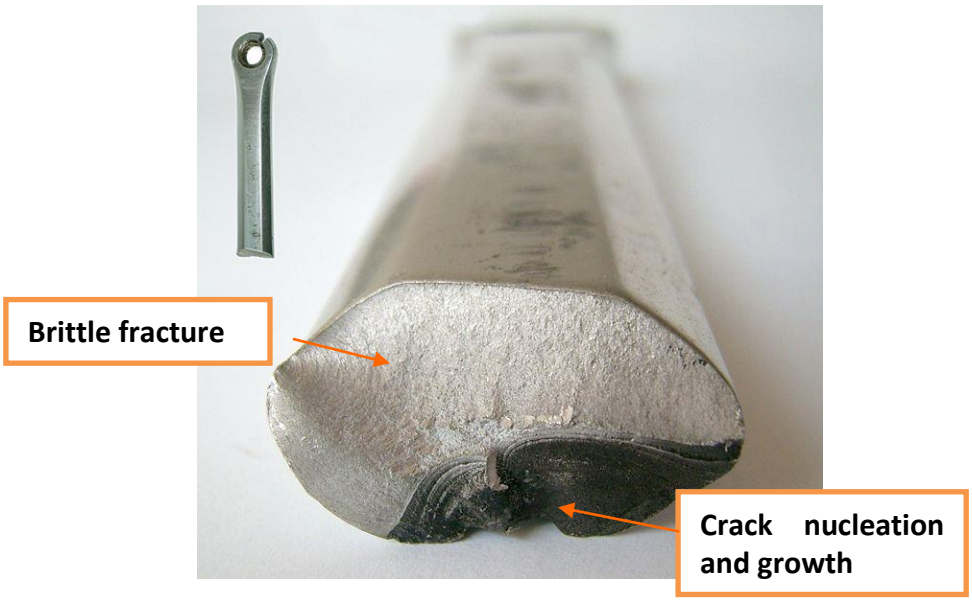

Figure 3-1 Fatigue crack nucleation and brittle fracture

According to ASTM, *fatigue life* N_f is the number of stress cycles of a specified character, that a specimen sustains before failure of a specified nature occurs.

3.1.2 S-N curves

A set of fatigue tests performed for specific material and specimen geometry under different stress ranges, can be illustrated as a fatigue resistant S-N curve, commonly known as Wohler curve. In these graphs, the horizontal axis is logarithmic and represents the stress cycles, while the vertical axis demonstrates the stress amplitude (maximum stress of applied stress range). Such diagrams are mainly used for medium ($2x10^6$ cycles) or high cycle fatigue ($>10^7$ cycles) analyses of welded joints, according to structural or notch stress approaches, as depicted in next paragraph.

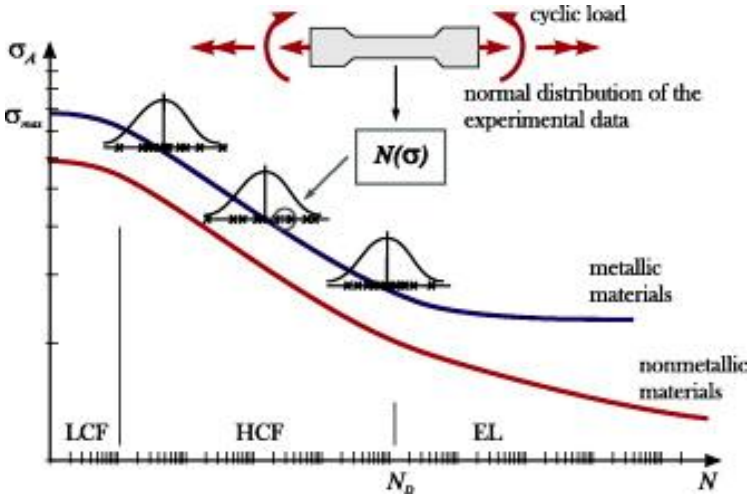

Figure 3-2 Wohler curves [47]

The endurance limit of a single specimen or a welded joint is dependent on the existence of a knee point (change of the line gradient), indicating no failure for unlimited number of cyclic loads and stress ranges not exceeding the stable value of the horizontal part of the graph on the right of the knee point.

3.2 Fatigue Life of welded joints

3.2.1 Fatigue analysis approaches

In reference to welded joints or notched bodies, according to Fricke [40], main fatigue analysis approaches as developed till today could be concisely reported as follows:

1. The Nominal stress approach, neglecting the stress gradient due to structural detail or weld effect. It is evident, that this method should be followed by local approaches, according to Petinov et al [93].

2. The Structural or hot-spot stress approach, which takes into account the stress increase due to the structure and excludes the local weld geometry effect. Actually, the stress gradient in cases like fillet weld joints is not accurately considered since calculations or measurements at specific distances from the toe are linearly extrapolated up to this point. Such assumptions however are rarely accurate.

3. The notch stress and notch intensity approaches [96, 103], which take into account stress concentrations due to the effects of structural geometry, as well as the presence of welds. These approaches are based on the elastic notch stress range and Stress Intensity Factors respectively. Alternatively, a Finite or Boundary Element Analysis can be carried out. Whilst the notch stress approach is gaining increasing importance in industry, many theories are developed for a reliable local principal stresses or Von Mises Stresses calculation at weld toe or root areas. For example, Radaj et al. [95] proposes application of a fictitious weld toe radii ρ_f=1.00mm for thick plates (t>5mm) derived by the micro-support hypothesis of Neuber. Thus, calculation of the effective notch stress could be carried out without making use of Stress Concentration Factors. This concept is further clarified in [37, 103].

4. The Notch Strain concept is based on elastic-plastic strain theory to assess the fatigue strength.

5. The fracture mechanics concept or crack propagation approach, offers according to Fricke [40], *"the one and only way for several cases, such as a fitness for purpose assessment of structural members with flaws or other crack-like defects".*

To predict the number of cycles N that a structure is expected to operate prior to fatigue failure, S-N diagrams, procedures based on fatigue crack propagation considerations or direct fatigue testing of components may be applied.

Below Figure 3-3, illustrates the effort and accuracy of above approaches versus geometrical complexity of the structure [72].

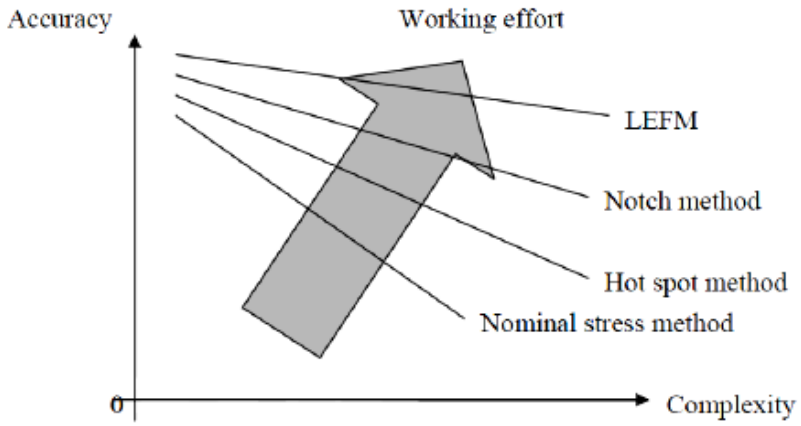

Figure 3-3 Accuracy of various fatigue analysis methods

3.2.2 Stress concentration in fillet weld joints

Fillet weld joints, as main structural components of marine structures, may contribute to the local and/or overall ship strength.

A typical full penetration fillet weld joint (or T-butt weld joint) is presented in Figure 3-4.

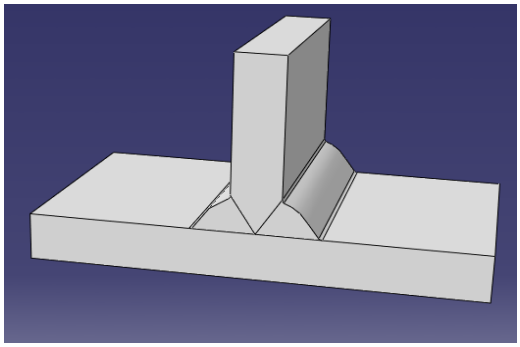

Figure 3-4 A fillet weld T- Joint

Typical ship areas of fillet welding against bending are the bulkhead structures of tank boundaries, while against tension is for example a transverse web, stiffening two longitudinal deck girders [82].

The main stress concentration areas are the weld toe [83] and root zones. Particularly, experimental data have shown [85] that it is possible to predict whether the crack initiation will take place at the weld toe or root, by an efficient notch stress analysis.

According to AWS [01]**,** in case of bending, the potential crack is *"initiating at weld toe, extending into base metal or initiating from root due to tension and then out through the weld"*. In case of tension respectively, it can be attributed to *"geometric discontinuities at toe of fillet extending into base metal*". Numerous are the references [38, 66, 74, 76, 85, 87, 88] indicating fillet weld toes as the most prone areas to crack initiations. This is also testified in Chapter 5, by finite element analyses of various fillet weld joint profiles under pure tension and bending.

The Stress Concentration Factors and their dependence on fillet weld geometry, have been studied by Monahan, Niu & Glinka, Peterson [89], Brennan [08], and others. Theoretical and experimental analyses [08, 18, 36, 61, 75, 76, 115] have shown that geometrical parameters with a significant contribution to fatigue are the flank angle, weld toe radius, weld throat or leg length, and carrying load plate thickness. Especially the latter, has an instant contribution to the size effect, which is conversely related to the fatigue life, according to [21, 35, 61] and others. A substantial cruciform joint analysis [76] has shown that the contribution of the weld leg length on stress concentration is less significant than the weld toe shape. Moreover in [115], it is referred that the critical parameter is the weld toe radius and an increase to the leg length without increasing the toe radius, would have neither effect to reducing stress concentrations nor to improving the fatigue life. Furthermore, in [61], cruciform joints analyses have shown that the weld size affects the crack initiation, propagation and finally, the fatigue life of the joint. Finally, the relative plate length to thickness has negligible influence on fatigue life, as depicted by [38].

In a recent work [110], D. Taylor developed an efficient variable-radius notch profile and approved that stress concentrations of every notched body can be reduced significantly by adopting such geometries. However, geometrical

optimization of fillet weld joints with respect to minimizing the SCFs and extending concurrently the fatigue life is still under investigation. Additionally, practical issues related to the welding procedures and efficiency in order to obtain compound fillet geometries though reliable welds should be addressed.

Consequently, Chapter 5 discusses an analysis in which, the 3 principal geometric parameters (weld angle, weld leg length and toe curvature radius) contribution is investigated, the surface stresses along the fillet welds are calculated and the geometry providing the minimum stresses is finally obtained. Afterwards, a number of geometric optimization suggestions are addressed for their potential to minimizing further the stress concentrations.

3.3 Fatigue life improvement

A number of critical parameters associated with the fatigue life of a welded joint are the following:

1. There is a theoretical and experimental background [09, 24], connecting the fatigue life with the geometry and design of a joint, under specific loading conditions. Notches and cross section geometrical variation are stress gradients, reducing the fatigue life of the joint through development of microcracks. Hence joint dimensioning is a challenge, not only because a strong joint is geometrically optimized but also because considerations of loading conditions, potential corrosion rates and economical aspects, concerning the post welding treatment should be made.

2. Existence of corrosive environments, accelerating the ageing effect, corrosion, erosion, gas-phase embrittlement.

3. Surface roughness, inducing stress concentrations at the surface of the material and surface flaws which may be evolved to propagating cracks.

4. Extreme high or low ambient temperatures.

5. Crack initiations and mechanisms of crack propagation and crack aspect development, a subject discussed further in §3.5.4.

6. Weld material and its lack of homogeneity, the sensitivity, inclusions and undercutting, along with plate deformations, residual tensile stresses due to welding or cutting and excessive distortions are crucial. Moreover, the aspects discussed in following § 3.4 regarding fabrication methods are critical.

7. Level of welding preparation (in respect of alignment of the plates and condition of the pre-welded sheet metal).

8. The surrounding ageing effects (as described above) in the structure which alter the actual stress conditions in the vicinity of the weld joint.

9. Thickness of a structural joint and the size effect. It has been observed [61] that as the wall thickness of the members is increased the fatigue strength is decreased.

Various techniques have been developed [07, 52, 84, 109] to arrest cracks or facilitate their detection before they become critical. Brennan [07], showed that by controlled peening it is possible to delay the propagation or arrest a crack, by creating a field of residual stresses in the vicinity of the weld. Many types of peening exist such as needle-, hammer-, shot-, brush-peening and ultrasonic. Furthermore, Okawa et al. [84] developed a technique in which cracks are urged to follow a tortuous path. By doing this, their detection is facilitated before they become critical. In [99], Brennan showed that by removing flaws and cracks from the weld toe, using a U-shaped or part circular repair profile, the Stress Concentration Factors can be mitigated and fatigue initiation life, in some cases, be improved. This is discussed further in Chapter 5. Besides, Rodríguez-Sánchez et al. [97] suggest weld toe grinding and crack removal, by profiling the new surface in order to improve the fatigue resistance without re-welding. Such process, when combined with an effective fatigue management program, could secure the structural integrity, by minimizing the repair costs.

In brief, the main post-welding treatments that can improve the fatigue resistance of welded joints are categorized [48] as follows:

1. Weld profile improvements (weld toe remelting by TIG/ plasma/ laser dressing, machining of the weld).

2. Residual stress improvements (peening, overstressing, stress relief).

3. Environmental condition improvements (resin coating, painting).

The fillet weld joint dealt within present work, will be geometrically optimized by mitigating Stress Concentration Factor in a way that joint's strength is not compromised. Such considerations as the extent of penetration of the weld are critical ones, since a full penetration is considered as offering stronger joints. In [73], which treats among others the lack of penetration, this parameter is synonymous to a reduction of the estimated fatigue lives of T-butts and cruciform joints.

In conclusion, the fillet weld joint as a part of a ship or offshore structure, contributes to the ageing of the overall structure. Hence, every improvement against its mechanisms (Chapter 2) is highly related to fillet weld joints design, fabrication and maintenance.

3.4 Fillet welding and testing

Fillet welds may be continuous or intermittent, based on the structural effectiveness of the member to be welded [34]. Satisfactory welding preparation is needed for a proper alignment of the plates and condition of the pre-welded sheet metal. Especially for thicker plates, beveling and profiling of their edges can ensure complete penetration of the weld metal. This is carried out usually by mechanical machining for higher tensile steel types, as it provides a better finish than the gas or plasma cutting.

The critical areas of many contemporary ships (midship, fore end, after end, bilge keel, deck plate) are reinforced by high tensile steels of AH, CH, EH and FH types with strength 32 up to 69 kg/m^2. However, in non-critical areas, grades A, B, C, D and E (ordinary mild steels) or cast iron may be used. As regards the fillet welding techniques, the manual arc welding, the MIG, TIG, SMAW and SAW are very common and useful in ship construction.

A fillet weld may be characterized as acceptable or unacceptable, according to the American Welding Code [01], as described in Figures 3-5, 3-6 and 3-7. However, a number of factors also affect the quality of a welded joint, the most

important being the unacceptable distortions (see Figures 3-8, 3-9 and [31]) caused by the cooling and contracting of the steel plate after the welding. Another problem arises from our effort to control distortions by restraining the plates, thus provoking high residual stresses in the structure. In order to mitigate above symptoms, a very fictitious welding consequence is needed. Particularly in fillet weld joints, the butt should be welded fully at first, then the seam edge duly prepared and finally the seam welding performed.

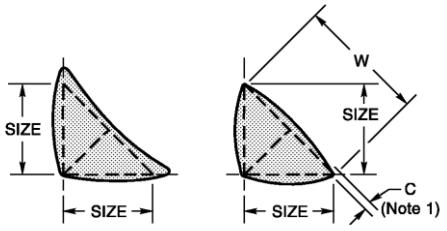

Figure 3-5 Desirable profiles

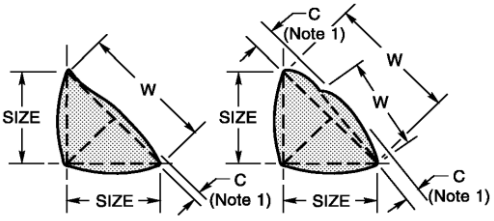

Figure 3-6 Acceptable profiles

Synoptically, the quality of a weld is influenced by the environmental conditions (i.e. welding in very low temperatures - ice conditions), fabrication methods, welder experience, any fatigue improvement techniques implemented and other factors described by AWS and other institutes.

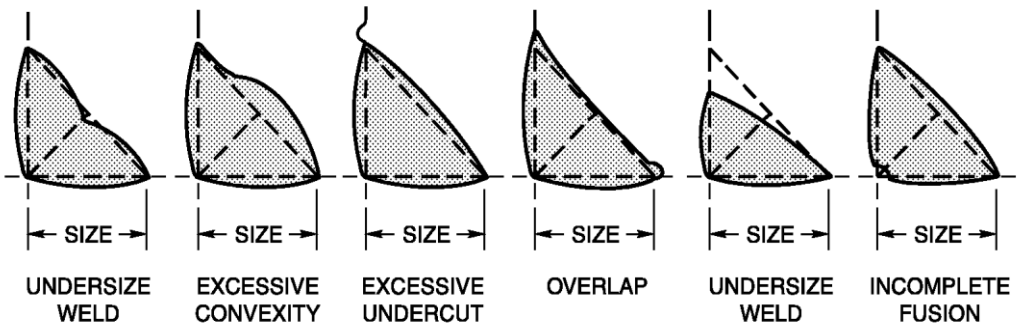

Figure 3-7 Unacceptable profiles

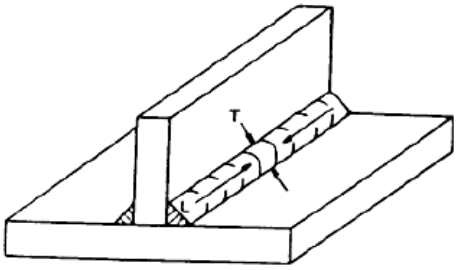

Figure 3-8 Longitudinal (L) and Transverse (T) shrinkage stresses

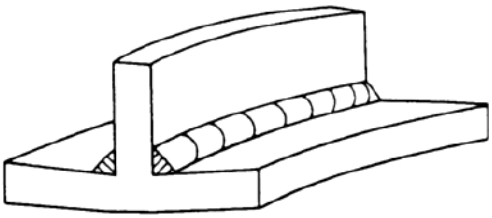

Figure 3-9 Distortions in a fillet weld joint

Further to the techniques mentioned in §2.4.2, the three dominant non-destructive weld testing methods are the periodical visual examination, the radiographic inspection and the ultrasonic energy technique. The dye penetrant and the magnetic particle testing are not extensively used today, since they are limited to surface crack examinations of the cast iron formulations in ship structures.

The ship hull inspection procedures are described in detail in IACS rules and respective Classification Societies guidance manuals. The most critical for the structural integrity of a ship fillet weld joints, among other important structural components, are inspected in annual basis (especially in bow, stern and midship areas) and more thoroughly during the intermediate and special surveys, the latter taking place every five years upon vessel's commissioning.

3.5 Fracture Mechanics

3.5.1 Basic principles and approaches

In mechanical theory and practice, Fracture Mechanics is the field of crack propagation analysis, based on elasticity and plasticity properties of materials and their crystallographic micro-defects. Developed by A.A. Griffith during 1st World War, Fracture Mechanics has been established on the assumption that raw materials always contain microscopic flaws. Under specific stress conditions and depending on their location in the structure, these flaws will

propagate, coalesce with adjacent cracks (if any) and may lead to a collapse of the cross section of material (bolt, plate, welded joint etc.).

The *Linear Elastic Fracture Mechanics* approach or LEFM is established on the following principles:

1. The material is linearly elastic and isotropic
2. The crack has been initiated & has started to propagate
3. The plastic zone surrounding the crack tip is small
4. The points of analysis are close to the crack tip

Basis on above, the *Critical Stress Intensity Factor* K_{ic} or the *Critical stored strain energy release rate* G_{ic} should be defined for establishing strength criteria.

Stress Intensity Factor, is the principal parameter in Fracture Mechanics and its calculation is performed through theoretical analysis of near crack tip stress field. Towards this, numerical solutions (BEM or FEA), handbook solutions and weight functions can be utilised.

As a theoretical construct, SIF is a measure of the stress state at the crack tip area and offers a criterion of fatigue strength for specimens under cyclic loads. Stress Intensity factor applies to homogeneous and linear elastic materials and is a function of crack geometry, distribution and magnitude of stresses at the crack tip area, crack position and size.

Three types of SIF corresponding to deformation modes of Figure 3-10 exist:

- Mode I: the symmetrically opening mode due to tensile in-plane stress
- Mode II: is the in-plane shear or sliding type mechanism
- Mode III: is the out-of-plane shear type mechanism

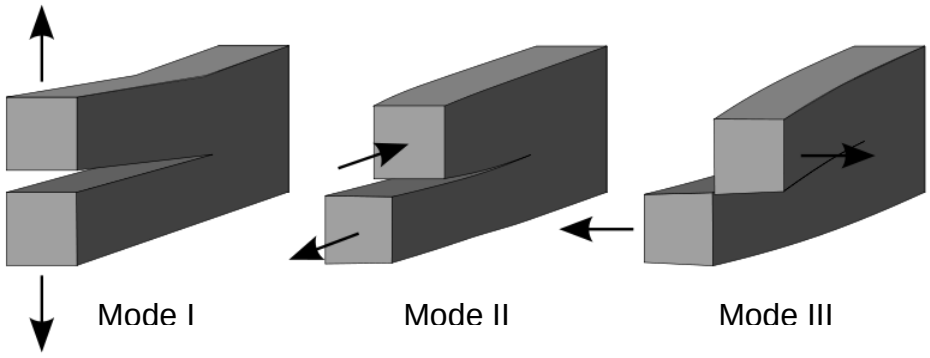

Figure 3-10 Fatigue analysis stress modes

Irwin [54] developed the following definition of Stress Intensity Factor (SIF) corresponding to fracture mode I :

$$K=\Delta S \bullet Y \bullet \sqrt{\pi \cdot \alpha}\left[MPa\sqrt{m}\right], \quad \text{where:} \qquad (3\text{-}1)$$

ΔS: *the stress range,*

Y: *the magnification/calibration factor dependant on crack geometry, modes and magnitude of loading and overall configuration of the body*

α: *depth of elliptical surface crack*

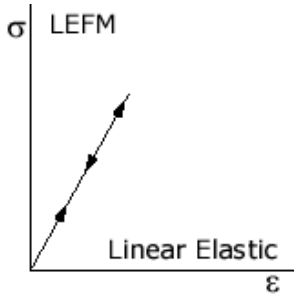

Figure 3-11 Linear Elastic material behaviour

Fracture toughness as a material specific property has been studied at first from Griffith and later from Irwin through the development of energy release rate G.

$$G=\left[\frac{\partial U}{\partial \alpha}\right]_P=-\left[\frac{\partial U}{\partial \alpha}\right]_u \quad , \text{ where:} \qquad (3\text{-}2)$$

U the elastic energy, *a* the crack length, *P* the load and *u* the displacement

A critical value of above strain energy rate G_{ic}, when released to a specimen may cause crack initiation by destroying structural bonds at the less stress resistant area of the material. Estimation of G_{ic} is an experimental process whilst determining the critical value of SIF, K_{IC} is a theoretical process of near crack tip stress field. The relationship between above values is as follows:

$$G = \frac{K_I^2}{E}, \text{ for Plane Stress} \qquad (3\text{-}3)$$

$$G = \frac{K_I^2}{E}\left(1-u^2\right), \text{ for Plane Strain} \qquad (3\text{-}4)$$

On the other hand, the *Elastic-Plastic Fracture Mechanics* (EPFM) concept is based on the following assumptions:

1. The crack has been initiated and is propagating
2. The material is elastic-plastic
3. The material is isotropic
4. The magnitude orders of the plastic zone at crack tip and the crack size are same
5. As the applied load is increasing, the size, shape and crack length of the plastic zone may change.

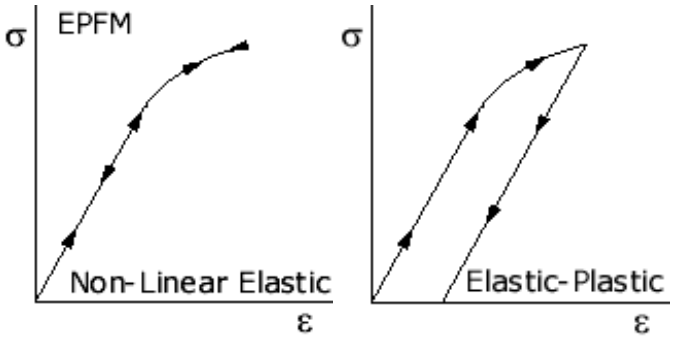

Figure 3-12 Non-linear elastic and Elastic-plastic behaviour

The critical parameters in EPFM analysis are the *Crack Tip Opening Displacement (CTOD) with critical value: δ_c*, and the *J-contour integral for strain energy fields calculations with critical value: J_c.*

Regarding crack tip opening displacement, the following formula applies:

$$\delta_t = \frac{8\sigma_Y}{\pi E}\alpha\left[\frac{1}{2}\left(\frac{\pi S}{2\sigma_Y}\right)+\frac{1}{12}\left(\frac{\pi S}{2\sigma_Y}\right)^4+\frac{1}{45}\left(\frac{\pi S}{2\sigma_Y}\right)^6+\ldots\right] \quad (3\text{-}5)$$

where α the half crack length, S the applied stress and σ_Y the crack edge stress.

Crack tip opening Displacement can be used as a failure criterion in a similar way to SIF and Energy Release Rate.

Finally, the J-integral is an alternative means for assessing fracture toughness of a non linear elastic body, based on energy release rate due to crack extension.

However, calculations of J-integral can be made both in linear and non-linear ranges of the σ-ε curve:

$$J = \frac{K_I^2}{E} = G_I \ [J/m^2] \ \text{, for Plane Stress} \quad (3\text{-}6)$$

$$J = \frac{K_I^2\left(1-u^2\right)}{E} = G_I \ [J/m^2] \ \text{, for Plane Strain} \quad (3\text{-}7)$$

For the purposes of this work, the evaluation of fatigue strength capacity is limited to Linear Elastic Fracture Mechanics analysis and deformation mode I.

3.5.2 Linear Elastic analysis

Paris-Erdogan relationship as provided below, associates the crack propagation rate to material properties (A and m constants) and Stress Intensity Factor range, ΔK.

$$\frac{da}{dn} = A\bullet\left(\Delta K\right)^m \quad (3\text{-}8)$$

The Paris' formula incorporating the K threshold range is modified as follows:

$$\frac{d\alpha}{dn} = A\left(\Delta K^{m} - \Delta K_{th}^{m}\right) \quad \text{where:} \qquad (3\text{-}9)$$

α: *depth of elliptical surface* crack

n: *number of stress cycles*

ΔK: *the SIF range*

ΔK_{th}: *the threshold SIF range*

A and **m**: *Paris coefficient and exponent (material constants)*

Combining the Paris' formula (3-8) with SIF formula (3-1), we obtain the number of fatigue stress cycles:

$$\left.\begin{aligned} d\alpha / dN &= A(\Delta K)^{m} \\ \Delta K &= Y(\Delta\sigma)\sqrt{\pi\alpha} \end{aligned}\right\} \Rightarrow$$

$$dN = \frac{d\alpha}{A(Y\Delta\sigma\sqrt{\pi\alpha})^{m}} \Rightarrow$$

$$N_f = \int_{\alpha_1}^{\alpha_2} \frac{d\alpha}{A(Y\Delta\sigma\sqrt{\pi\alpha})^{m}} \Rightarrow$$

$$N_f = \frac{2}{(2-m)A \cdot Y^{m} \cdot \Delta\sigma^{m}\pi^{m/2}} \left[\alpha^{\frac{2-m}{2}}\right]_{\alpha_1}^{\alpha_2} \quad , \quad \text{where:} \qquad (3\text{-}10)$$

Δσ: *Applied stress range*

N_f: *Number of stress cycles till failure*

Y: *Stress Intensity Calibration Factor*

Therefore, if we could determine the SIF distribution along crack fronts it would be possible to calculate the number of cycles required for the propagation of crack through the plate thickness from depth a_1 to a_2. Relevant parametric equations [06] of Stress Intensity Factors and particularly Y factors have been used in Chapter 6 for the purposes of subject work, aiming at maximizing the fatigue life of various geometries of fillet weld joints.

3.5.3 Weld magnification factors

Reference is made to BS 7910 [15], concerning assessment of the Stress Intensity Factor K_I at weld toes, by introducing the weld correction or magnification factor M_k. It is evident that initial cracks located at or in the vicinity of weld toes, will be affected by the stress concentration field during their propagation life.

In BS 7910 the above necessity is clearly stated:

"Unless the K_I solution being used already incorporates the influence of the stress concentration, it is necessary to introduce the correction factor M_k, which is a function of crack size, geometry and loading."

However, weld magnification factor equations do not account for weld geometry details (weld toe radius, angle), except for the attachment size.

Weld toe Correction Factor definition:

$$M_k = \frac{K_1}{K_2}, \text{ where:} \qquad (3\text{-}11)$$

K_1: *the SIF in plate with attachment and*

K_2: *the SIF in same plate without attachment*

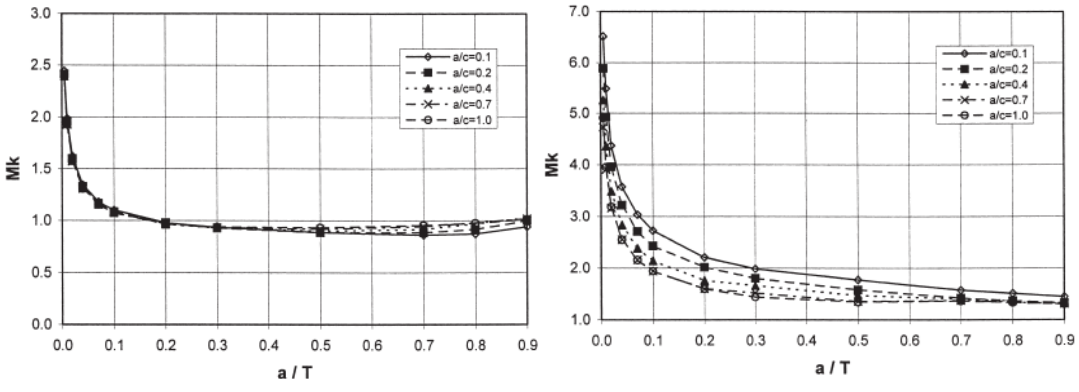

Deepest point ***Crack ends***

Figure 3-13 Magnification factors in membrane loading

According to [99]**,** in shallow cracks the K is increased due to *notch stress* effects while in deep cracks is reduced due to *restraining effects*. The crack

opening and the plate deformation have been reduced due to the attachment presence (and restraining effect) whilst in case of bending, the neutral surface is comparatively raised.

3.5.4 Crack propagation and aspect ratio evolution

Cracks incorporated in fillet weld joints will propagate in a different manner than geometrically same surface cracks in finite plates without attachment plate. This behavior can be attributed to a number of factors including but not limited to the magnitude of Stress Concentrations, the material inhomogeneity (inclusions, small cavities) and toughness, existence of thermal affected zones and residual stresses in welded areas.

The geometrical evolution of the crack will additionally depend on [67] the nature of the stress (bending, tension), the stress mode (I, II, III) and amplitude [94]**,** the stress ratio R and alterations frequency, the plate thickness etc.

Numerous are the references in literature [10,12,46,63,67,70,71,94,102,104, 107,108,114,117], concerning the crack geometry evolution after initiation stage, which usually represents the 5-10% of the total fatigue life of a welded joint [83]. However, higher loads will lead to shorter fatigue initiation lives. The same applies also to manual and automatic welds, the former leading to shorter initiation lives due to the formation of deeper toe defects.

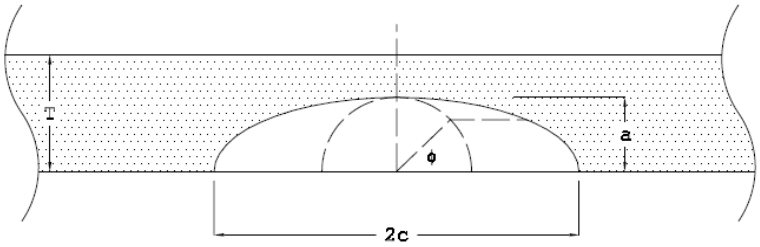

Figure 3-14 Semi-Elliptical Surface Crack [60]

In case of bending load exerted on a welded joint, the fatigue crack growth rate through the plate thickness has been proved to be lower than in surface direction [16]. This phenomenon is strictly related with the neutral axis downshift, which in combination with the ever decreasing stress at the crack tip

area (the bending stress is reduced towards the neutral axis under constant nominal load) and the fact that the higher bending stress is evidenced at the surface of the material, is leading to an ever decreasing crack aspect ratio (a/c). Another factor contributing to the above growth rate reduction is the plasticity of crack tip areas approaching the back plate surface creating a lower stress resistant area accompanied by a reduction of Stress Intensity Factor. Hence the aforementioned stress reduction at the crack tip area may prohibit any further propagation at the crack depth “a” direction when the back plate surface has also become plastic [67].

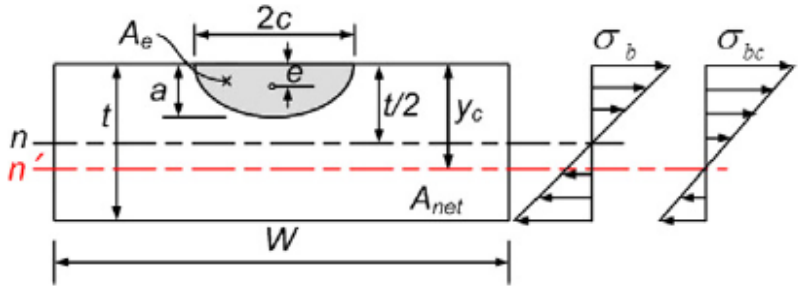

Figure 3-15 Neutral axis shift due to uncracked area reduction [16]

It should be underlined that the critical factor in case of alternating bending is the weakening of the plate due to the neutral axis downshift. Various studies and experiments on crack propagation under bending load have noticed very low crack aspect ratios (around 0.1) for crack depth exceeding the half thickness of the cross section. An indicative crack depth limit for examining the fatigue life of welded joints under bending is the half thickness of the plate e.g. a/T=0.5. In this case, the failure mechanism consists of a plastic collapse of plate’s unaffected cross section due to development of a lengthy crack in surface direction to an extent that the remaining cross section cannot withstand the exerted stress.

On the contrary, in alternating tension the failure mechanism is quite different. The crack will usually propagate beyond the depth of a/T=0.5 and reach the limit of a/T=0.8 before a brittle fracture is experienced. Besides, regarding failure criterion, the collapse is expected to occur when Stress Intensity Factor K has reached the critical value K_{cr}. Due to higher stresses and SIF values at

crack tip area, shorter cracks propagating in vertical direction are developed which under the alternating/pulsating tension will lead to a brittle fracture of the unaffected cross section. A substantial difference to bending failure mechanism is that the fracture toughness due to weakening of the cross section has become lower in comparison to the crack tip SIF.

An initial semi-circular crack in tension usually grows to semi-elliptical shape of about 0.7 -0.8 aspect ratio. On the contrary, if the initial ratio is low, the crack is developed in through thickness (vertical to surface) direction, before increasing again in free edge-surface direction in the range of 0.7 to 0.8.

In addition to above, another important factor in predicting the crack aspect ratio evolution for both tension and bending cases is the crack coalescence.

According to [83], three phases of surface cracks development and coalescence have been recognized:

1. Existing or fatigue induced microcracks along the weld toe at microgeometric discontinuities tending to form small semi-ellipses with aspect ratio $0.1<a/c<0.3$.

2. Microcracks growth leading to a maximum of $a/c=0.5$ at crack depth of about 0.1 to 0.3mm

3. The crack aspect ratio will decrease in a discontinuous manner mainly due to coalescence.

In several cases, a sudden reduction in a/c rate has been observed, due to a rapid crack coalescence, especially in bending [16]. However, we should reiterate that the stress magnitude can determine the evolution of a single crack or multiple cracks included in the plate material. Especially in case of high exerted stresses, multiple crack coalescence will occur, leading to much lower a/c values as the crack is propagating through plate's thickness. In contrary, low stresses will usually result to single crack propagation, since not all the initial cracks will propagate. but mainly the one affected mostly by the higher stresses.

Lin & Smith [67], based on experimental results of surface cracks growing under tension and bending, have observed a so-called *"preferred propagation path"* (PPP). The independence of the initial crack aspect ratio to the final ratio under the same loading conditions is clearly illustrated in the following diagram of Figure 3-16. Yan-Lin Lu [117] demonstrated an engineering process for calculating Crack Aspect Development Curves of surface cracks at weld joints. It is important to note that fatigue life predictions should not be based on an assumed crack growth path but on CADC, especially in case of weld joints with residual stresses. Therefore, the most accurate estimation of the crack growth pattern could be succeeded by a 3D analysis for precise CADC calculations and obtaining the actual distribution of SIF along the crack front and SIF values at the crack tip and crack end.

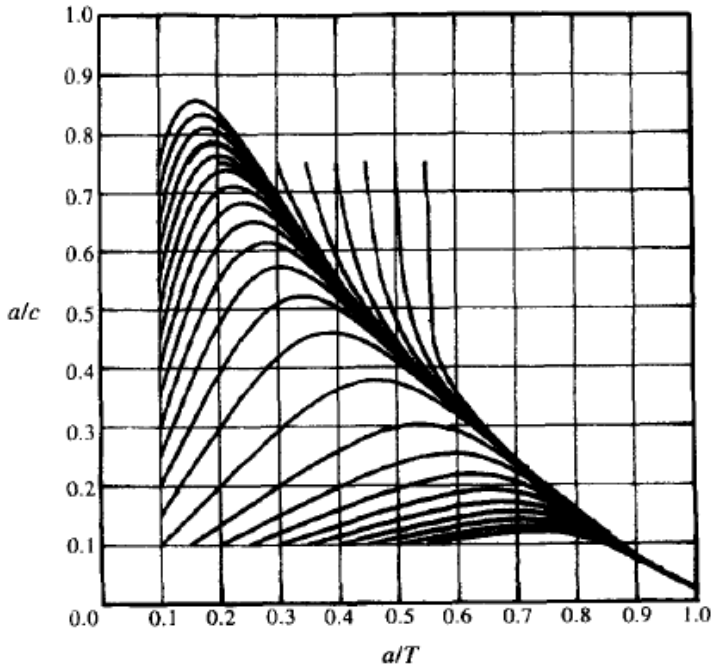

Figure 3-16 CADC for a fillet weld joint in bending [29]

Another important factor of the crack evolution model is the plate thickness. According to [04], thinner plates under pure bending load, have shown resistance in a through thickness growth while axial tension could lead to yield before a brittle crack failure occurs. On the other hand, thick plates are more prone to through plate thickness cracks.

3.5.5 Empirical Equations of crack aspect ratio

Various researchers have developed in the past parametric equations for easier calculations of the crack aspect ratio a/c, as a function of crack depth and/or stress for a variety of materials and geometries (mostly surface cracks, butt and T-butt welds). Particularly:

- Bell & Vosikovsky [12], through experimental results of cracks propagating in fillet weld joints under 3-point bending, developed the following equation:

  $$\frac{a}{c} = e^{-ka}$$, where: (3-12)

  k is a function of stress level and weld toe geometry as follows:

  $$k = 2.09 \bullet 10^{-6} (S_{max})^{1.93}$$ (3-13)

  where S_{max} refers to the maximum stress calculated or measured at the weld toe area. The recommended value for Paris law exponent m is 3 and for Paris coefficient A is 5.36×10^{-12}.

- Portch [94], has developed a number of parametric equations for surface crack propagation both for bending and tension dependant on the crack depth.

- Kawahara & Kurihara [63], through experimental results of surface flaws propagation developed a set of equations not only for pure bending and tension but also for a combination of these two loading types.

- Iida [53] similarly, developed a set of equations both for bending and tension dependent on crack depth.

- Wu Shang-Xian [107], developed a set of analytical solutions based on Paris law (separately for the crack tip and surface point) and incorporating the Newman-Raju's equation $C_A = 1.1^m C_B$ (3-14), both for bending and tension cases in surface cracks.

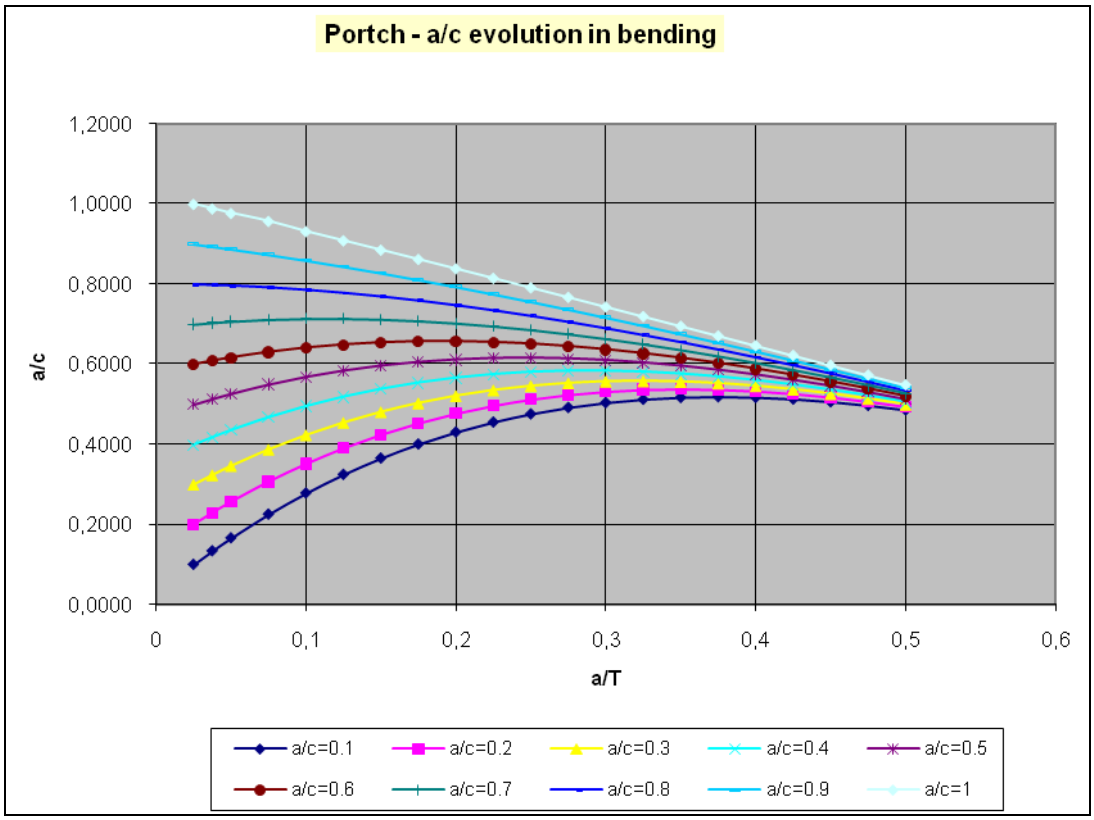

Figure 3-17 Portch - Crack aspect development curves (bending)

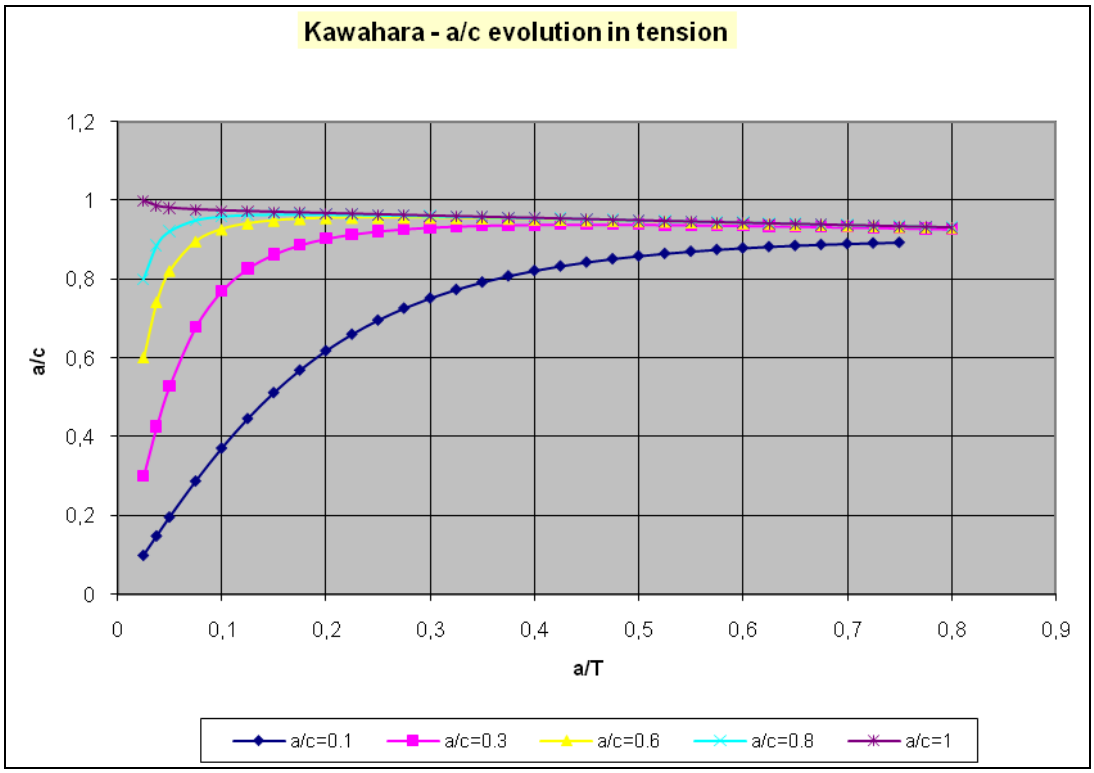

Figure 3-18 Kawahara - Crack aspect development curves (tension)

Indicative Crack Aspect Ratio evolution curves, computed on the basis of above Parametric Equations of Portch, Kawahara & Kurihara (commencing from different initial crack aspect geometries) and Bell & Vosikovsky (medium cycle for the 9 geometries) are demonstrated in Figures 3-17, 3-18 and 3-19 respectively.

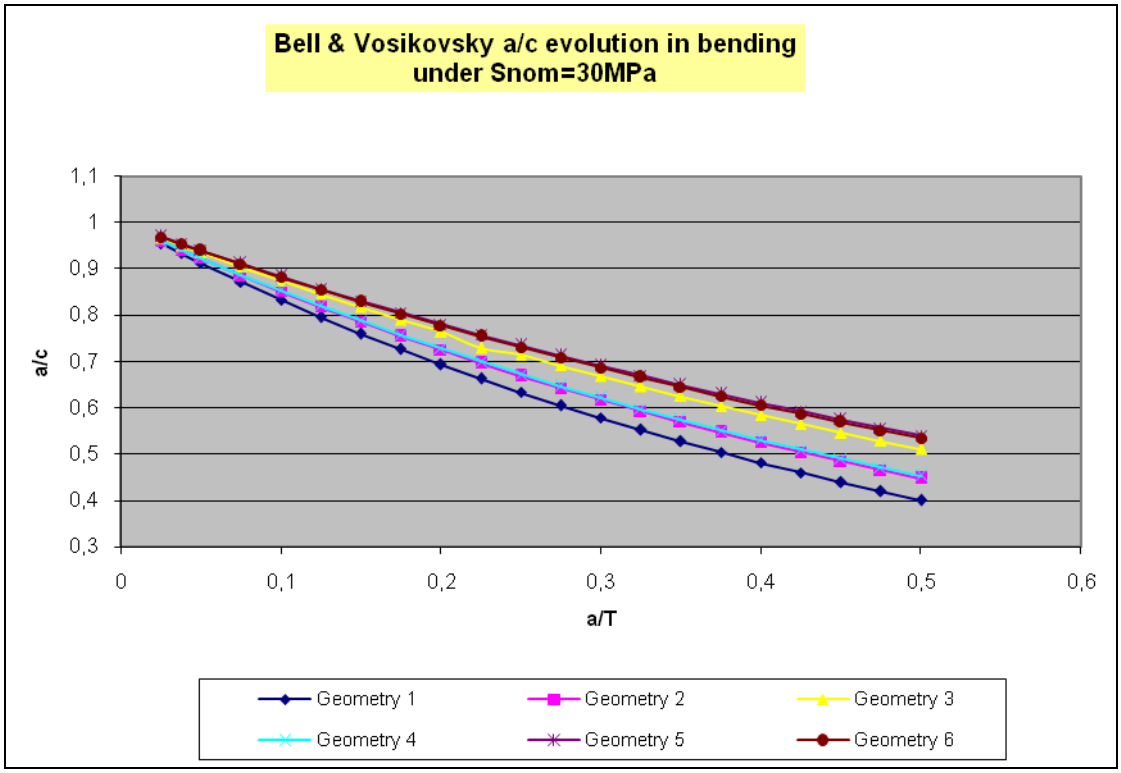

Figure 3-19 Bell & Vosikovsky - Crack aspect development curves (bending)

GEOMETRY	1	2	3	4	5	6
Length overall (mm)	150	150	150	150	150	150
Full penetration weld length L (mm)	30	30	30	20	30	30
Base plate thickness (mm)	20	20	20	20	20	20
Attached plate thickness (mm)	10	10	10	10	10	10
Fillet weld angle (deg)	45	45	30	45	30	30
Weld radius on attachment side (mm)	1	1	1	1	1,3	1,3
Weld toe radius (mm)	1	1,3	1	1,3	1,3	1,3
Penetration (weld root)	√	√	√	√	√	-

Table 3-1 Details of 6 geometries considered in figure 3-19

4 STRUCTURAL RELIABILITY ASSESSMENT

4.1 Background

Traditionally, uncertainties would be incorporated in design as safety factors, uniformly applied to the structure, accounting for any strength inconsistencies or combination of “unknown factors”, leading to overstressing and collapse of the structural member.

Nowadays, structural reliability in ship and offshore platform construction has become a powerful tool, due to an increasing demand for complex, unconventional geometries and critical designs.

Especially, focusing on ageing mechanisms of marine structures, factors influencing corrosion and fatigue may be highly stochastic and therefore any prediction in corrosion rates or fatigue capacity will fail, if such variables are considered deterministically. Loads, ambient factors, properties of materials, design and fabrication methods are indicative ones.

Structural reliability analysis identifies critical uncertainty contributors, combination of which is the actual stress and strength of each structure. Our confidence on every joint and plate of considered structure can be illustrated in reliability indices. Such procedures, not only can be applied repetitively for obtaining the optimum design, but also for in-service analysis of the ageing structure, through a sophisticated inspection regime.

Reliability, according to [25], *is the probability that a system will perform its function over a specified period of time and under specified service conditions.*

On the other hand, *Structural Reliability aims at predicting limit-state violations of a structure during its service life*.

According to [30], structural reliability methods are classified to following levels:

Level I: The uncertain variables are represented by single values and therefore a load may have only a specific magnitude. This level is called deterministic.

Level II: Incorporating two values for the representation of any uncertain variable (i.e. mean and variance) and an additional correlating measure of those variables (for example the covariance).

Level III: Introducing the joint probability distribution of all the uncertain variables. In this level, probability of failure is the main reliability measure. Advanced mathematical techniques, approximate analytical methods (1^{st} and 2^{nd} order methods) and simulation methods such as Monte Carlo simulation belong to this category.

Level IV: Used mostly for establishing acceptance criteria for level III analyses, this level takes into account uncertainty in engineering economic analysis, to produce an optimized cost – benefit calculation for decision making.

4.2 Time invariant methods

Similarly to physical phenomena, stability problems actually are time dependent hence, any accurate and analytical mathematic modelling is a demanding and laborious task. Considering exclusively random variables we can simplify above analyses by converting the problem into time invariant. Towards this, any random variable may be given a specific distribution or a steady state may be assumed.

In the following paragraph, a short reference to time invariant methods is made and especially to Level III methods.

In reference to variables used in structural reliability field, a specific distribution $f_x(\mathbf{X})$ is assigned to any vector $\mathbf{X}$ of n-dimensions. On the other hand, functional requirements, $g_j(\mathbf{X})$, commonly known as limit state functions, associate the initial state to the result, as a negative or positive value, corresponding to failure or success correspondingly and null, if limit condition is observed. Such $g_j(\mathbf{X})$ functions should be equal in number to functional requirements. Finally, global function $g(\mathbf{X})$, combining all $g_j(\mathbf{X})$ functions is a tool providing indication of the overall satisfaction of limit states.

Before we define the probability of failure P_f, it is necessary to introduce the Probability Density Function or PDF. This function, offers indication of the potential of occurrence of a random variable at a specific point.

Integration of this function extended in the domain of g(X)<0, will produce the probability of failure.

According to [119], the probability of failure is the likelihood that the variables lay inside the limit state area:

$$P_f = \text{Prob}\{g(X) < 0\} = \int_{g(X)<0} \text{PDF}(x)\, dx \quad (4\text{-}1)$$

On the other hand, reliability is the complementary of P_f, thus

$$P_r = 1 - P_f \quad (4\text{-}2)$$

Finally, the generic limit state function is

g(X)=R(X)-S(X), where **S***: the Stress and* **R** *the Resistance* (4-3)

4.3 Reliability Assessment Methods

Reference is made to level III methods for their simplicity, accuracy and for providing reliable structural optimization solutions as well.

4.3.1 First and Second order approximation methods

All basic variables {X} are transformed to normal uncorrelated Gaussians {Y}:

$$Y_j = \frac{X_j - \mu_{xj}}{\sigma_{xj}} \quad (4\text{-}4)$$

Limit state functions are approximated around a selected point (Y*), by functions (linear or quadratic) of below form:

$$g'(Y) = g(Y^*) + A\,(Y - Y^*) + B\,(Y - Y^*)^2 \quad (4\text{-}5)$$

In case of quadratic functions as stated above, the method is called SORM (Second Order Reliability Method) whilst for linear functions it is a FORM (First Order Reliability Method)

First Order Reliability method, provides a substantial simplification of PDF, since curves of same probability become circles, offering an easier calculation of probability of failure.

4.3.2 Hazofer and Lind method

This method is also a characteristic FORM in which a first order function approximates the limit state function g(Y)=0.

The reliability index can be obtained, based on geometry and according to β calculations formula:

$$\beta = \frac{\mu_g}{\sigma_g} = \frac{\mu_R - \mu_\sigma}{\sqrt{\sigma_R^2 + \sigma_S^2}}, \text{ where:} \quad (4\text{-}6)$$

μ stands for mean and σ for standard deviation of S and R, whilst β is the inverse of variation coefficient of the limit state function g(R,S).

The corresponding probability of failure is derived as:

$P_f=\Phi(-\beta)$, where Φ is the cumulative normal distribution.

4.3.3 Monte Carlo simulation method

Monte Carlo Simulation (MCS), has been established as the principal random sampling method for obtaining random sets of numerical data. Initially founded by E. Fermi in 1930s, it was further investigated and nominated as MCS by Von Neumann.

The generation of random sets of uncertain variables is an invaluable tool when we approximate in probabilistic terms the outcome of a stochastic process. Especially in structural reliability, simulations are based on sampling sets and the outcome is the structure’s response.

Instead of the great variety of existing MCS methods , the main pattern of all MCS can be summarized as follows:

1. Definition of the input data domain
2. Use of a probability distribution for random generation of input data
3. Deterministic analysis of data
4. Output data aggregation

Upon random generation of input variables X_i drawn from respective distribution $f_{xi}(X)$, the Probability of failure is the probability of $g(X_i)<0$.

Using MCS for reliability analysis purposes, the indicator function I(x) should be introduced as follows:

$$I(X) = \begin{cases} 1 & \text{if } G(X) \leq 1 \\ 0 & \text{if } G(X) > 1 \end{cases} \quad (4\text{-}7)$$

The corresponding probability of success is expressed as:

$$P_E = \frac{1}{N} \sum_{i=1}^{N} I(X_i) \quad (4\text{-}8)$$

where the nominator represents the successful realizations and denominator N the number of samples.

In terms of computational time and cost, this method is very demanding especially in case of a large number of input variables or low probability of failure. It is evident, that detecting and calculating one per billion probability of failure entails a corresponding number of simulations which should consist of no less than one billion repetitions.

4.3.4 Application on fillet weld joints

For the purposes of this work, a reliability analysis concerning main geometrical parameters impact on fatigue life of fillet weld joints, based on Monte Carlo simulation method has been carried out.

This process has been applied for obtaining random sets of uncorrelated input variables, for further evaluation and analysis. Upon this, the reliability of a range of geometries under particular fatigue strength criteria has been calculated.

It should be underlined, that several studies [04,17,23,25,30,42,44,45,62,119] concerning probabilistic analysis of stiffened plates and other structural members of marine structures such as welded joints have been made, but few of them have outlined the importance and made considerations towards a meaningful geometrical optimization aiming at a reduction of the failure probability P_f.

According to [32], upon a theoretical fracture mechanics analysis of 42 specimens supported by relevant experiments, the scatter in constant amplitude fatigue life is dependent on the following factors, ranked as per their impact order:

1. Weld geometry variability (specific reference is made to weld toe radius)
2. Initial crack shape and size
3. Material parameters

Above sequence is indicative of the importance of geometry in reliability of welded joints. It is evident that the geometrical variability dominates over other mechanisms, in determination of the final fatigue life of fillet weld joints.

5 FILLET WELD JOINTS STRESS ANALYSIS

5.1 Finite Element Method

Computer Aided Engineering (CAE) especially during last two decades has been an invaluable tool for analysis of complex systems for avoiding hand and laborious calculations. Numerical resolution of such technological challenges and problems is possible due to huge development of software applications facilitating this process.

Computer Aided Design on the other hand incorporates mathematical models for design and is an additional tool to numerical analysis software that usually are both offered as CAD/CAE.

Finite Element analysis (FEA) is one of the domains of CAE whilst Finite Element Method (FEM) is a numerical/simulation technique established on variational methods for resolving boundary value problems.

FEM's expansion use in domains like fluid dynamics, aerodynamics, heat transfer, structural analysis and others goes back to '70s.

In structural analysis, FEM through model discretization and creation of small subdomains, commonly known as finite elements, reduces the initial and complicated mathematical problem, whose analytical solution is in many cases impossible, to the solution of a linear combination of basic functions.

The finite elements as figure 5-1 depicts, may have one, two or three dimensions, each element consisting of nodes defining its geometry and incorporating displacement factors.

On each node, a force or reaction is assumingly exerted. The unknown factors-degrees of freedom in this problem are the coefficients of above combination. On the other hand, degrees of freedom are a characteristic feature of elements and in structural analysis they are the nodal displacements. Finally, structural elements incorporate linear, plastic or elastoplastic behavior, relevant elasticity modulus and Poisson's ratio.

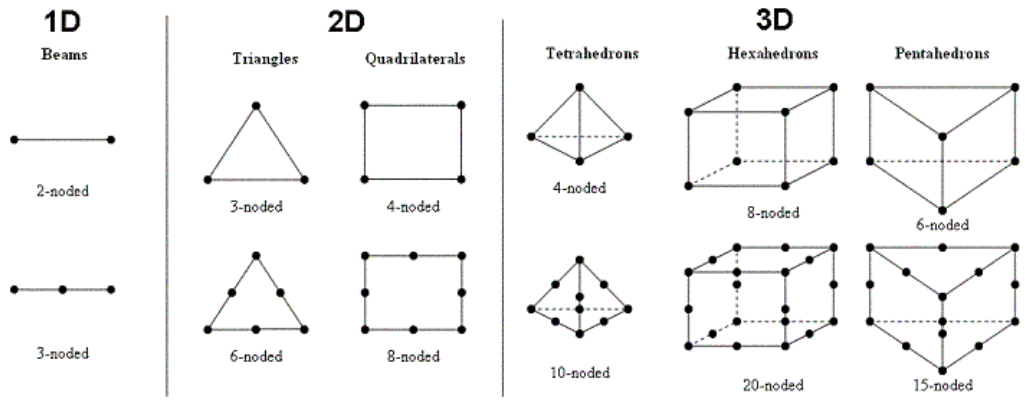

Figure 5-1 Different types of finite elements

The following basic principle applicable to structural analysis is that the virtual work of external forces (left part) should be in equilibrium to the one of internal forces (induced ones-right part):

$$\int_A uFdA + \int_V ufdV = \int_V \varepsilon\sigma dV \text{ ,where:} \quad (5\text{-}1)$$

F: *is the vector of external forces*

f: *is the vector of body forces* f=Ku *(**K**: Global stiffness matrix)*

A: *is the integration surface*

V: *is the integration volume*

u: *is the vector of displacement*

ε: *is the vector of strain, where:* ε=Bu *(**B:** strain-displacement matrix)* (5-2)

σ: *is the vector of stress, where* σ=Eε *(**E:** Elasticity matrix)* (5-3)

In Finite Element analysis, the following procedure is usually followed:

a) Unit system definition (if applicable)
b) Discretization of model into a grid of nodes and elements (meshing)
c) Definition of basic analysis parameters
d) Definition of the element type and parameters
e) Application of loads and constraints

f) Assembly of element stiffness matrices
g) Linear algebraic equations system solution
h) Calculation of results
i) Review and reporting of results

5.2 Model development

5.2.1 Fundamentals

Further to theoretical aspects of main geometric variables (Figure 5-2) impact on stress concentration of fillet weld and cruciform joints, analytically discussed in § 3.2.2, a two dimensional model was developed in Abaqus CAE V6.9 software.

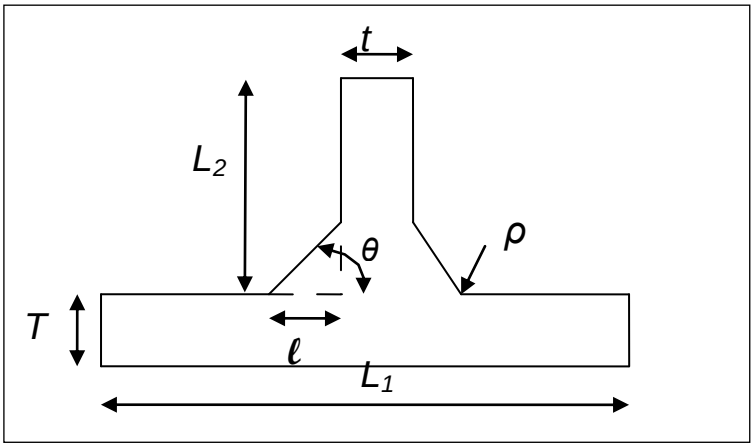

Figure 5-2 Fillet weld geometry

Since strains and deflections of a fillet weld joint section under planar pure tension or pure bending, lie on the same plane with stresses, a 2D planar shell part was considered satisfactory. To investigate the geometric dependence of Stress Concentration Factors, effects related to the presence of the weld were not taken into account. Instead, a homogeneous elastic steel with Young modulus $E=210 \times 10^9$ and Poisson ratio $\rho=0.3$ was assumed for the entire section. No elastic-plastic or plastic analysis was carried out.

Two loading cases are illustrated in Figure 5-3. Firstly, pure tension is formed by two uniformly distributed pressures at the left and right edges of the model,

whilst pure bending stress is formed by two sets of opposing shear concentrated forces.

The main geometric variables considered are the length of weld angle θ and weld root radius over thickness ρ/T (§5.3.1), the weld leg length over base plate thickness l/T (§5.3.2) and relative plate thickness (§5.3.3). The base plate thickness was assumed constant at 20mm and the vertical plate as 10mm. Besides, Table 5-1 demonstrates the selected values of the above variables.

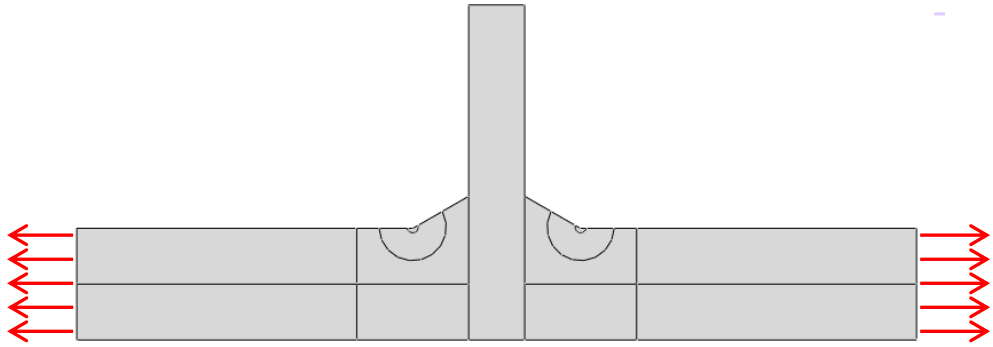

(a) Pure Tension

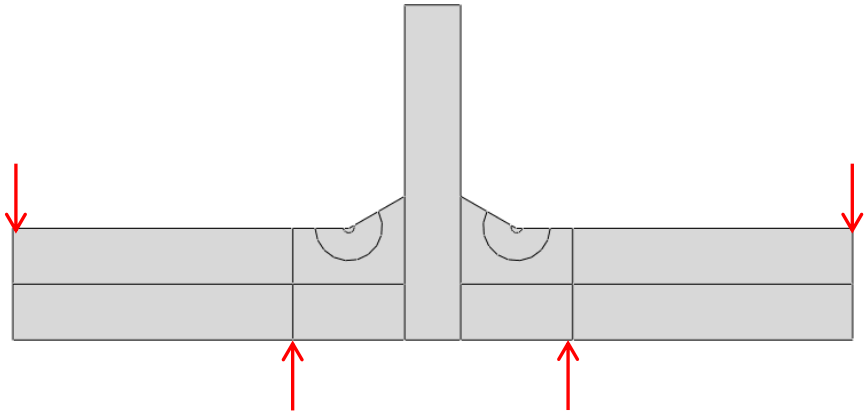

(b) Pure Bending

Figure 5-3 The two loading scenarios: Pure tension and pure bending

For the purposes of this LEFM analysis the stress ratio:

$$R = \frac{S_{min}}{S_{max}} \tag{5-4}$$

was assumed zero, thus the load is pulsating as depicted in Figure 5-4.

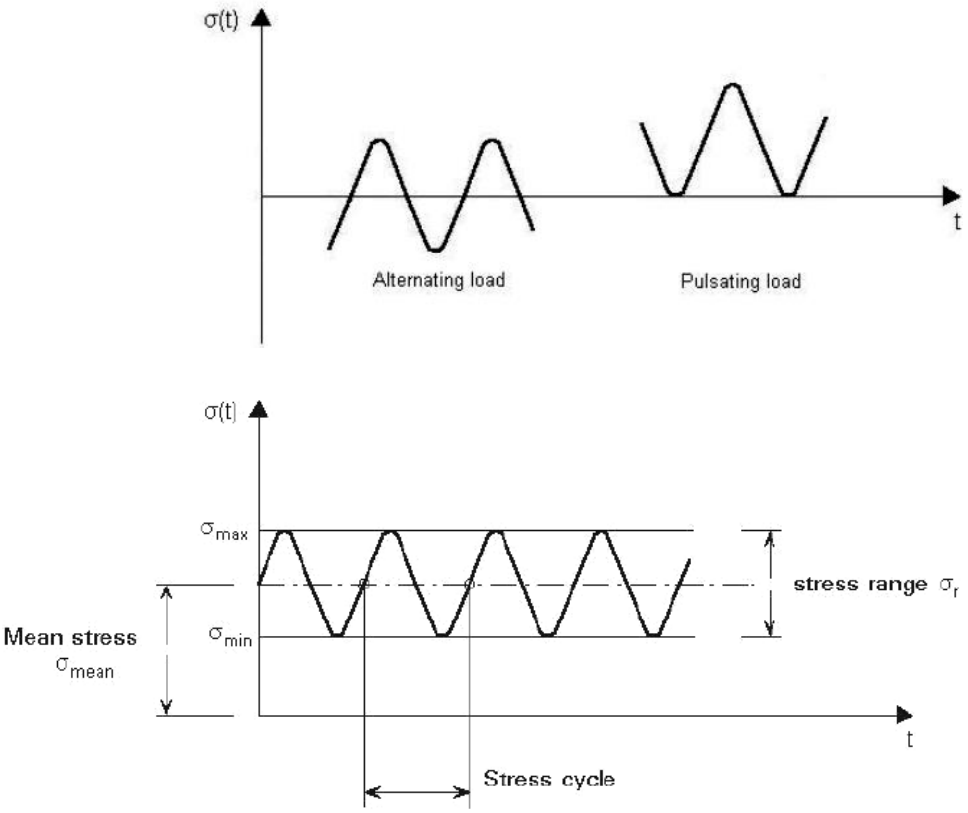

Figure 5-4 Fluctuating stress with constant stress amplitude and constant mean stress

Sixty models were developed in total, for which a mesh optimization process (see appendix B) and stress concentration factors convergence analysis (Figures 5-6, 5-7) were carried out. Doing this, a number of elements was set out as a threshold for over-refinement of the mesh at weld toes has a negative impact on the process, due to an increased number of distorted quadrilateral elements with acute angles less than 10 degrees. A substantial analysis of the above effect is presented in the following paragraph §5.2.3 The aforementioned threshold represents the optimum number of model elements, leading to a minimum acceptable deviation of calculated stress concentration factors opposed to several literature sources.

Geometrical variables		
ρ/T	**l/T**	**θ (deg)**
0.01	0.25	30
0.02	0.5	45
0.04	1	60
0.066	1.5	

Table 5-1 Values of geometrical parameters

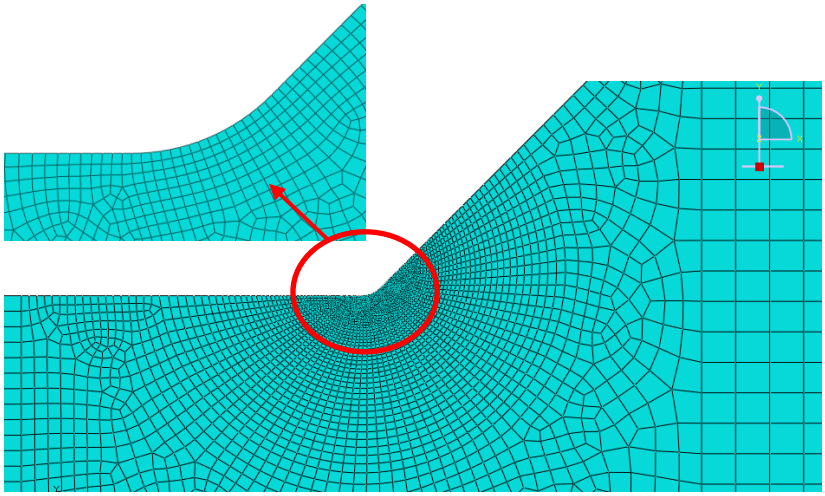

Figure 5-5 Detail of the weld toe mesh

5.2.2 Stress concentration factors calculations

The SCF values were derived by considering the maximum principal in-plane stresses derived from the FEA analysis over the nominal tension and bending stresses. The latter are calculated using the bending moment formula [1] for rectangular cross-sections:

$$\sigma_b = \frac{6 \cdot M_b}{h \cdot t^2}$$, where: (5-5)

σ_b : *bending stress*

M_b: *bending moment*

h: *loaded plate thickness (considered as 1mm)*

t: *loaded plate width*

Referring to the nominator of SCF, the maximum principal stresses for the current 2D elastic analysis apply to this analysis better, as they represent the maximum in-plane stresses in contrary to respective V.Mises stresses whose values are lower. According to Fricke (IIW recommendations, [37]), since plane strain restrictions are imposed to the plate, a biaxial stress state in the notch area is evident. Therefore, in notch stress analysis, the criteria of Table 2.1 (in ref [37]) apply and for proportional loading, the principal stresses should be used.

Finally, regarding the denominator, the nominal tension stress is equal to the imposed pressure on the right edge of the plate.

5.2.3 Convergence tests of SCF

For the purposes of subject 2D planar stress/strain analysis, relevant models have been shaped to obtain an outline (generic dimensioning) and upon selection of a proper partitioning pattern (see Appendix B) and assignment of meshing properties, the accurate discretization and number of introduced elements have been studied for their impact on Maximum Principal Stress at fillet weld toes.

An indicative convergence procedure is illustrated in Figures 5-6 and 5-7 and relevant SCF values versus number of elements of subject model have been collected in Table 5-2. Subject result concerning geometry #2 of Appendix C, Table C-1 with following particulars: $\rho/T=0.01$, $l/T=0.5$, $\theta=30^0$, T=20mm, t=10mm and 11286 number of elements has been duly validated from various sources [08, 89, 120] as per Figure 5-8 and Table 5-3 for tension.

From below trend of derived SCFs, the number of 10,000 elements is derived as an absolute minimum for obtaining an acceptable level of accuracy as per §5.2.4.

#ELEMENTS	SCF-TENSION	CPU TIME TENSION	SCF-BENDING	CPU TIME BENDING
452	1,941	0,5	2,052	0,5
673	2,072	0,7	2,216	0,6
1115	2,136	0,9	2,304	0,7
1651	2,104	0,9	2,268	0,8
3749	2,269	1,5	2,431	1,2
7082	2,585	2,1	2,768	1,8
8275	2,973	2,1	3,187	2,1
11286	**3,007**	**2,7**	**3,225**	**2,7**
23940	3,121	6,4	3,349	5,3

Table 5-2 SCF values emanating from model refinement

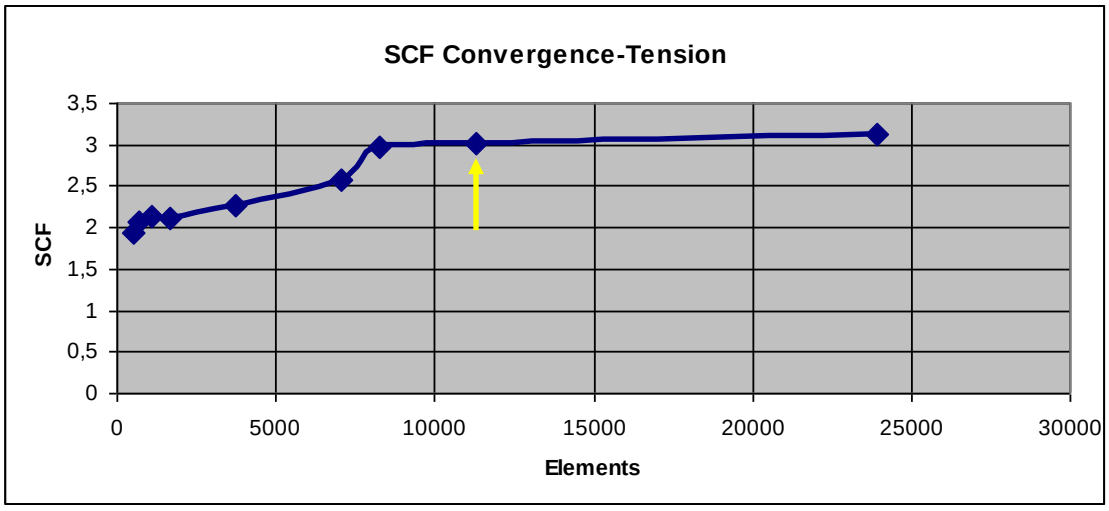

Figure 5-6 SCF convergence - tension

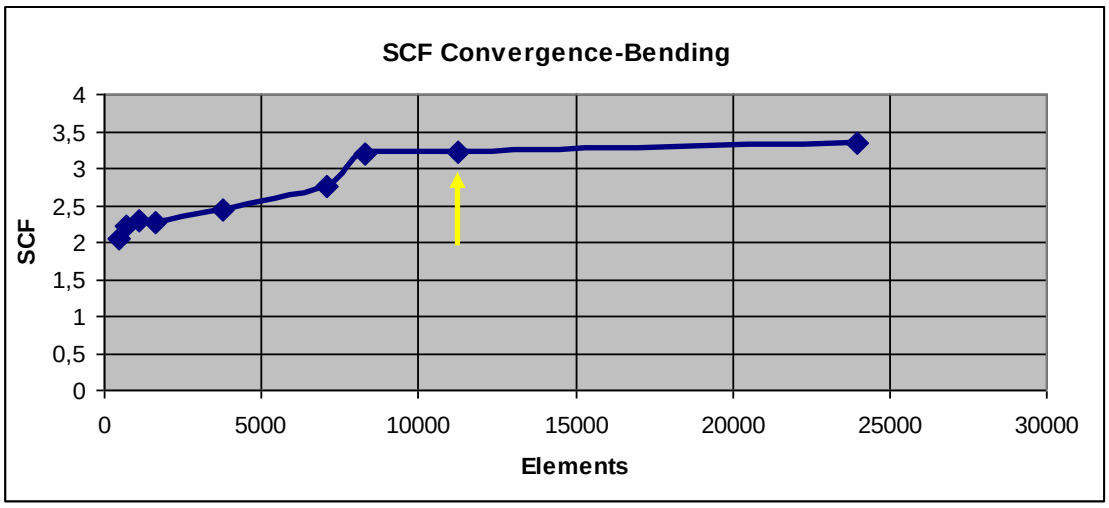

Figure 5-7 SCF convergence – bending

In case of pure tension, in our model of 11286 elements a SCF of 3,007 has been derived instead of 2,835 of Brennan's [08] simple equations (deviation 6,1%). Table 5.3 presents reference values from literature, pertinent to geometry l/T=0.525 and $\theta=30^0$.

On the other hand, in case of pure bending, subject model depicts a SCF of 3,225 against Brennan's 3,042 (deviation 5,7%).

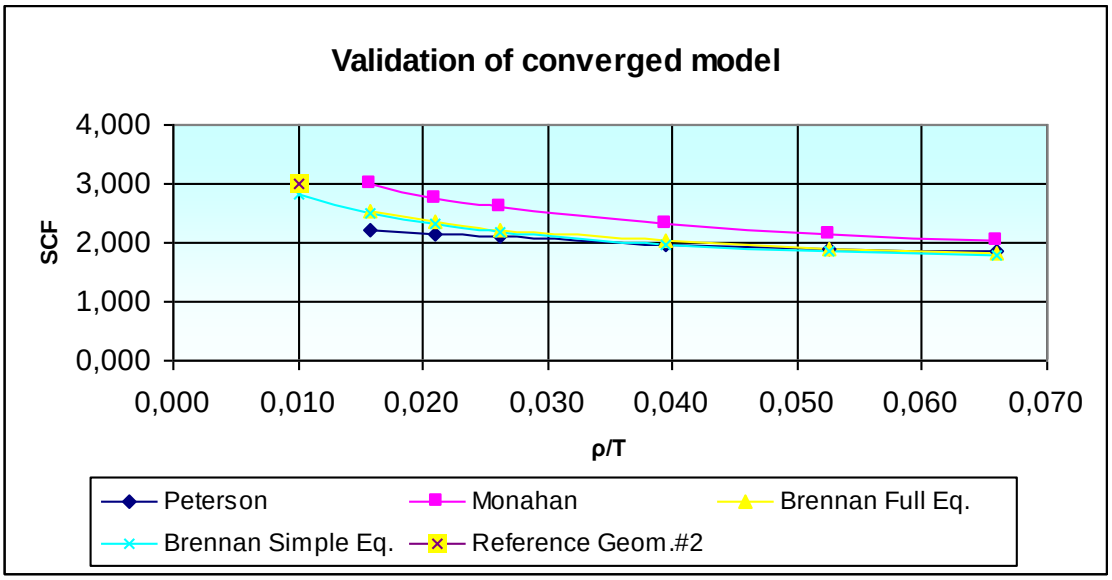

Figure 5-8 SCF validation of converged model– tension

ρ/T	Geometry #2	Brennan Simple Eq.	Brennan Full Eq.	Peterson	Monahan
0,010	3,007	2,835			
0,016		2,500	2,540	2,200	3,010
0,021		2,320	2,350	2,140	2,760
0,026		2,190	2,220	2,090	2,590
0,039		1,980	2,020	1,980	2,330
0,053		1,860	1,900	1,900	2,160
0,066		1,780	1,820	1,840	2,050

Table 5-3 Pure tension: SCF - comparison with published values

5.2.4 Simulations data validation

For further validation of our models, a number of different model SCF predictions have been compared with Brennan's respective SCF derived from

analytical parametric equations [08] and some indicative solutions of Peterson and Monahan. The results are presented accordingly in Table 5-4.

θ	ρ/T	l/T	t/T	SCF Tension	SCF Bending	Brennan Tension	Brennan Bending	Deviation Tension (%)	Deviation Bending (%)
30	0,066	1	0,5	1,960	2,085	1,913	2,107	2,38	1,06
30	0,066	1,5	0,5	1,999	2,125	1,966	2,153	1,65	1,30
45	0,066	1	0,5	2,110	2,382	1,988	2,237	5,76	6,08
45	0,066	1,5	0,5	2,123	2,391	2,064	2,354	2,79	1,54
60	0,066	1	0,5	2,138	2,480	2,013	2,294	5,87	7,52
60	0,066	1,5	0,5	2,130	2,508	2,126	2,510	0,21	0,07
						Peterson Tension	Monahan Tension	Peterson Deviation (%)	Monahan Deviation (%)
30	0,066	0,5	0,5	1,957		1,840	2,050	5,98	4,75
						Peterson Tension	Monahan Tension		
30	0,04	0,5	0,5	2,167		1,980	2,330	8,63	7,52

Table 5-4 SCF deviations from [08, 89, 120]

5.3 Diagrams and conclusions

The diagrams that follow, illustrate the geometric parameter effects on SCFs. It should be noted that the observed Maximum Principal Stresses both in tension and bending were located at the surface of the fillet weld profile at the weld toe area, as depicted in Figure A-3 of Appendix A.

Two sets of diagrams for tension and bending respectively are provided below, the former for weld leg to thickness ratio l/T=0.25 and the latter for l/T=0.5.

5.3.1 Weld angle and toe radius effects

It can be concluded that by gradually increasing θ or/and decreasing ρ, the SCFs are increased.

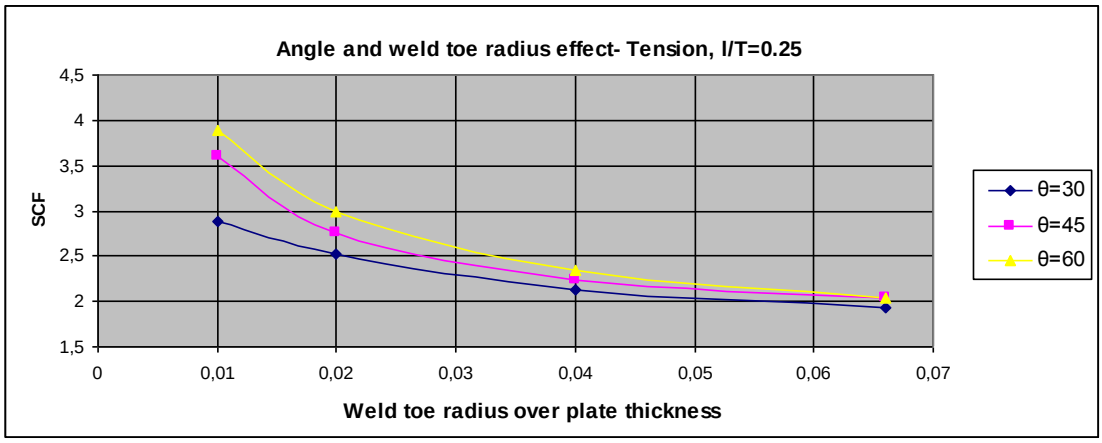

Figure 5-9 The angle and weld toe radius effect on SCF, l/T=0.25, Tension

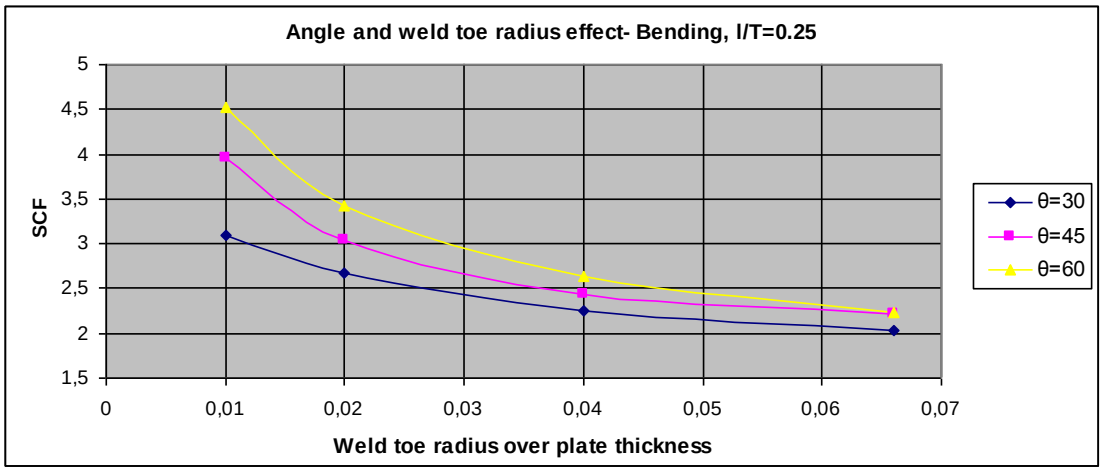

Figure 5-10 The angle and weld toe radius effect on SCF, l/T=0.25, Bending

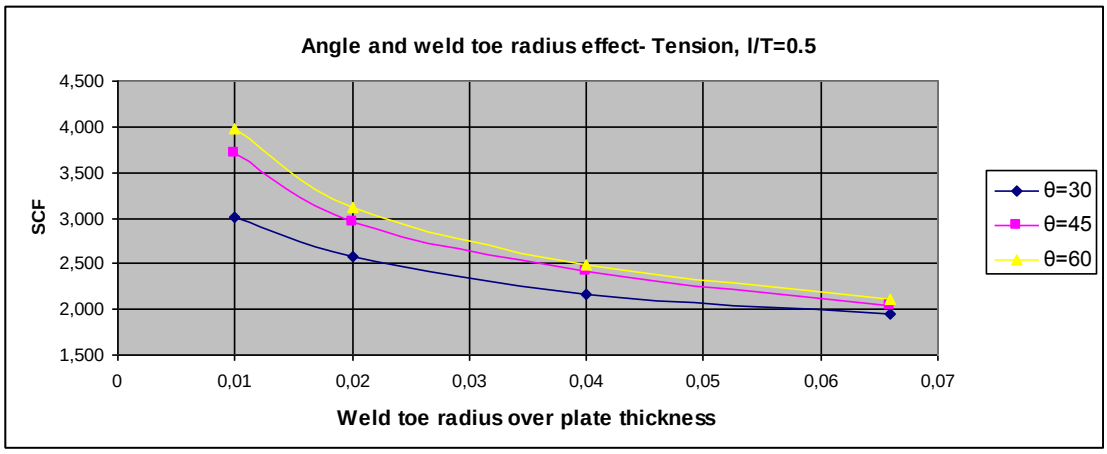

Figure 5-11 The angle and weld toe radius effect on SCF, l/T=0.5, Tension

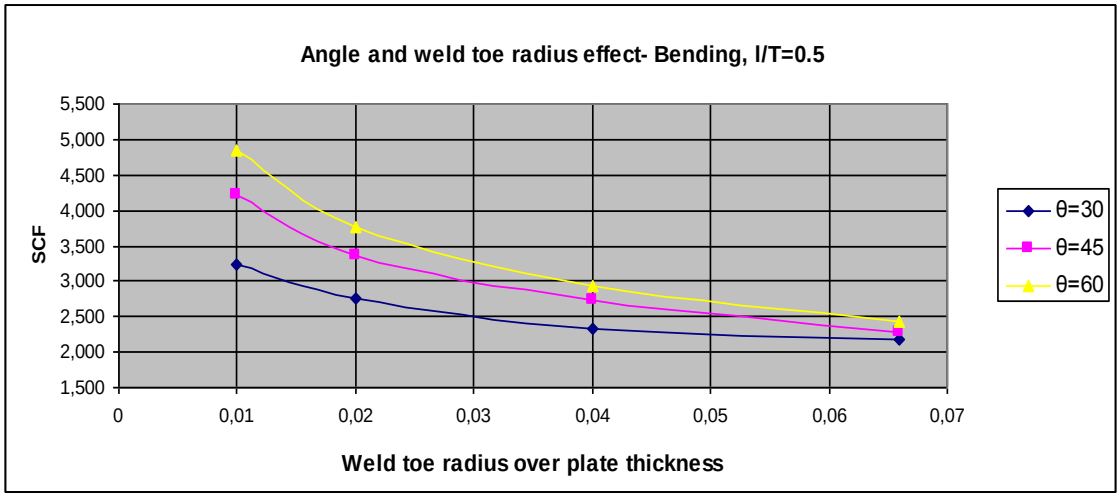

Figure 5-12 The angle and weld toe radius effect on SCF, l/T=0.5, Bending

5.3.2 The weld leg length effect

The following diagram illustrates the effect of leg length (l/T) on SCFs.

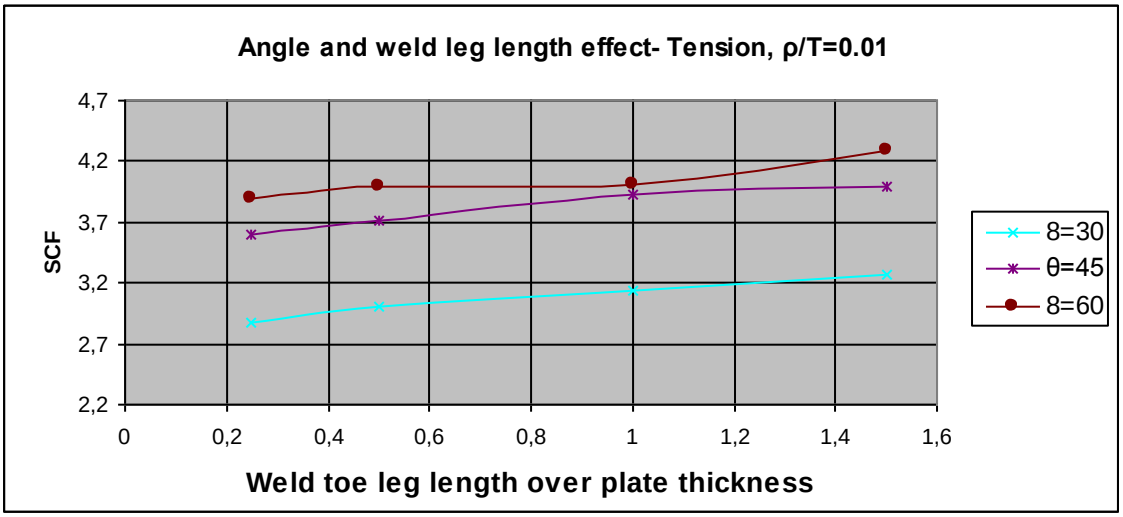

Figure 5-13 The leg length and weld angle effect on SCF, ρ/T=0.01, Tension

Despite minor fluctuations, an increase of SCF in all cases has been identified, when the leg length increases and this especially is observed at the lower ranges of respective ratios l/T (0.25 towards 0.5).

5.3.3 The relative plate thickness effect

The geometry ρ/T=0.066, θ=30^0, 45^0 and 60^0, l/T=0.5, T=20 is tested under five different attachment plate thicknesses, t=10mm, 13mm, 16mm, 18mm and

20mm and the results are presented in the following diagrams (Figures 5-14, 5-15). It is apparent that there is almost no dependence of the SCFs on the relative thickness t/T, since an eligible increase in SCF is observed when thickness is increased.

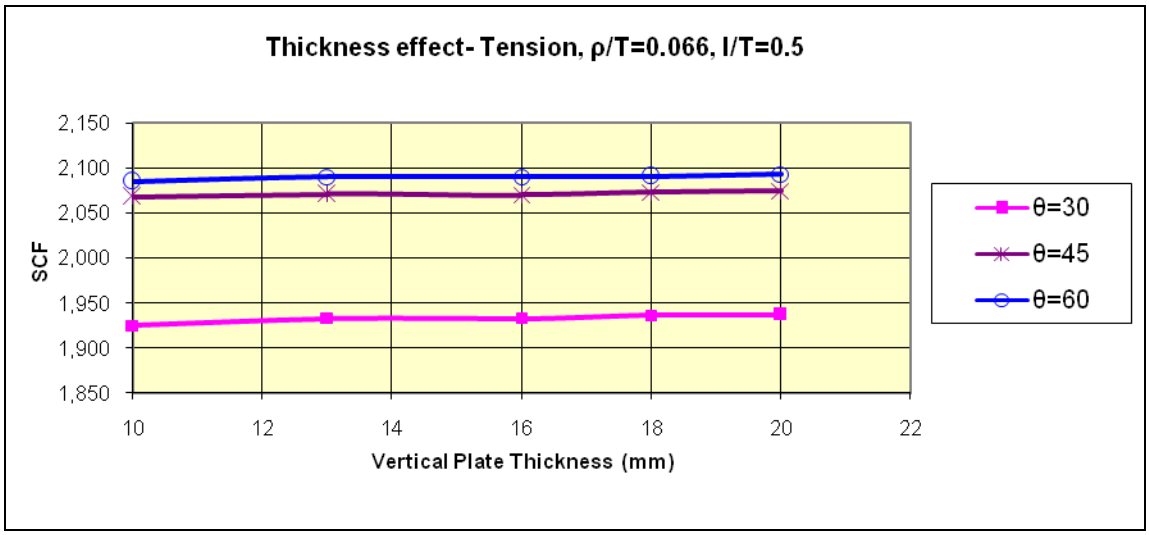

Figure 5-14 The relative thickness effect on SCF, Tension

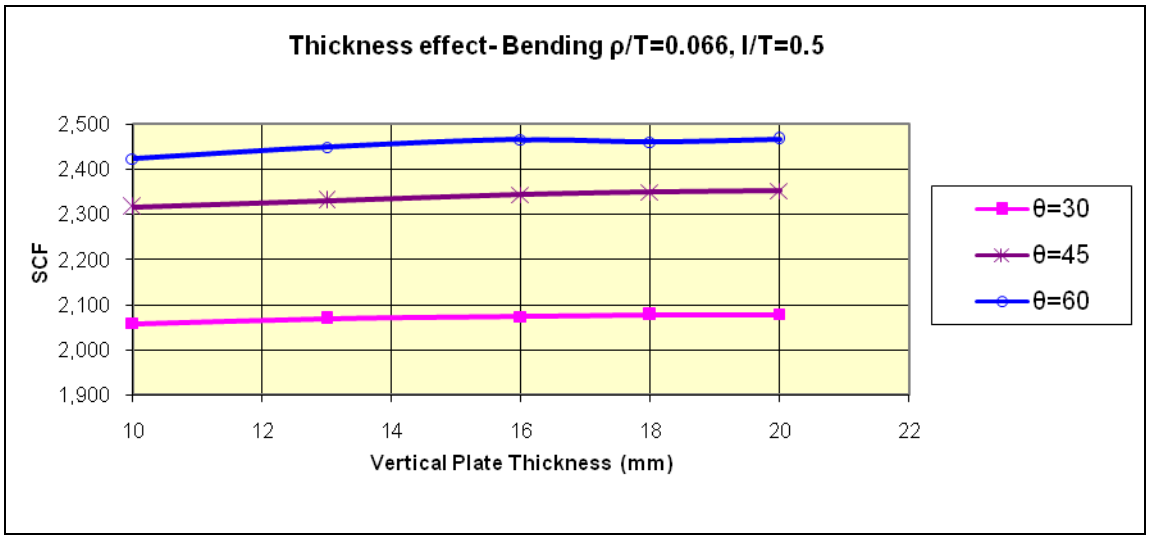

Figure 5-15 The relative thickness effect on SCF, Bending

5.3.4 Simulations and results

In Appendix C, a summarizing table with respective SCF values is provided. Meanwhile, Table 5-5 presents the minimum values of Concentration Factors for pure tension and bending respectively. The last row represents the calculated SCF values, based on Brennan's parametric equations [08]. An obvious deduction is that both minimum stress concentration factors are emanating from the same geometry.

$\theta=30^0$	$\rho/T=0.066$	$l/T=0.25$	Minimum SCF Tension	Minimum SCF Bending
Reference geometry #13 Table C-1			1,933	2,035
Calculation based on Brennan's SCF parametric equations [08]			1,723	1,895
Deviation (%)			10,874	6,894

Table 5-5 The optimal geometry

It is worth mentioning that the minimum angle and weld length values, along with the maximum weld root radius are strictly related to the optimal geometry. However, the minimum weld throat provided above, is not necessarily reversely related to the fatigue life since, according to Lee et al [66], a strong correlation between them could not be established.

Last but not least, we should underline that the minimum stress concentration factor in tension is lower than in bending. This applies to the majority of the results and is indicative of the sensitivity of SCF on applied loading mode and type. In pure bending, the maximum stress observed at the surface is reduced towards neutral axis hence the increased sensitivity to any surface geometrical discontinuities and notches than in pure tension, where a stress is uniformly exerted to the cross section.

5.4 Stress concentration factors mitigation

A number of actions towards mitigating the maximum surface stresses are provided:

1. Circular and U shaped repair profiling
2. The root slot effect
3. Model trees and the variable radius notch concepts

5.4.1 Circular and U shaped repair profiling

According to Rodriguez et al [99], by adopting a carefully shaped notch configuration in areas which contain flaws and cracks and by cutting out the material, it is possible that stress concentrations are mitigated and fatigue initiation life improved. The notch geometry can be either part circular or U-shaped. The parameters of a U-notch configuration are illustrated in Figure 5-16.

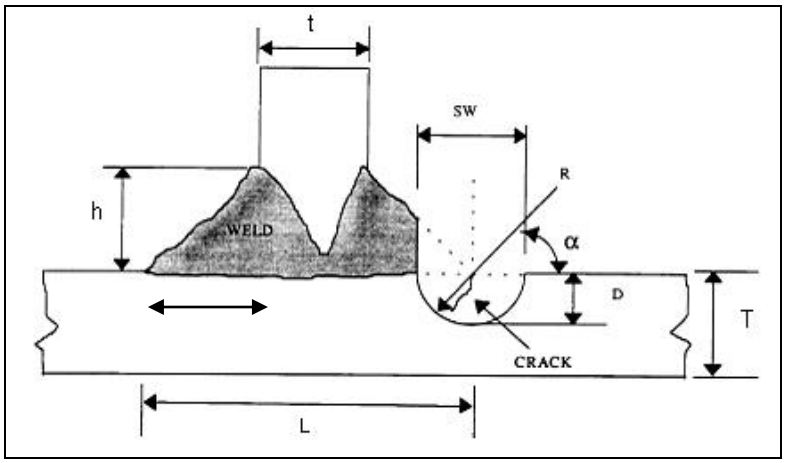

Figure 5-16 U-notch repair profile

In [88] and [98] is also referred that such treatments, like the weld toe grinding, can improve the fatigue life of a fillet weld joint. Pang estimates this as 53% and proposes a grounded weld toe radius of ρ=5mm instead of other lower values investigated. Doing this, the lowest SCF value of 1,948 is obtained.

In an attempt to verify the above statement, a part-circular notch with ρ=5mm, a=45^0, l=15mm and D=4mm (therefore ρ/D=1,25) was tested under pure tension. The outcome was confirmative, since a SCF of 1,953 was obtained.

At next stage, an analysis of various geometries which aims at providing comparative SCF values to the ones presented in § 5.3 and Appendix C for uncracked joints has been carried out. Through this analysis, the sensitivity of SCFs on R and D parameters (the most important ones according to [99]), is examined. The results are compared with those derived from [99] and are summarized in Table 5-6. The fillet weld geometry parameters are: l/T=0.5 for the models 1-9, l/T=0.75 for the models 10-18, a=45^0 and the considered minimum and maximum values of R were 1,34mm and 8mm respectively. Finally, the lowest SCF for tension and bending was obtained in case Nr.18, which involves the maximum R/D value, as illustrated in Figure 5-18.

	R/D	SCF tension	SCF tension by [48]	Deviation %	SCF bending	SCF bending by [48]	Deviation %
1	0.25	**6,782**	6,940	2,277	**4,615**	4,780	3,452
2	0.33	**5,245**	5,420	3,229	**3,969**	4,120	3,665
3	0.5	**4,010**	4,090	1,956	**3,409**	3,470	1,758
4	0.5	**5,555**	5,710	2,715	**3,721**	3,820	2,592
5	0.67	**4,258**	4,510	5,588	**3,164**	3,340	5,269
6	1	**3,279**	3,490	6,046	**2,731**	2,890	5,502
7	0.75	**4,853**	4,980	2,550	**3,223**	3,290	2,036
8	1	**3,755**	3,930	4,453	**2,760**	2,870	3,833
9	1.5	**2,898**	3,050	4,984	**2,383**	2,480	3,911
10	1	**4,405**	4,560	3,399	**2,891**	3,000	3,633
11	1.33	**3,445**	3,580	3,771	**2,503**	2,600	3,731
12	2	**2,670**	2,780	3,957	**2,170**	2,240	3,125
13	1.25	**4,212**	4,280	1,589	**2,757**	2,810	1,886
14	1.67	**3,266**	3,360	2,798	**2,363**	2,430	2,757
15	2.5	**2,534**	2,630	3,650	**2,047**	2,110	2,986
16	1.5	**4,015**	4,070	1,351	**2,621**	2,670	1,835
17	2	**3,112**	3,190	2,445	**2,252**	2,300	2,087
18	3	**2,422**	2,510	3,506	**1,950**	2,000	2,500

Table 5-6 Stress Concentration Factors in U-shaped and part-circular profiles

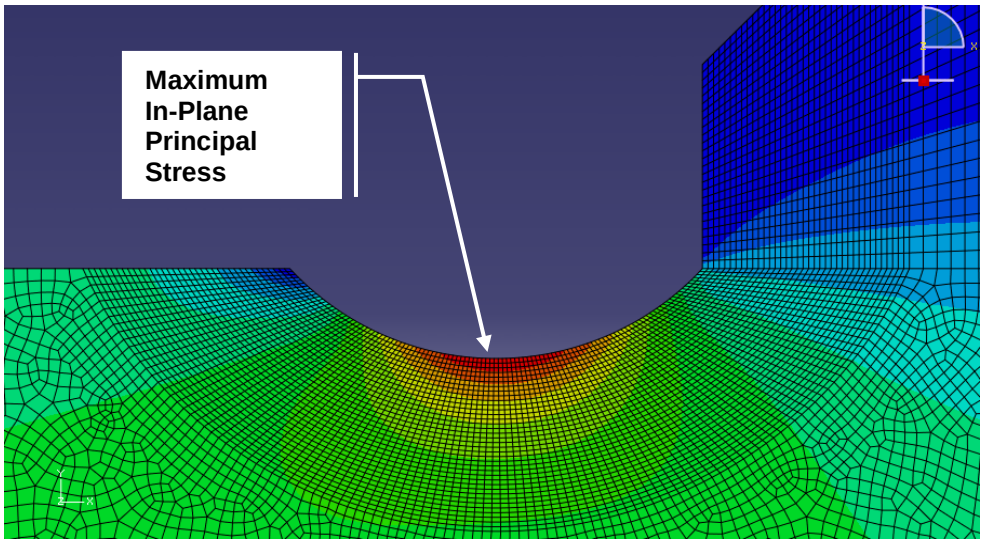

Figure 5-17 The optimum part-circular profile of table 5-6

Consequently, the maximum R values along with the minimum D values can minimize the stress concentration in a grounded weld toe (see Figure 4-19).

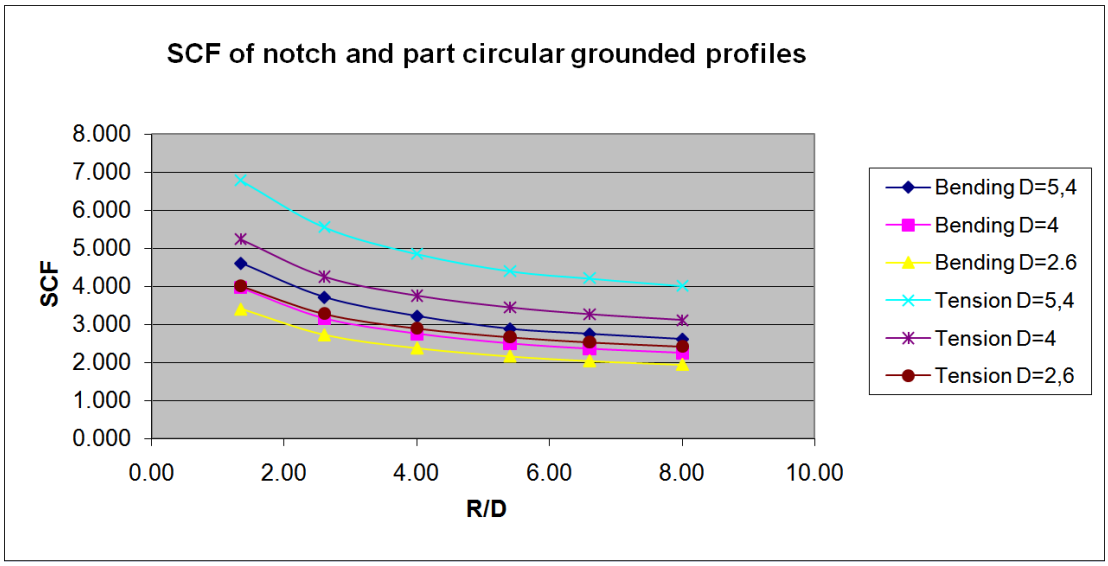

Figure 5-18 The SCF dependence on R and D values

5.4.2 The root slot effect

Where a non full penetration weld is present, the root slot can reduce significantly the surface stress concentration in the fillet weld toe area. The impact of the root gap on SCFs is illustrated in Figures 5-20 and 5-21 for a number of different geometries as those of Figure 5-19.

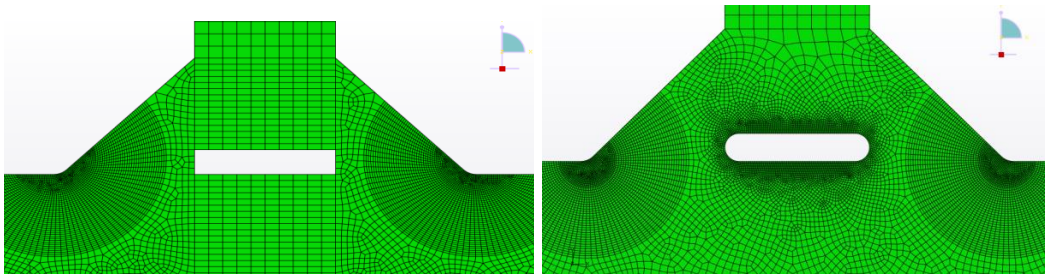

A. A rectangular slot **B. Slot with rounded edges**

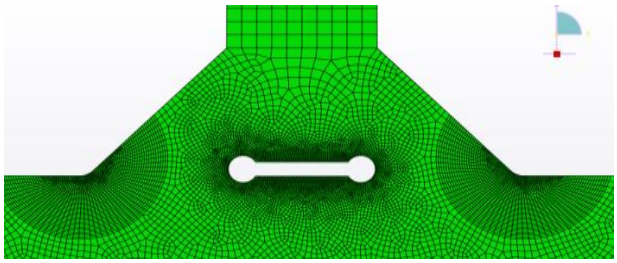

C. Slot with keyholes

Figure 5-19 Different root slot geometries

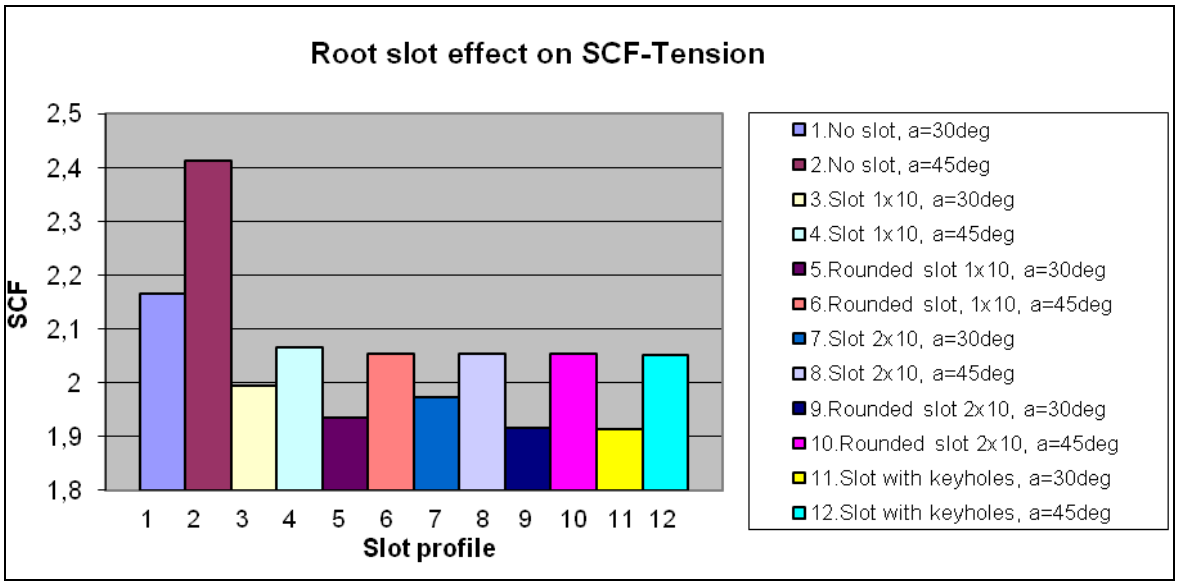

Figure 5-20 SCF dependence on weld root slot geometry - tension

From this analysis, it is evident that the root gap can reduce the stress concentration up to 14,9% in case of tension (profile 2 vs 12) and 15,6 % in case of bending (profile 2 vs 8).

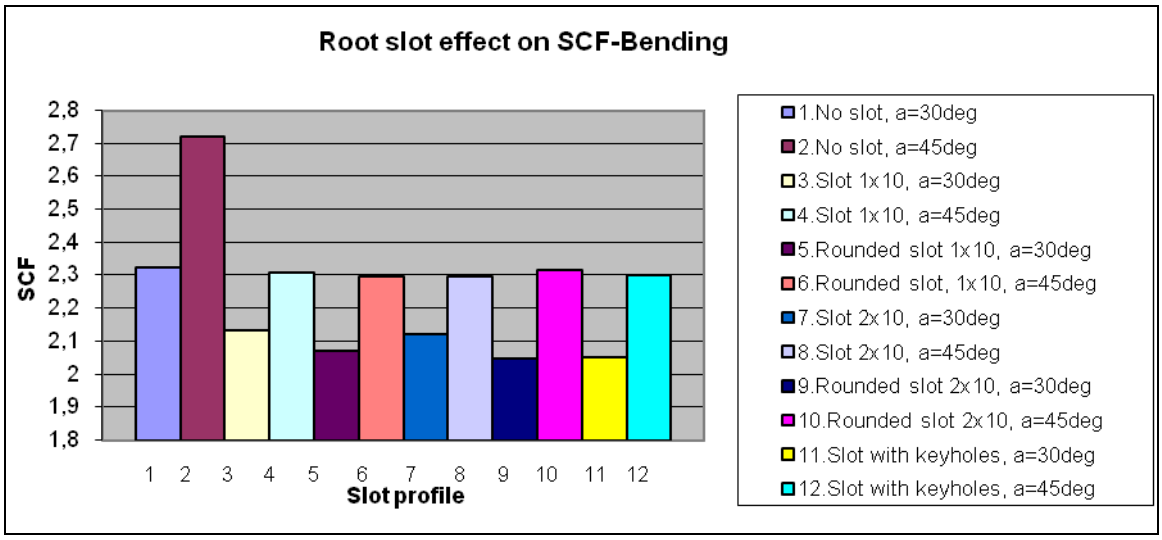

Figure 5-21 SCF dependence on weld root slot geometry - bending

5.4.3 The variable radius notch

In a recent work [110], Taylor developed a theory of redesigning the constant fillet notch radius ρ profile, by adopting a function ρ(r), where r is the distance from the one end of the fillet. Based on previous works of Mattheck [77] and others, he developed the Local Curvature Method for rapid calculations of the most efficient profiles and another method incorporating finite element analysis, making use of parametric inputs of ρ. Finally, the variable radius notch made possible to reduce the stress concentration factor of a 90^0 notch fillet down to 1,05.

As mentioned in §3.2.2, this method is applicable mostly on notched bodies and geometries of machines or structural components since the variable weld radius is not manageable and cost effective solution in the contemporary ship building practice. However, the potential benefits emerging from this application would be remarkable in a long term perspective. As Figure 4-22 depicts, in his analysis [77], Mattheck proved that adopting tree geometries we can successfully produce notches with significantly lower SCF values.

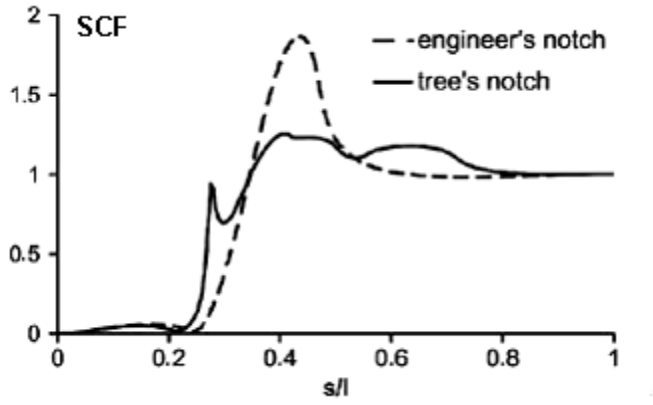

Figure 5-22 Mattheck: A tree buttress root vs a shoulder fillet

6 Fillet weld joints reliability assessment

6.1 Geometrical aspects

Based on performed structural analysis, a Linear Elastic Fracture Mechanics analysis has been carried out to estimate the fatigue life of 9 selected geometries, demonstrated in Table 6-1.

Afterwards, a reliability analysis will follow, to examine the variability of fatigue life predictions and our confidence on certain fillet weld configurations under stochastic fluctuations of their geometry.

Figure 6-1, illustrates the weld root of geometries 3 and 4 while in Figure 6-2, the model sketch of geometry Nr.2 is presented. Respective Stress Concentration Factors are provided in Table 6-2.

GEOMETRY	1	2	3	4	5	6	7	8	9
Length overall (mm)	150	150	150	150	150	150	150	150	150
Full penetration weld length L (mm)	30	30	20	20	30	20	30	30	30
Base plate thickness (mm)	20	20	20	20	20	20	20	20	20
Attached plate thickness (mm)	10	10	10	10	10	10	10	10	10
Fillet weld angle (deg)	30	30	30	30	45	45	45	60	60
Weld radius on attachment side (mm)	1	1,32	1,32	1,32	1	1	1	1	1
Weld toe radius (mm)	1	1,32	1,32	1	1	1,32	1,32	1	1,32
Lack of penetration	-	-	√	√	-	-	-	-	-

Table 6-1 Values of geometrical parameters

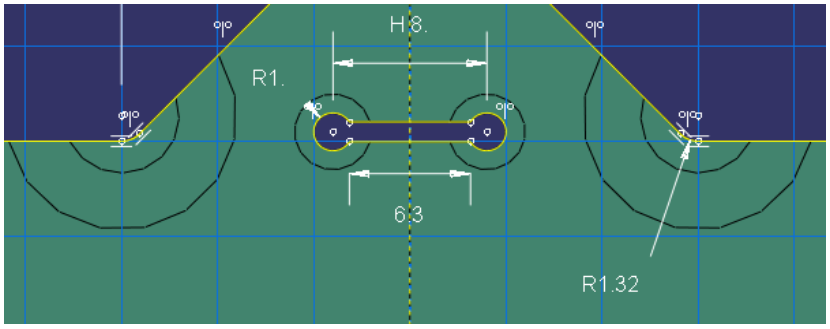

Figure 6-1 Detail of weld root slot with circular edges

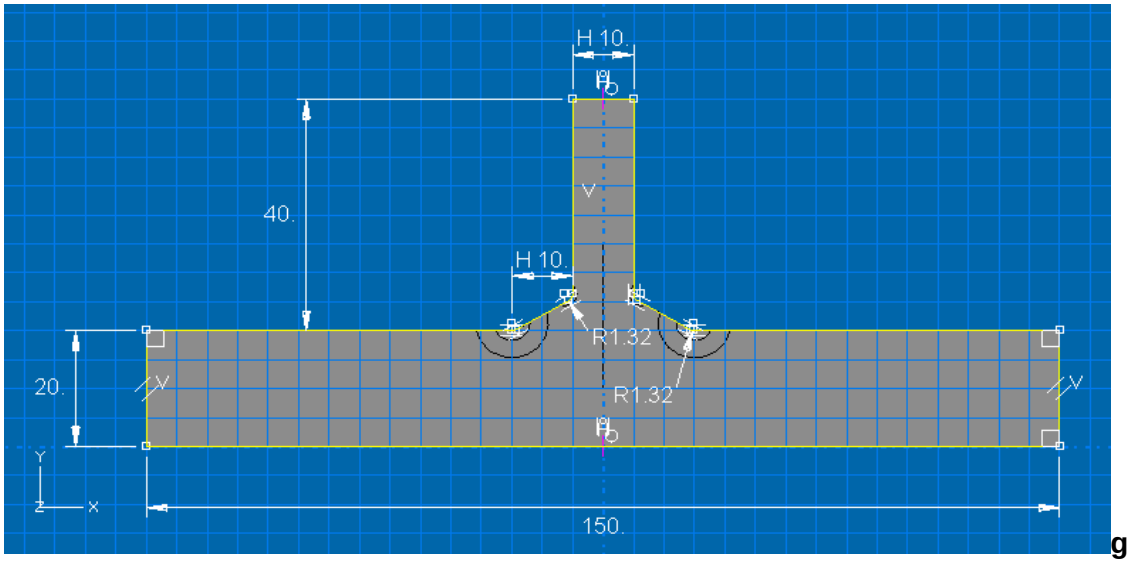

g

Figure 6-2 Dimensioning of model Nr.2

GEOMETRY	SCF Tension	SCFBending
1	2.031	2.174
2	*1.953*	*2.086*
3	1.744	2.020
4	1.787	2.035
5	2.231	2.509
6	2.002	2.165
7	2.080	*2.329*
8	*2.248*	*2.629*
9	2.143	2.494

Table 6-2 SCFs of considered geometries of Table 6-1

6.2 SIF calculations

Crack Aspect Ratios computed by Parametric Equations of Kawahara & Kurihara, Shang-Xian and Bell-Vosikovsky have been incorporated in present LEFM analysis. Along with relevant Brennan's [06] parametric equations for SIF predictions, they have been integrated in a MATLAB code enabling correction factor Y and respective stress cycle calculations each time for a specific

geometry as per Table D-1 of Appendix D. Subject Stress Intensity Factors for surface cracks emanating from weld toe flaws or defects, account for the deepest crack point (crack tip). For the purposes of Y function calculations, respective Fracture Mechanics parameters of Table 6-3 have been considered.

Upon analysis of geometrical impacts on fatigue life, a further integration of the initial MATLAB code to account for a large number of stochastically derived geometries was made, enabling the reliability analysis of various fillet welds under several thousands of stress cycles.

FRACTURE MECHANICS	
Paris exponent (m)	3
Paris coefficient	5,36E-12
Initial crack aspect ratio in bending	1
Initial crack aspect ratio in tension	0,6
Initial flaw depth (mm)	0,5
Final flaw depth tension/ bending (mm)	16/10

Table 6-3 Fracture mechanics parameters

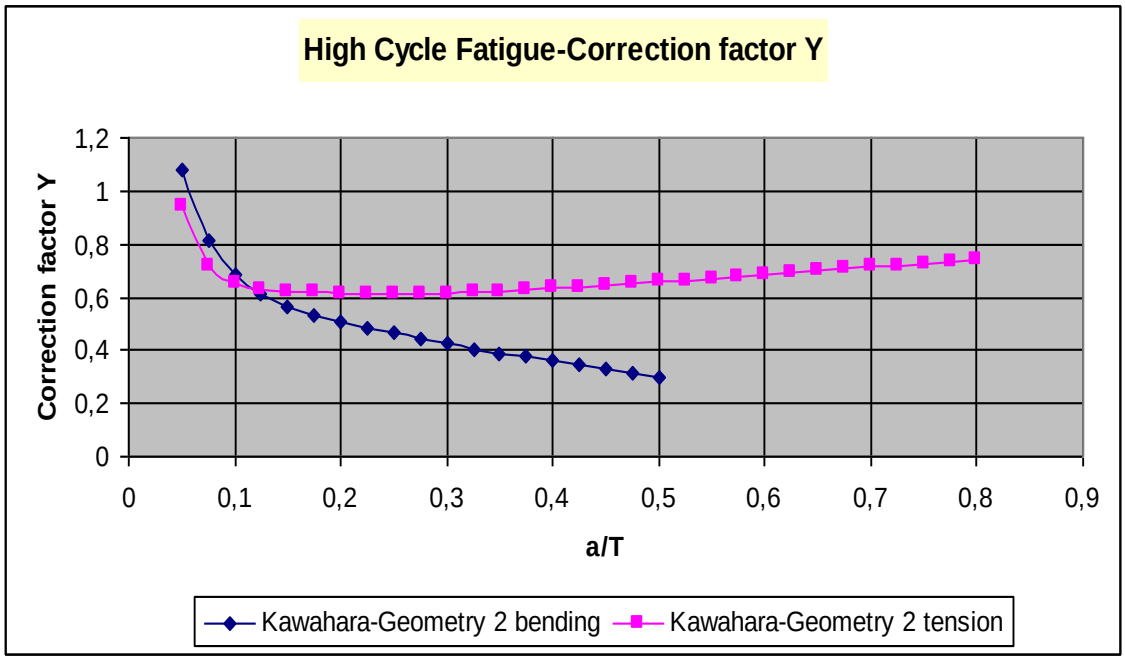

Figure 6-3 Y factors in High cycle fatigue

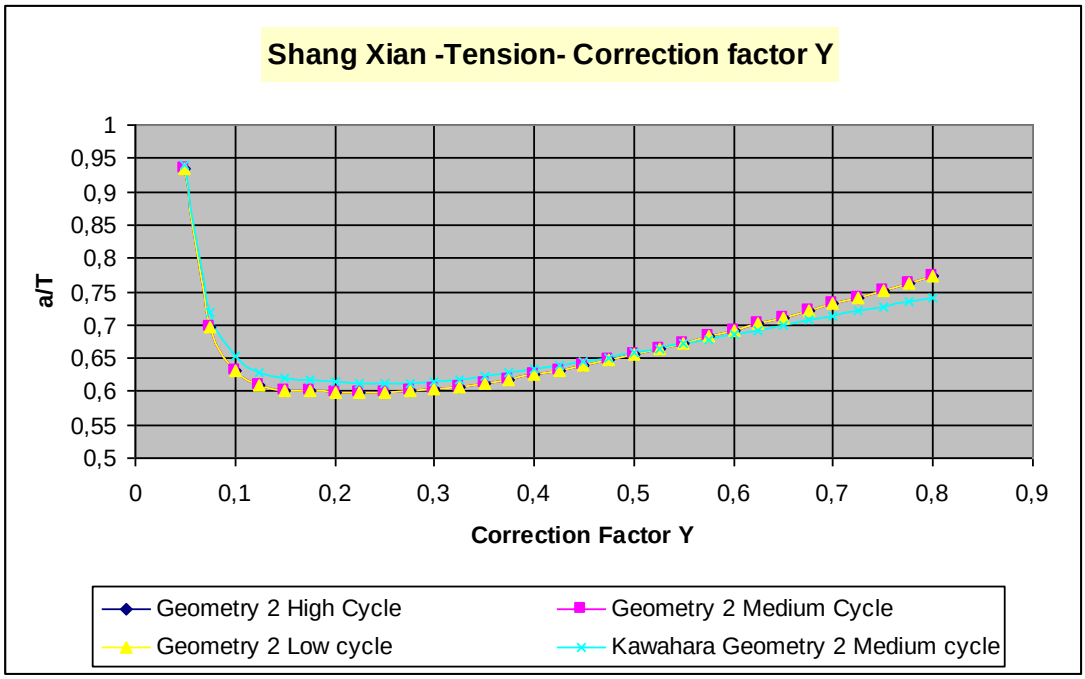

Figure 6-4 Y factors in Tension

6.3 Fatigue life predictions

For the considered weld joint geometries of Table 6-1, a number of different nominal stresses were inserted in the Finite Element Model according to Table 6-4. The Maximum Principal Stresses in all models have been detected at fillet weld toes.

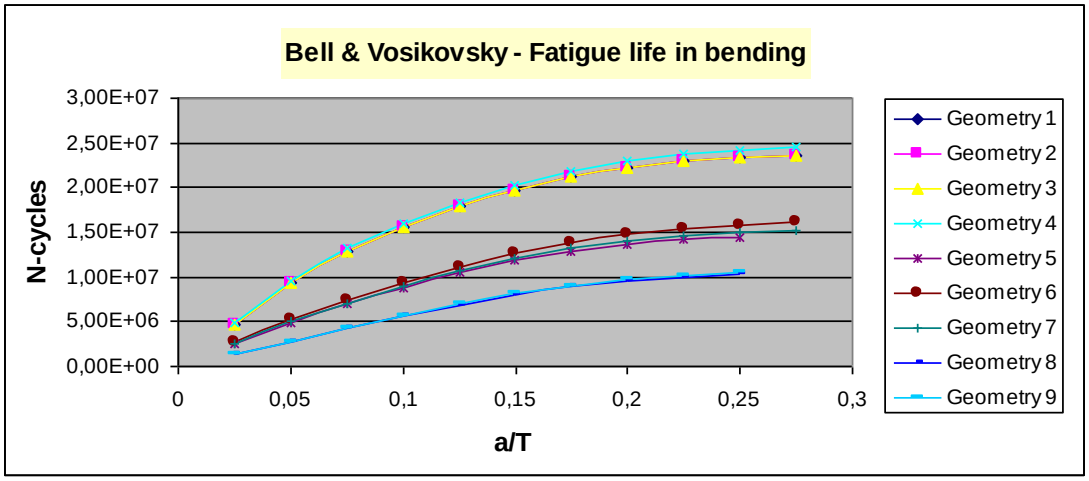

Figure 6-5 Fatigue life – high cycle bending

Figures 6-5 and 6-6 demonstrate fatigue life in cycles N over the crack depth a/T for bending and tension respectively.

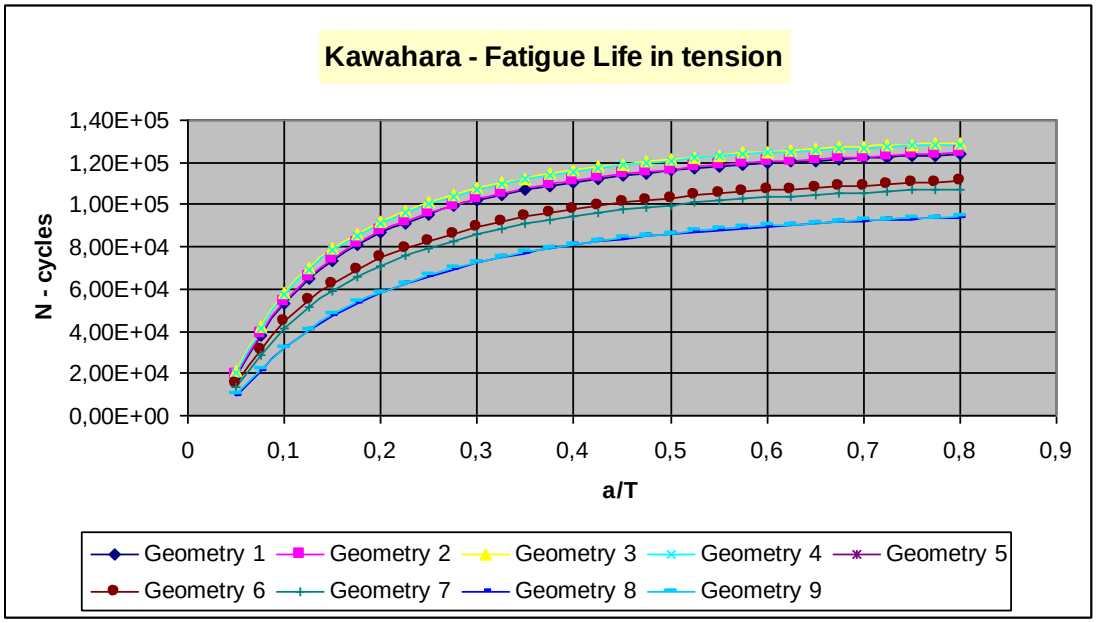

Figure 6-6 Fatigue life – low cycle tension

Bell & Vosikovsky's crack propagation in vertical direction seems to be lower than Kawahara's predictions since cracks obtained maximum aspect ratios of a/c<0.2 at about 30% of plate thickness.

	Max value Bending		Max value Tension	
Nominal Stress	***Bell & Vosikovsky Geometry 3***	***Kawahara & Kurihara Geometry 3***	***Kawahara & Kurihara Geometry 3***	***Shang Xian Geometry 3***
25 Mpa	2,48E+07	3,44E+07	1,42E+07	1,52E+07
50Mpa	2,25E+06	4,30E+06	1,78E+06	1,90E+06
120Mpa	7,98E+04	3,11E+05	1,29E+05	1,37E+05
	Min value Bending		**Min value Tension**	
Nominal Stress	***Bell & Vosikovsky Geometry 8***	***Kawahara & Kurihara Geometry 9***	***Kawahara & Kurihara Geometry 8***	***Shang Xian Geometry 8***
25 Mpa	1,03E+07	2,11E+07	1,03E+07	1,10E+07
50Mpa	8,18E+05	2,63E+06	1,29E+06	1,37E+06
120Mpa	2,57E+04	1,91E+05	9,35E+04	9,94E+04

Table 6-4 Minimum and maximum values of fatigue life

In Appendix D, Table D-1 concisely demonstrates fatigue life calculations for each of the 9 fillet weld joint geometries in high, low and medium cycle fatigue

analyses. From the results, it is evident that the optimal geometry of lowest SCF, maximizing the fatigue life both in tension and bending is No. 3. Even non-full penetration weld, the weld root is substantially small and rounded at the edges, the maximum stress concentration is located at the weld toe, therefore the weld toe is the most prone area to crack initiations.

From a comparative analysis of above results (see table 6-4) the following conclusions can be drawn:

- In medium cycle bending, the maximum fatigue life benefit according to Kawahara is 63,09%. Corresponding analysis of Bell & Vosikovsky depicts a higher benefit of 175% that is mostly due to much more conservative predictions in comparison to Kawahara whose analysis concerns semi-elliptical surface cracks at finite plates without notch effects. Above benefits have been observed between geometries #3 (SCF=2,02) and #8 (Bell & Vosikovsky) or #9 Kawahara (SCF=2,629 and 2,494 respectively). The maximum corresponding stress concentration reduction is 30,1%. Relevant benefits in low and high cycle bending are 63,095% and 63,096 % respectively.

- Comparatively to the benefits in bending benefits in case of tension are substantially lower. Relevant observations depict 37,83% benefit in high cycle, 37,92% benefit in medium and 37,93% in low cycle fatigue. In tension, the corresponding stress concentration reduction is 28,9%.

- The effect of weld angle is evident when comparing geometries 1 (30deg) 5 (45deg) and 8 (60deg) whilst keeping constant the other parameters. In high cycle fatigue, relevant reduction of fatigue life varies from geometry to geometry: Between 1 to 5 we read 24,4% whilst between 5 and 8 it is 17,3% due to a SCF mitigation of 15,4 and 4,8% respectively.

- Regarding weld toe radius, a comparison between geometries 1 (ρ=1,0mm) and 2 (ρ=1.32mm) depicts a maximum fatigue life improvement of 5% in case of medium cycle bending. Respective SCF mitigation observed is 4,05%.

- As far as weld toe leg length effect is concerned, a comparison between geometries 6 and 7 depicts a stress concentration factor increase of 7% due to a rise of 50% in leg length. Respective fatigue life is improved by 37% in high cycle fatigue life.

- The effect of SCF reduction over the number of fatigue life cycles is illustrated in figure 6-7. In high cycle fatigue, the nominal stress of 25MPa applies to all geometries both in tension and bending and respective correlation between Stress Concentration Factors and Fatigue Life Estimations is presented accordingly.

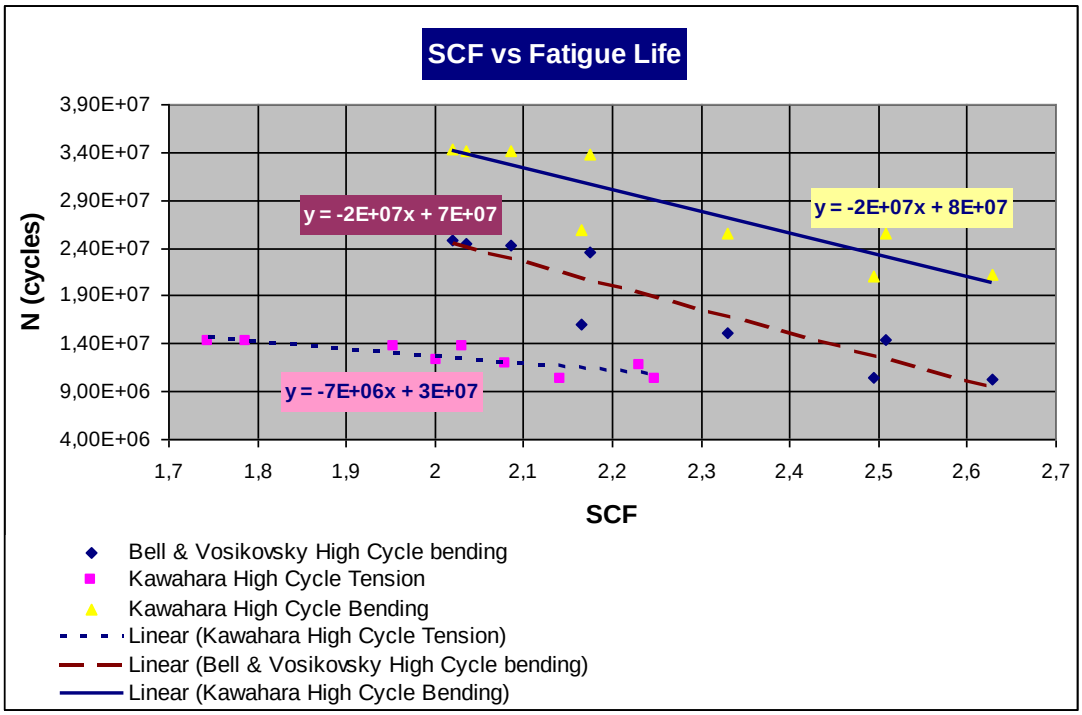

Figure 6-7 SCF effect on fatigue life

6.4 Reliability analysis

For the purposes of the present analysis, stochastic geometrical parameters (angle, weld toe radius and length) have been checked for their impact on total fatigue life.

In case of Tension, an analysis in medium cycle fatigue has been carried out incorporating all geometries 1-9 and considering a threshold of $1{,}4 \times 10^6$ cycles.

In all geometries, the following mean values and standard deviations were considered:

	Mean value	Standard deviation
θ	30	5
(deg)	45	5
	60	5
ρ/T	0.05	3
	0.066	3
l/T	1	1
	1.,5	1

Table 6-5 Mean values and standard deviations

A representative analysis of 10,000 random combinations of above stochastic input variables for a specific geometry under the nominal stress of 50MPa provides the demonstrated in Table 6-6 values of reliability and inverse cumulative distribution function accordingly.

RELIABILITY: Medium Cycle Tension				
Geometry	**B**	**P_f**	**Rel**	**N_{95}**
1	2,5364	0,0056	0,9944	2,312E+06
2	2,6437	0,0041	0,9959	2,321E+06
3	2,9112	0,0018	0,9982	2,435E+06
4	2,7944	0,0026	0,9974	2,445E+06
5	1,1636	0,1223	0,8777	1,962E+06
6	1,4502	0,0735	0,9265	2,044E+06
7	1,2092	0,1133	0,8867	1,972E+06
8	-0,30969	0,6216	0,3784	1,696E+06
9	-0,29709	0,6168	0,3832	1,694E+06

Table 6-6 Combined effect of all variables

Above table provides for all nine geometries, the inverse normal cumulative distribution function of P_f, the probability of failure P_f, the Reliability and Maximum value of fatigue life over the 95% of the total sample. An observation would be that under same failure criteria, the geometry #3 is considered the strongest one whilst #8 is the less reliable.

In order to demonstrate the impact of each variable separately from others, an analysis based on failure less than $1{,}8 \times 10^6$ cycles has been carried out and relevant data have been collected in Table 6-7. Figures 6-8, 6-9 and 6-10 represent the total fatigue life N distributions of considered configurations.

Sensitivity analysis of Geometry #2				
Case	**B**	**P_f**	**Rel**	**N_{95}**
All effects	-0,01003	0,504	0,496	2,265E+06
Angle effect	0,047644	0,481	0,519	2,299E+06
+10%	-0,19422	0,577	0,423	2,253E+06
+20%	-0,56217	0,713	0,287	2,150E+06
Weld toe effect	1,2536	0,105	0,895	2,546E+06
+10%	1,1552	0,124	0,876	2,905E+06
+20%	1,3346	0,091	0,909	2,934E+06
Weld leg length effect	0,82038	0,204	0,794	1,917E+06
+10%	0,26631	0,395	0,605	1,889E+06
+20%	-0,19422	0,577	0,423	1,857E+06

Table 6-7 Effect of each variable in medium cycle tension

Application of a uniform tensile stress over the same geometry with variations to a specific characteristic each time, provides an indication of its weight and impact on fatigue life. It should be underlined that under the uniformly applied failure criterion of $1{,}8 \times 10^6$ cycles our intention is only to demonstrate this relation of parameters to fatigue life.

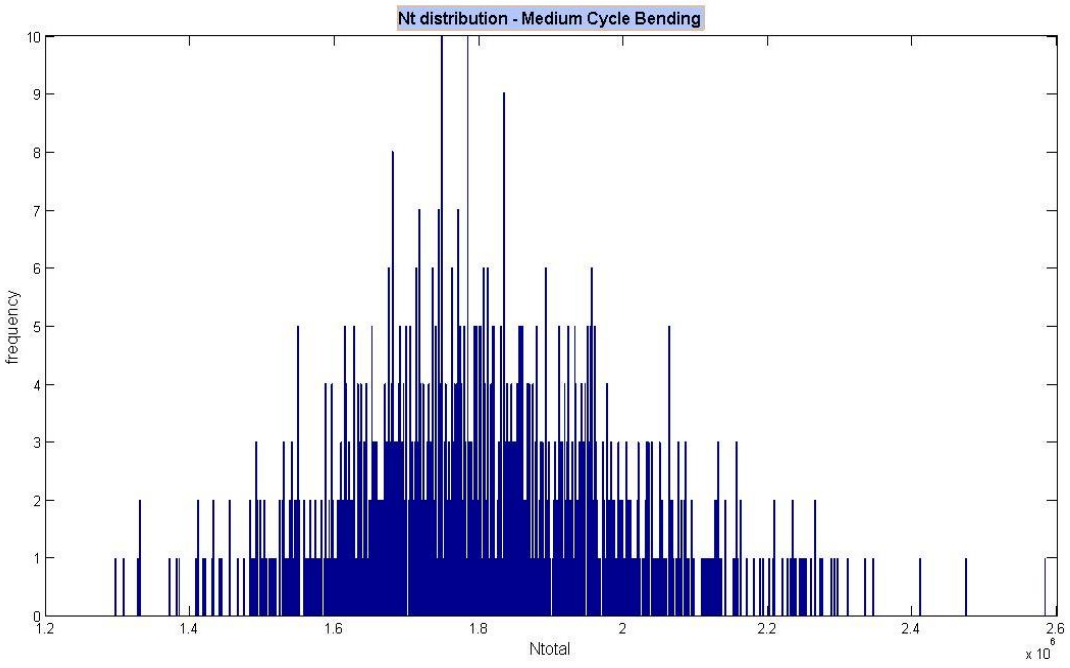

Figure 6-8 Distribution of N_t with stochastic parameters (θ, ρ, l)

It is evident so far, that an increase of weld angle by 10% may have an impact on fillet weld reliability of 22,7%. On the other hand, an increase of weld leg by 10% may decrease the reliability by 31,2%. The weld toe, offering the maximum value of $N_{95,}$ is less sensitive as regards reliability, although it provides the higher reliability values. This is mainly due to its lower standard deviation in comparison to angle but also due to its counter-impact in comparison to other geometrical parameters whose increase is related with reduction of fatigue life.

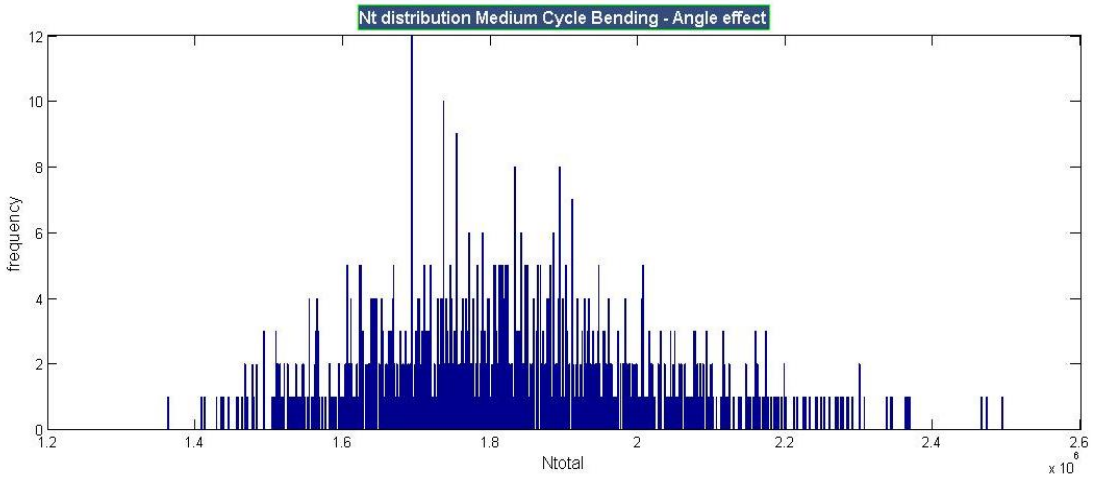

Figure 6-9 Distribution of N_t with stochastic angle θ

In case of bending, an analysis involving all 9 geometries of Table 6-1 with standard deviation 5 for angle, 2 for toe radius and 1 for leg length is provided in Table 6-8. Each model has been tested under three stress levels (25MPa, 50MPa, 120MPa) accounting for high, medium and low cycle fatigue and 10.000 samples from each geometry have been produced and tested against fatigue life and reliability. Respective threshold level for low cycle fatigue was set at $2.89x10^4$ cycles, for medium cycle at $9.65x10^5$ cycles and for high cycle at 10^7 cycles.

The corresponding reliability of geometry #1 has been regulated to equivalent levels of reliability for safer comparison of reliability fluctuations.

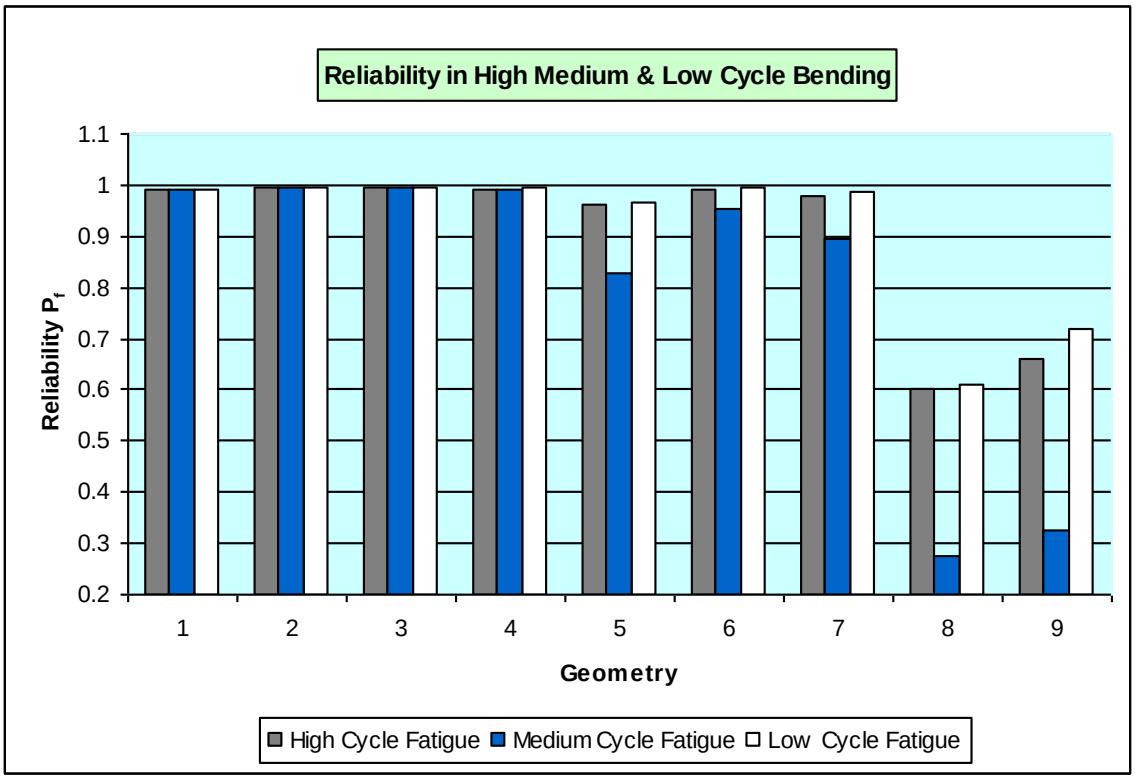

Figure 6-10 Reliability in bending stress

RELIABILITY: High Cycle Bending				
Geometry	**B**	**P_f**	**Rel**	**N_{95}**
1	2.3656	0.009	0.991	1.54E+08
2	2.6437	0.0041	0.9959	6.90E+07
3	2.6783	0.0037	0.9963	7.42E+07
4	2.3954	0.0083	0.9927	2.45E+08
5	1.7829	0.0373	0.9627	5.69E+07
6	2.3999	0.0082	0.9918	3.45E+07
7	2.0558	0.0199	0.9801	3.19E+07
8	0.2622	0.3966	0.6034	1.99E+07
9	0.4138	0.3395	0.6605	2.01E+07
RELIABILITY: Medium Cycle Bending				
Geometry	**B**	**P_f**	**Rel**	**N_{95}**
1	2.3656	0.009	0.991	1.28E+07
2	2.5556	0.0053	0.9947	6.37E+06
3	2.6693	0.0038	0.9962	6.92E+06
4	2.4228	0.0077	0.9923	1.47E+07
5	0.94708	0.1718	0.8282	4.19E+06
6	1.6922	0.0453	0.9547	3.04E+06
7	1.2541	0.1049	0.8951	2.99E+06
8	-0.60046	0.7259	0.2741	1.68E+06
9	-0.44766	0.6728	0.3272	1.77E+06

RELIABILITY: Low Cycle Bending				
Geometry	**B**	**P_f**	**Rel**	**N_{95}**
1	2.3656	**0.009**	**0.991**	3.68E+05
2	2.5899	0.0048	0.9952	2.16E+04
3	2.6693	0.0038	0.9962	2.08E+05
4	2.5427	0.0055	0.9945	4.60E+05
5	1.8068	0.0354	0.9646	1.90E+05
6	2.5241	0.0058	0.9942	1.02E+05
7	2.1917	0.0142	0.9858	9.16E+04
8	0.27619	0.3912	0.6088	5.75E+04
9	0.57928	0.2812	0.7188	5.96E+04

Table 6-8 Reliability in High, Medium and Low Cycle Bending Fatigue

7 CONCLUSIONS

Despite the variety of parameters affecting the fatigue life of welded joints, it is widely common today that both stress distributions inside the weld and in surface of the weld joint are leading factors in fatigue life, since they affect the micro-crack initiation time and propagation till failure.

This work has examined the fatigue capacity of fillet weld joints and resulted in a comparative analysis of different geometries under stochastic variation of their dimensions. A Mode Carlo simulation was inserted in a MATLAB code incorporating also the Stress Intensity Factor calculations for rapid exporting of fatigue life and reliability index. Reference to this code is made in Appendix E.

In case of pure bending - mode I fatigue analysis, the surface stress is one of the dominant parameters since the bending moment is maximized as the FEA stress analysis depicted. Besides, as per FEA stress analysis, in case of pure tension - mode I, the maximum principal stresses found again at the surface areas of weld toes, as in case of pure bending, the main difference being the relatively lower Stress Concentration Factors. Additionally, fracture mechanics calculations have depicted an effect of the exerted (nominal) stress on fatigue life, since in case of low cycle bending, the calculated fatigue life was greater than in tension, but in high and medium cycle the above is reversed.

It is worth mentioning that fillet weld joints and cruciform joints are heavily affected by the weld geometries in comparison to butt welds. The stress concentration of those types of weld joints may differ from geometry to geometry. In our analysis the main parameters studied were the weld toe angle, weld toe radius and weld leg length. The relative plate thickness showed minor effect on stress concentration, given that the attachment plate is a non-load carrying plate. As regards weld throat that is mentioned in many publications and references, it is the outcome of a specific angle and leg length. Although important for the increased strength of a joint, experiments have shown that increased weld throats may have counter-impacts on fatigue lives, due to scale

effects and is not just simple as to increase the thickness of a weld in order for the joint to withstand the maximum stress alterations.

Stress concentrations have been correlated within this work with the stress cycles till failure, in order to identify their relationship. It has been shown so far that the stress concentration in case of high cycle pure tension has a reduced impact on fatigue life in comparison to pure bending. As per figure 6-7, the gradient of the $N=f(SCF_{tens})$ is less than $N=f(SCF_{bend})$. One of the most important remarks is that under the same bending or tensile stress, the joints fatigue lives will be almost proportional to their stress concentration factors (with a negative gradient).

Useful reliability analysis results correlating the fatigue life of stochastic geometrical fluctuations with their geometries have depicted minor discrepancies in comparison to the previous analysis.

Subject stress analysis has depicted a decreasing impact of an increasing weld toe radius to SCF. The above effect is stronger for higher weld angle values. Indicatively, for angle 30^0, an increase of the toe radius from 0.8 to 1.32mm (65%), may reduce the SCF by 34.9%, while at 60^0 the benefit would be 47.2%. In case of bending, the benefit would be 9% higher. As regards reliability analysis, the ρ/T fluctuation under a two steps increase of 10% and 20% with a standard deviation 3, depicted a minor impact on fatigue life if other parameters are constant. It has been shown therefore that a percentage change of weld toe radius has the lowest effect in comparison to other parameters. However, the reliability of the as-welded fillet weld (without weld toe radius) will be substantially increased after this treatment since the initial (before treatment) toe radius would be zero and in practical terms it is the easiest and best way to reduce the stress gradient and remove the weld flaws and defects in the most stress affected area of the joint.

As regards weld leg length effect, it has been shown that the leg increase will affect negatively the SCF and therefore the increased stress concentration will lead to shorter fatigue life. Comparison between geometries 6 and 7 (30mm and 20mm respectively) of table 6-1, depicts an increase of 7,4% and 3,3% in

medium cycle bending and tension respectively. In reliability terms, the fluctuation with standard deviation 1, demonstrated the higher impact on fatigue life which is also evident in fracture mechanics analysis.

Finally, the lower weld angle towards the stressed plate is strictly related with the lowest SCF and maximum fatigue life. Relevant reliability analysis of the weld angle demonstrated a medium effect to fatigue life, meaning that a change of 1% may have higher impact on fatigue life than the weld toe radius and less than the weld leg length.

Although the geometry No.3 of table 6-2 depicted the lowest SCF and the maximum fatigue life and reliability comparatively to the others both in bending and tension, a specific analysis for evaluation of the minimum suggested weld throat is required. It is important to note that minimizing the weld leg and angle is a way for minimizing the SCF whilst wiping out the surface micro defects by grounding of weld toes reduces the potential of micro-crack initiations. The strength of the joint might be enhanced by retaining the increased leg of 30mm whilst minimizing the angle to 30^0 and applying the maximum toe radius of 1.32mm in order to retain a relatively thicker weld throat.

What is more, the effect of a U-shape repair profiling has improved the SCF if the radius is maximized. Nonetheless, it is important again to outline that over-increasing the radius R, has been tested (through experiments in literature) to be conversely related to fatigue life after a critical value.

Last but not least, the effect of the weld root, in case of a non-full penetration weld, even if it is traditionally avoided when considering about stronger joints, it seems to have stress mitigating effects in case of a treatment that would remove any root surface defects and apply semicircular or keyhole edges, acting as a stiffener of the tensile and compressive stresses under the welded joint and in way of the attachment plate.

REFERENCES

01. American Welding Society. (2004). *Structural Welding Code-Steel*, 19th ed. AWS, Florida.
02. Abaqus 6.9 *Theory Manual*, (2009). Dassault Systems Simulia, United States of America, 2009.
03. Atzori, B. Lazzarin, P., Meneghetti, G. (2009). Fatigue strength of welded joints based on local, semi-local and nominal approaches. *Theoretical and Applied Fracture Mechanics*, 52, p. 55-61.
04. Ayala-Uraga, E., Torgein, M. (2007). Fatigue reliability-based assessment of welded joints applying consistent fracture mechanics formulations. *International Journal of Fatigue*, Vol. 29, p.444-456.
05. Besuner, P.M., Tetelman, A.S. (1977). Probabilistic Fracture Mechanics. *Nuclear Engineering and Design*, Vol.43, p.99-114.
06. Brennan, F.P., Dover, W.D., Kare R.F., Hellier, A.K. (1999). Parametric equations for T-butt weld toe stress intensity factors. *International Journal of Fatigue,* 21, p. 1051-1062*.*
07. Brennan, F.P., Ngiam, S.S., Lee, C.W. (2008). An experimental and analytical study of fatigue crack shape control by cold working. *Engineering Fracture Mechanics*, Vol. 75, No.3-4, p. 355-363.
08. Brennan, F.P., Peleties, P., Helier, A.K. (2000). Predicting weld toe stress concentration factors for T and skewed T-joint plate connections. *International Journal of Fatigue,* 22, p. 573-584*.*
09. Baptista, R., Infante, V., Branco, C.M. (2008). Study of the fatigue behavior in welded joints of stainless steels treated by weld toe grinding and subjected to salt water corrosion. *International Journal of Fatigue*, 30, p. 453-462.
10. Branco, R., Antunes F.V. (2008). Finite element modelling and analysis of crack shape evolution in mode-I fatigue Middle Cracked Tension speciments. *Engineering Fracture Mechanics*, Vol. 75, p.3020-3037.
11. Bell, R., Vosikovsky, O. (1992). A fatigue life prediction model for multiple cracks in welded joints for offshore structures. *OMAE, Materials Engineering,* ASME 1992, Vol. III-B.
12. Bell, R., Vosikovsky, O. et al. (1987). A fracture mechanics model for life prediction of welded plate joints*. Proc. Intl. Offshore Conf. on Steels in Marine Structures,* Paper TS-53, Delft.
13. Bell, R., Vosikovsky, O., Bain, S.A., (1989). The significance of weld toe undercuts in the fatigue of steel plate T-joints. *International Journal of Fatigue,* 11, p. 3-11.
14. Bowness, D., Lee, M.M.K. (2000). Prediction of weld toe magnification factors for semi-elliptical cracks in T-butt joints. *International Journal of Fatigue*, Vol. 22, p.369-387.
15. BS 7910:1999. *Guide on methods for assessing the acceptability of flaws in metallic structures*.
16. Baik, B., Yamada, K., Ishikawa, T. (2011). Fatigue crack propagation analysis for welded joint subject to bending. *International Journal of Fatigue*, p. 746-758.

17. Bhattacharya, B., Basu, R., Ma, K. (2001). Developing target reliability for novel structures: the case of the Mobile Offshore Base. *Marine Structures*, 14, p. 37-58.
18. Bouchard, R., Vosikovsky, O., Rivard, A. (1991). Fatigue life of welded plate T joints under variable-amplitude loading. *International Journal of Fatigue*, Vol.13, No.1, p. 7-15.
19. Bowness, D., Lee, M.M.K. (2000). Weld toe magnification factors for semi-elliptical cracks in T-butt joints – comparison with existing solutions. *International Journal of Fatigue,* Vol. 22, p.389-396.
20. Bowness, D., Lee, M.M.K. (1996). Stress intensity factor solutions for semi-elliptical weld toe cracks in T-butt geometries. *Fatigue & Fracture of Engineering Materials & Structures,* Vol. 19, p.787-797.
21. Berge, Stig. (1985). On the effect of plate thickness in fatigue of welds. *Engineering Fracture Mechanics*, 21(2), p. 423-435.
22. Cox, B.N., Morris, W.L. (1988). Monte Carlo simulations of the growth of small fatigue cracks. *Engineering Fracture Mechanics*, Vol.31, No.4, p.591-610.
23. Camara, M.C., Ramalho Cyrino, J.C. (2011). Structural reliability applications in design and maintenance planning of ships subjected to fatigue and corrosion. In: *30th ASME International Conference on Ocean, Offshore and Arctic Engineering*, OMAE2011-50133, June 19-24, 2011 Rotterdam.
24. Caccese, V., Blomquist, P.A. et al. (2006). Effect of weld geometric profile on fatigue life of cruciform welds made by laser/ GMAW processes. *Marine Structures,* , 19, p.1-22.
25. Choi, S., Grandhi, R.V., Canfield, R.A. (2007). *Reliability-based structural design*, 1st ed, Springer-Verlag London Ltd, p.1-6.
26. Carpintieri, A., Brighenti, R., et al. (2005). Fatigue growth of a surface crack in a welded T-joint. *International Journal of Fatigue*, Vol. 27, p. 59-69.
27. Chahardeli, A., Brennan, F.P., Steuwer, A. (2010). The effect of residual stresses arising from laser shock peening on fatigue crack growth. *Engineering Fracture Mechanics*, 77, p. 2033-2039.
28. DNV, Casualty Information, (2003), Crack in deck plating
29. DNV, Casualty Information, (1995), Fatigue cracking of side longitudinal
30. DNV, *Structural Reliability Analysis of Marine Structures*, Norway. Classification No. 30.6. July 1992
31. Deng, D., Liang, W., Murakawa, H. (2007). Determination of welding deformation in fillet-welded joint by means of numerical simulation and comparison with experimental measurements. *Journal of Materials Processing Technology,* 183, p.219-225.
32. Engesvik, K., Moan, T. (1983). Probabilistic analysis of the uncertainty in the fatigue capacity of welded joints. Engineering Fracture Mechanics, Vol.18, No.4, p.743-762.
33. Ersdal, G., Hornlund, E., Spilde, H. (2011). Experience from Norwegian programme on ageing and life extension. In: *30th ASME International Conference on Ocean, Offshore and Arctic Engineering*, OMAE2011-50046, June 19-24, 2011 Rotterdam.

34. Eyres, DJ. (2008). *Ship construction*, 6th ed. Butterworth-Heinemann, Oxford.
35. Ferreira, J.M., Branco, C.M. (1988). Influence of weld and plate geometry on the fatigue strength of cruciform joints. *Theoretical and Applied Fracture Mechanics,* 9, p. 23-32.
36. Ferreira, J.M., Branco, C.M. (1989). Influence of the radius of curvature at the weld toe in the fatigue strength of fillet welded joints. *International Journal of Fatigu*e, 11(1), p. 29-36.
37. Fricke, W. (2010). Guideline for the fatigue assessment by notch stress analysis for welded structures. *International Institute of Welding*, IIW document- XIII-2240r2-08.
38. Ferreira, J.M., Branco, C.M. (1988). Influence of fillet weld joint geometry on fatigue crack growth. (1991). *Theoretical and Applied Fracture Mechanics,* 15 p. 131-142.
39. Fu, B., Haswell, J.V., Bettess P. (1993). Weld magnification factors for semi-elliptical surface cracks in fillet welded T-butt joint models. *International Journal of Fracture,* Vol. 63, p.155-171.
40. Fricke, W. (2003). Fatigue analysis of welded joints: state of development. *Marine Structures*, 16, p. 185-200.
41. Feng, C.G., Garbatov, Y., Soares C.G. (2012). Probabilistic model of the growth of correlated cracks in a stiffened panel. *Engineering Fracture Mechanics,* Vol.84, P.83-95.
42. Feng, C.G., Garbatov, Y., Soares C.G. (2012). Fatigue reliability of a stiffened panel subjected to correlated crack growth. Structural Safety, Vol. 36-37, p.39-46
43. Garbatov, Y., Soares G. (2012). Uncertainty assessment of fatigue damage of welded ship structural joints. *Engineering structures*, Vol.44, P.322-333.
44. Guo, J., Wang, G., Perakis, A., Ivanov, L. (2012). A study on reliability-based inspection planning- Application to deck plate thickness measurement of aging tankers. *Marine Structures,* 25, p. 85-106.
45. Garbatov, Y., Soares, C.G. (2001). Cost and reliability based strategies for fatigue maintenance planning of floating structures. *Reliability Engineering and System Safety,* 73, p. 293-301.
46. Gorner, F., Mattheck, C., Munz, D. (1983). Change in geometry of surface cracks during alternating tension and bending. *Materialwissenschaft und Werkstofftechnik,* Vol.14, 1, p. 11-18.
47. Han, M., Bouriga, M. et al. (2013). Life time prediction of metallic materials with the Discrete-Element Method. *Computational Materials Science*, Vol. 71, p. 146-156.
48. Hobbacher, A. (2008). Recommendations for fatigue design of welded joints and components. *International Institute of Welding*, IIW document-1823-07.
49. Hou, C.Y. (2007). Fatigue analysis of welded joints with the aid of real three-dimensional weld toe geometry. *International Journal of Fatigue,* 29, p.772-785.
50. International Ship and Offshore Structures Congress. 2009. Committee IV.1, *Design principles and criteria*, Seoul, Korea.

51. International Ship and Offshore Structures Congress. 2009. Committee V.6, *Condition Assessment of aged ships and offshore structures*, Seoul, Korea.
52. International Ship and Offshore Structures Congress. 2009. Committee III.2, *Fatigue and fracture*, Seoul, Korea.
53. Iida, K. (1980). *Aspect ratio expressions for part-through fatigue crack*. IIW Doc. XIII-967-80.
54. Irwin, G.R. (1948). Fracture dynamics. *Fracturing of metals ASM Cleveland.*
55. IMO, SOLAS International Convention (2009).
56. Irwin, G.R. (1962). Crack-extension force for a part-through crack in a plate. Journal of Applied Mechanics, p. 651-654.
57. Juvinall, R.C, Marshek, K.M. (2006). *Fundamentals of machine component design*, 4th ed. John Wiley and Sons Ltd, New York.
58. Jeong-Woo, H., Kwon-Hee, L., Seung-Ho, H. (2012). Three dimensional weld toe magnification factors for various welded joints. *Journal of Mechanical Science and Technology,* Vol. 26(7), p.2121-2124.
59. Kim, S., Frangopol, D.M. (2011). Optimum inspection planning for minimizing fatigue damage detection delay of ship hull structures. *International Journal of Fatigue,* 33, p. 448-459.
60. Kou, K.P. (2005). The SIF for long-deep semi-elliptical surface crack in finite thickness plate. *Abaqus Users' Conference* 2005.
61. Kihla D., Sarkanit, S. (1997). Thickness effects on the fatigue strength of welded steel cruciforms. *International Journal of Fatigue,* 19 (1), p. S311-S316.
62. Kolios, A. (2010). *A multi configuration approach to reliability based structural integrity assessment for ultimate strength*, PHD Thesis, Department of Offshore, Process& Energy Engineering, Cranfield University.
63. Kawahara M., Kurihara, M. (1977). Fatigue crack growth from a surface flaw. *Fracture,* vol.2, ICF4, Waterloo, Canada.
64. Lie, S.T., Zhao, Z., Yan, S.H. (2000). Two-dimensional and three-dimensional magnification factors for non-load-carrying fillet welds cruciform joints. *Engineering Fracture Mechanics*, Vol. 65, p.435-453.
65. Lloyd's Register. (2007). Common Structural Rules for double hull oil tankers.
66. Lee, C.H, Chang,K.H. et al. (2009). Effect of weld geometry on the fatigue life of non-load carrying fillet welded cruciform joints. *Engineering Failure Analysis,* 16, p.849-855.
67. Lin, X.B., Smith, R.A. (1999). Finite element modelling of fatigue crack growth of surface cracked plates, part II: Crack Shape Change.. *Engineering Fracture Mechanics*, Vol. 63, p. 523-540.
68. Landet, E., Oma, N., Ersdal, G. et al. (2011). Assessment of ageing structures. In: *30th ASME International Conference on Ocean, Offshore and Arctic Engineering*, OMAE2011-49959, June 19-24, 2011 Rotterdam.
69. Martinez, L.L. (2011). Fatigue life extension of offshore structures. In: *30th ASME International Conference on Ocean, Offshore and Arctic Engineering*, OMAE2011-49935, June 19-24, 2011 Rotterdam.

70. Mahmoud, M.A. (1988). Growth patterns of surface fatigue cracks under cyclic bending- A quantitative analysis. *Engineering Fracture Mechanics*, Vol. 31, No.2, p. 357-369.
71. Mahmoud, M.A., Hosseini, A. (1986). Assessment of Stress Intensity Factor and Aspect Ratio Variability of Surface Cracks in Bending Plates. *Engineering Fracture Mechanics,* Vol. 24, No.2, p. 207-221.
72. Martinsson, J. (2005). *Fatigue Assessment of complex Welded Steel Structures* PHD Thesis, Devision f Lightweight Structures, Department Aeronautical and Vehicle Engineering, Royal Institute of Technology, Stockholm.
73. Motarjemi, A.K., Kokabi, A.H., Burdekin, F.M.. (2000). Comparison of fatigue life for T and cruciform welded joints with different combinations of geometrical parameters. *Engineering Fracture Mechanics*, 67, p. 313-328.
74. Motarjemi, A.K., Kokabi, A.H et al. (2000). Comparison of the stress intensity factor of T and cruciform welded joints with different main and attachment plate thickness. *Engineering Fracture Mechanics*, 65, p. 55-66.
75. Mellor, B.G., Rainey, R.C.T, Kirk, N.E. (1999). The static strength of end and T fillet weld connections. *Materials and Design*, 20, p. 193-205.
76. Mashiri, F.R., Zhao, X.L., Grindy, P. (2001). Effects of weld profile and undercut on fatigue crack propagation file of thin-walled cruciform joint. *Thin-Walled Structures*, 39, p. 261-285.
77. Mattheck, C. (2006). Teacher tree: The evolution of notch shape optimization from complex to simple*. Engineering Fracture Mechanics*, 73, p.1732-1742.
78. Newman, J.C. (1973). Fracture analysis f surface and through-cracked sheets and plates. *Engineering Fracture Mechanics*, Vol. 5, p.667-689.
79. Newman, J.C., Raju, I.S. (1979). Analyses of surface cracks in finite plates under tension or bending loads. *NASA*, technical paper 1578.
80. Newman, J.C., Raju, I.S. (1981). An empirical stress-intensity factor equation for the surface crack. *Engineering Fracture Mechanics*, Vol. 15, p. 185-192.
81. Nguyen, T.N., Wahab, M.A. (1998). The effect of weld geometry and residual stresses on the fatigue of welded joints under combined loading. *Journal of Materials Processing Technology*, 77, p. 201-208.
82. Okumoto, Takeda, Mano, Okada. (2009). *Design of ship hull structures*, 1st ed. Springer-Verlag, Berlin Heidelberg.
83. Otegui, J.L., Kerr, H.W., Burns, D.J., Mohaupt, U.H. (1989). Fatigue crack initiation from defects at weld toes in steel. *International Journal of Pressure Vessels & Piping,* Vol. 38, p.385-417.
84. Okawa, T., Sumi, Y., Mohri, M. (2006). Simulation-based fatigue crack management of ship structural details applied to longitudinal and transverse connections. *Marine Structures,* 19, p. 217-240.
85. Park, W., Chitoshi, M. (2008). Fatigue assessment of large-size welded joints based on the relative notch stress approach. *International Journal of Fatigue,* 30, p.1556-1568.
86. Patsouris, E. (2004). *Structural integrity monitoring of ships*, MSc thesis. University College of London.

87. Pang, H.L.J. (1993). Analysis of weld toe profiles and weld toe cracks. *International Journal of Fatigue*, 15(1), p.31-36.
88. Pang, H.L.J. (1994). Analysis of weld toe radius effects on fatigue weld toe cracks. *International Journal of Vessels and Piping*, 58, p. 171-177.
89. Pilkey, Walter. (2008) *Peterson's stress concentration factors*, 3d ed. John Wiley and Sons Ltd, New York.
90. Papanikolaou, Guedes Soares, Jasionowski et al. (2009). *Risk based ship design*, 1st ed., Springer-Verlag, Berlin Heidelberg.
91. Peishi, Y., Wanlin, G. (2012). An equivalent thickness conception for prediction of surface fatigue crack growth life and shape evolution. Engineering Fracture Mechanics, Vol. 93, p. 65-74.
92. Pang, H.L.J., Gray, T.G.F. (1993). Fatigue analysis of surface cracks at fillet welded toes. *Fatigue Fracture Engineering Material Structures,* Vol. 16, No. 2, p.151-164.
93. Petinov, S.V. et al. (1999). The similitude of fatigue damage principle: Application in S-N curves based fatigue design. *Fatigue Design and Reliability,* 23, p. 219-228.
94. Portch, D.J. (1979). An investigation into the change of shape of fatigue cracks initiated at surface flaws. *Central Electricity Generating Board,* Research Division, Berkeley Nuclear Laboratories.
95. Radaj, D. (1990). *Design and analysis of fatigue resistant welded structures*. Abington Publishing Ltd, Cambridge.
96. Radaj, D., Sonsino, C.M., Fricke, W. (2009). Recent developments in local concepts of fatigue assessment of welded joints. *International Journal of Fatigue,* 31, p. 2-11.
97. Rodríguez-Sánchez, J.E., Dover, W.D., Brennan, F.P. and Rodríguez Castellanos, A. (2005). Fracture mechanics analysis of fatigue crack repaired joints. *Journal of Offshore Mechanics and Arctic Engineering*, 127:2, 182-189.
98. Rodriguez, J.E, Dover, W.D, Brennan, F.P. (1998). Application of short repairs for fatigue life extension. *International Journal of Fatigue,* 26, p. 413-420.
99. Rodriguez, J.E, Brennan, F.P., Dover, W.D. (1998). Minimization of stress concentration factors in fatigue crack repairs. *International Journal of Fatigue,* 20 (10), p. 710-725.
100. Rawson, K.J, Tupper, E.C. (2001). *Basic ship theory vol.1,* 5th ed., Butterworth-Heinemann, Oxford.
101. Raju, I.S., Newman, J.C. (1979). Stress Intensity Factors for a wide range of semi-elliptical surface cracks in finite-thickness plates. *Engineering Fracture Mechanics*, Vol. 11, p. 817-829.
102. Radon, J.C. (1993). The shape of surface cracks in fatigue. *International Journal of Pressure Vessels and Piping,* Vol. 55, p.265-285.
103. Sonsino, C.M., Fricke, W., Bryune, F. et al. (2012). Notch stress concepts for the fatigue assessment of welded joints – Background and applications. *International Journal of Fatigue,* 34, p. 2-16.
104. Smith, I.F.C., Smith R.A. (1983). Fatigue crack growth in a fillet welded joint. *Engineering Fracture Mechanics*, Vol. 18, p. 861-869.

105. Sommer, E., Hodulac, L., Kordisch, H. (1977) Growth characteristics of part-through cracks in thick-walled plates and tubes. ASME *Journal of Pressure Vessel Technology,* 99 106-111.
106. Smith, I.F.C., Gurney, T.R. (1986). Changes in the fatigue life of plates with attachments due to geometrical effects. *Welding Research Supplement*, p.244-250.
107. Shang-Xian, W. (1985). Shape change of surface crack during fatigue growth. *Engineering Fracture Mechanics*, Vol. 22, No.5, p. 897-913.
108. Smith, I.F.C, Smith, R.A. (1982). Defects and crack shape development in fillet welded joints. *Fatigue of Engineering Materials and Structures*, Vol. 4, No.2, p. 151-165.
109. Ting W., Dongpo, W., Lixing, H., Yufeng, Z. (2009). Discussion on fatigue design of welded joints enhanced by ultrasonic peening treatment (UPT). *International Journal of Fatigue, 31, p.644-650.*
110. Taylor, D., Kelly, A., Toso, M., Susmel, L. (2011). The variable radius notch: Two new methods for reducing stress concentration. *Engineering Failure Analysis*, 18, p. 1009-1017.
111. Tanker Structure Cooperative forum in association with IACS. (1995). *Guidelines for the inspection and maintenance of double hull tanker structures,* 1st ed. Witherby & Co. Ltd, London.
112. Tovo, R., Lazzarin, P. (1999). Relationships between local and structural stress in the evaluation of the weld toe stress distribution. *International Journal of Fatigue,* 21, p. 1063-1078.
113. US Department of the Army. (1993). *Welding Theory and Application, Training Circular No 9-237*, Washington.
114. Wallbrink, C., Peng, D. et al. (2006). Predicting the fatigue life and crack aspect ratio evolution in complex structures. *Theoretical and Applied Fracture Mechanics*, Vol. 46, p.128-139.
115. Xiao, Z., Yamada, K. (2002). Correlation of fatigue life of fillet welded joints based on stress at 1mm in depth. *Advances in Steel Structures*, Vol II, p. 1001-1008.
116. Yan-Ping L., Cuan-Yao, S. et. al. (2010). Fatigue life prediction of semi-elliptical surface crack in 14MnNbq bridge steel. *Engineering Failure Analysis,* Vol. 17, p.1413-1423.
117. Yan-Lin, L. (1995). Crack aspect development curves and fatigue life prediction for surface cracks at weld toes in the presence of residual stress. *International Journal of Fatigue*, Vol.17, p.551-557
118. Xue Yibin, (2010). Modeling fatigue small-crack growth with confidence-A multistage approach. *International Journal of Fatigue*, Vol.32, p. 1210-1219.
119. Hohenbichler, M., Gollwitzer, S. et al. (1987). New light on First and Second Order Reliability Methods. Structural Safety, Vol.4, p.267-284.
120. Monahan CC. (1995). Early fatigue crack growth at welds-Topics in engineering. *Computational Mechanics,* Southampton, Brebbia CA, Connor JJ, editors. vol. 26.

APPENDICES

Appendix A Models mesh and partitioning

The following Figures A-1 up to 4 illustrate the stress fluctuations on indicative fillet weld joints by means of contours.

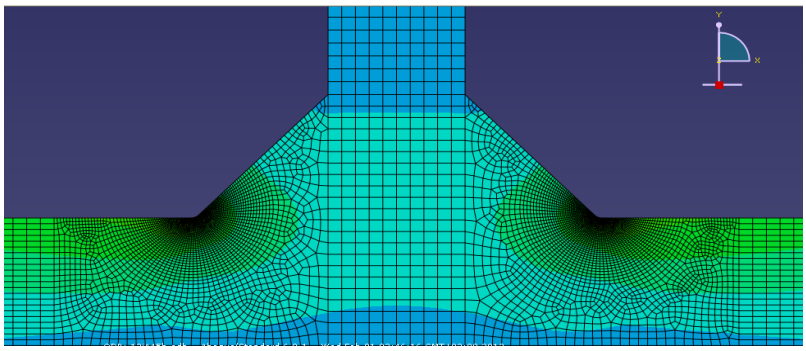

Figure A 1 Model mesh

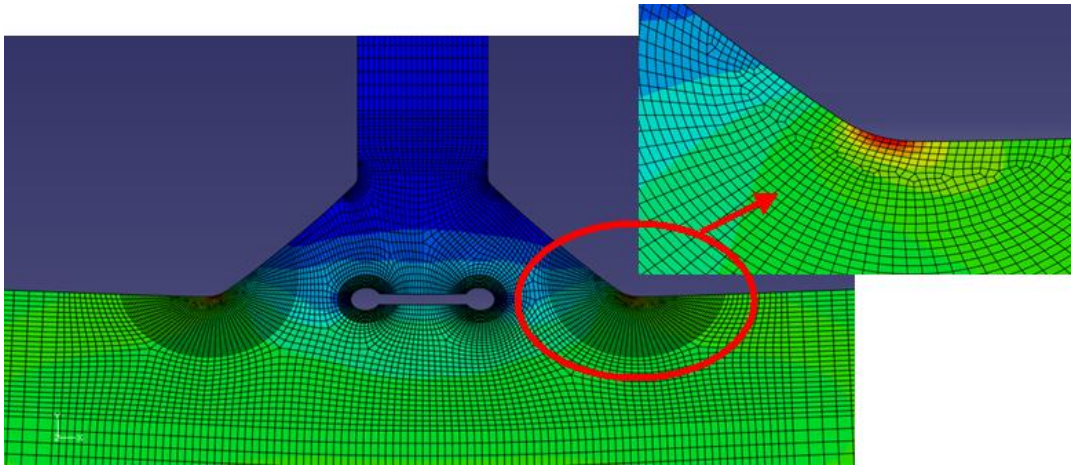

Figure A 2 Weld Toe Detail

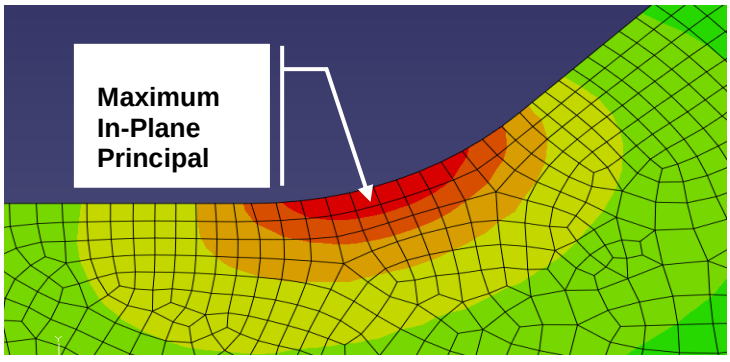

Figure A 3 Model mesh at weld toe

Figure A-4 illustrates model's partitioning. The ping colored areas were the ones that a "structured" mesh could not be created and subsequently an "advancing front" mesh was applied.

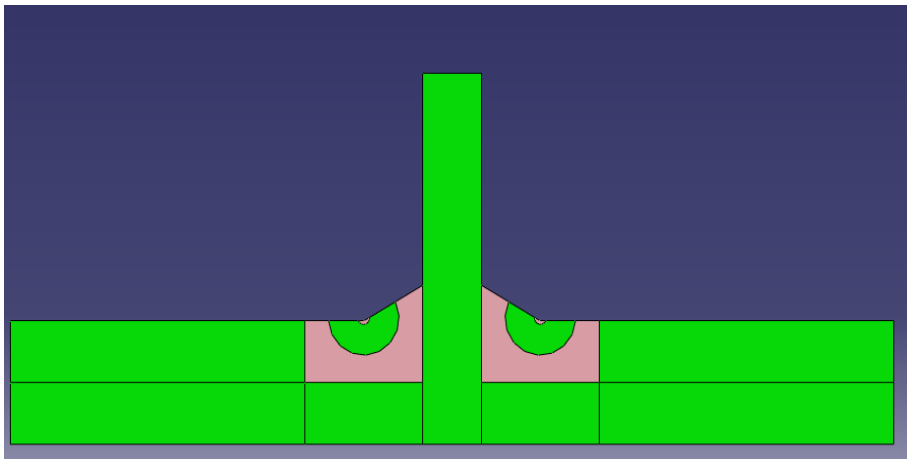

Figure A 4 Model partitioning

In order to eliminate the effect of an increasing number of distorted elements in meshes exceeding 9000 elements, the trapezoid partitioning of figures A 5 and A 6 in weld toe area was substituted by the two homocentric cycle concept of Figure A 4. Above consideration emerges also from the necessity for a better refinement of the weld toe area.

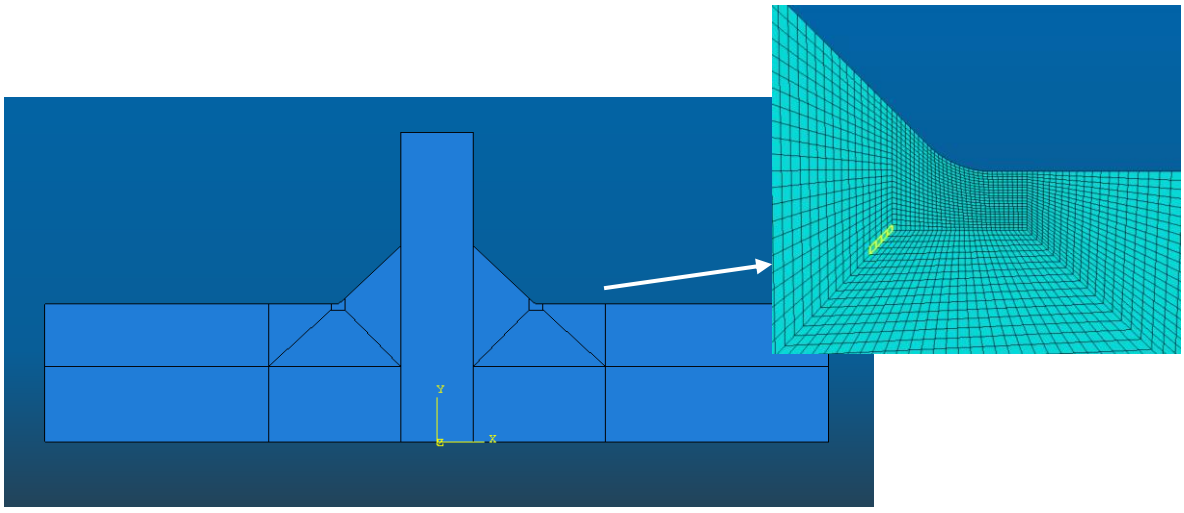

Figure A 5 Rectangular model partitioning at weld toe

The yellow highlighted finite elements of illustrated models in figures A-5 and A-6 are distorted elements with geometric deviation factor 0.00655. Above model is a 9100 finite element model with 40 distorted elements.

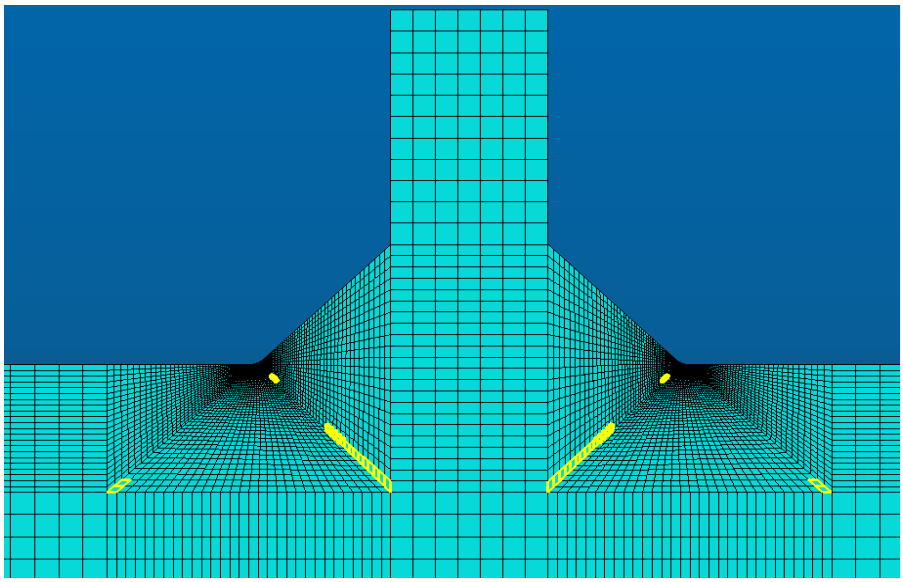

Figure A 6 Distorted elements in rectangular partitioning

Appendix B Mesh Optimization

A mesh refinement process at weld toe high stress concentration area is presented, making use for reference purposes the model of Table 6-1 geometry #5, consisting of 11.348 elements and a weld toe radius of 1mm. Stress analysis of weld toe configurations with 45^0 angle as our reference model, depicts higher stress concentration factor under mode I pure tension, at an approximately 1/3 distance of reference part-circular weld toe length, counting from the intersection node between toe and base plate.

Four models have been developed each one consisting of an increasing number of elements (3, 6, 8, 10) at weld toe. Respective SCFs have been calculated and relevant node from lower toe intersection point compared to total number of weld toe nodes and elements have been included in table B-1.

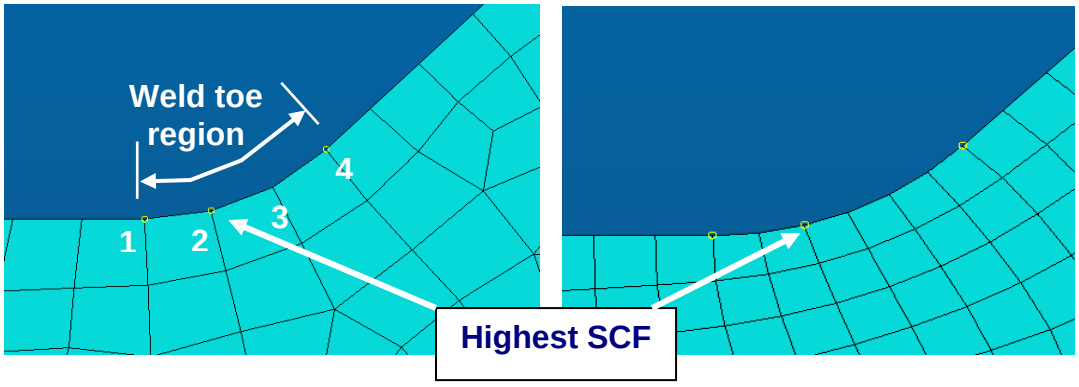

Model #1: 3 Elements **Model #2: 6 Elements**

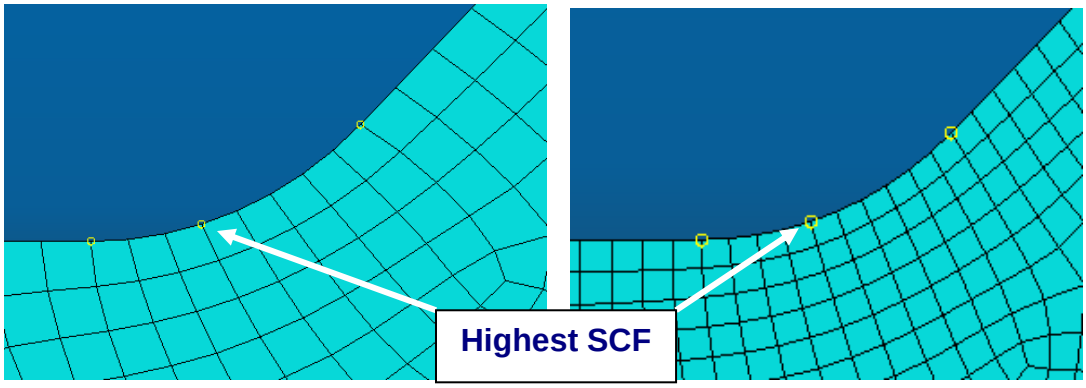

Model #3: 8 Elements **Model #4: 10 Elements**

Figure B 1 Finite elements at weld toe

	MODEL 1	MODEL 2	MODEL 3	MODEL 4
Total # of Elements	6944	8563	10519	11348
Elements at weld toe	3	6	8	10
Number of nodes at weld toe	4	7	9	11
Position of SC, node #	2	3	4	5
SCF	1,881	2,104	2,167	2,230

Table B 1 Weld toe model refinement and SCF evolution

Appendix C Stress Concentration Factors Index

C.1 Geometrical Parameters

Geometrical parameters considered: weld angle, toe radius and weld length.

Geometry	θ	ρ/T	l/T	t/T	SCF Tension	SCF Bending
1	30	0,01	0,25	0,5	2,879	3,092
2	30	0,01	0,5	0,5	3,007	3,225
3	30	0,01	1	0,5	2,787	3,084
4	30	0,01	1,5	0,5	2,967	3,160
5	30	0,02	0,25	0,5	2,517	2,671
6	30	0,02	0,5	0,5	2,573	2,761
7	30	0,02	1	0,5	2,505	2,673
8	30	0,02	1,5	0,5	2,587	2,66
9	30	0,04	0,25	0,5	2,124	2,245
10	30	0,04	0,5	0,5	2,167	2,324
11	30	0,04	1	0,5	2,176	2,323
12	30	0,04	1,5	0,5	2,135	2,261
13	30	0,066	0,25	0,5	1,933	2,035
14	30	0,066	0,5	0,5	1,957	2,184
15	30	0,066	1	0,5	1,986	2,192
16	30	0,066	1,5	0,5	1,999	2,199
17	45	0,01	0,25	0,5	3,594	3,964

18	45	0,01	0,5	0,5	3,710	4,213
19	45	0,01	1	0,5	3,473	3,991
20	45	0,01	1,5	0,5	3,551	4,081
21	45	0,02	0,25	0,5	2,755	3,037
22	45	0,02	0,5	0,5	2,962	3,359
23	45	0,02	1	0,5	2,764	3,167
24	45	0,02	1,5	0,5	2,833	3,187
25	45	0,04	0,25	0,5	2,231	2,427
26	45	0,04	0,5	0,5	2,413	2,721
27	45	0,04	1	0,5	2,423	2,751
28	45	0,04	1,5	0,5	2,427	2,756
29	45	0,066	0,25	0,5	1,997	2,208
30	45	0,066	0,5	0,5	2,042	2,277
31	45	0,066	1	0,5	2,110	2,382
32	45	0,066	1,5	0,5	2,123	2,391
33	60	0,01	0,25	0,5	3,898	4,520
34	60	0,01	0,5	0,5	3,985	4,843
35	60	0,01	1	0,5	3,665	4,575
36	60	0,01	1,5	0,5	3,889	4,924
37	60	0,02	0,25	0,5	2,993	3,420
38	60	0,02	0,5	0,5	3,117	3,759
39	60	0,02	1	0,5	3,051	3,788

40	60	0,02	1,5	0,5	3,010	3,775
41	60	0,04	0,25	0,5	2,346	2,642
42	60	0,04	0,5	0,5	2,493	2,944
43	60	0,04	1	0,5	2,422	2,949
44	60	0,04	1,5	0,5	2,492	3,044
45	60	0,066	0,25	0,5	2,043	2,234
46	60	0,066	0,5	0,5	2,105	2,431
47	60	0,066	1	0,5	2,138	2,480
48	60	0,066	1,5	0,5	2,130	2,508

Table C 1 Geometrical effects

C.2 Attachment plate thickness effect

Geometry	θ	ρ/T	l/T	t/T	SCF Tension	SCF Bending
1	30	0,066	0,5	10	1,925	2,058
2	30	0,066	0,5	13	1,933	2,069
3	30	0,066	0,5	16	1,933	2,073
4	30	0,066	0,5	18	1,936	2,077
5	30	0,066	0,5	20	1,937	2,078
6	45	0,066	0,5	10	2,068	2,316
7	45	0,066	0,5	13	2,071	2,330

8	45	0,066	0,5	16	2,070	2,343
9	45	0,066	0,5	18	2,073	2,349
10	45	0,066	0,5	20	2,074	2,352
11	60	0,066	0,5	10	2,085	2,423
12	60	0,066	0,5	13	2,09	2,449
13	60	0,066	0,5	16	2,09	2,465
14	60	0,066	0,5	18	2,091	2,460
15	60	0,066	0,5	20	2,093	2,467

Table C 2 Relative plate thickness effect

Appendix D Fracture mechanics index

Geometry 1				
Nominal bending stress	Max principal stress	SCF bending	Bell & Vosikovsky	Kawahara & Kurihara
25,00	54,35	2,174E+00	2,36E+07	3,39E+07
50,00	108,71	2,174E+00	2,07E+06	4,24E+06
120,00	260,90	2,174E+00	6,80E+04	3,06E+05
Nominal tensile stress	Max principal stress	SCF tension	Kawahara & Kurihara	Shang Xian
25,00	50,77	2,031E+00	1,36E+07	1,45E+07
50,00	101,54	2,031E+00	1,71E+06	1,82E+06
120,00	243,70	2,031E+00	1,23E+05	1,31E+05
Geometry 2				
Nominal bending stress	Max principal stress	SCF bending	Bell & Vosikovsky	Kawahara & Kurihara
25,00	52,15	2,086E+00	2,42E+07	3,41E+07
50,00	104,30	2,086E+00	2,16E+06	4,26E+06
120,00	250,32	2,086E+00	7,59E+04	3,08E+05
Nominal tensile stress	Max principal stress	SCF tension	Kawahara & Kurihara	Shang Xian
25,00	48,83	1,953E+00	1,37E+07	1,46E+07
50,00	97,67	1,953E+00	1,71E+06	1,83E+06
120,00	234,40	1,953E+00	1,24E+05	1,32E+05
Geometry 3				
Nominal bending stress	Max principal stress	SCF bending	Bell & Vosikovsky	Kawahara & Kurihara
25,00	50,49	2,020E+00	2,48E+07	3,44E+07
50,00	100,99	2,020E+00	2,25E+06	4,30E+06
120,00	242,37	2,020E+00	7,98E+04	3,11E+05
Nominal tensile stress	Max principal stress	SCF tension	Kawahara & Kurihara	Shang Xian
25,00	43,59	1,744E+00	1,42E+07	1,52E+07
50,00	87,18	1,744E+00	1,78E+06	1,90E+06
20,00	209,24	1,744E+00	1,29E+05	1,37E+05
Geometry 4				
Nominal bending stress	Max principal stress	SCF bending	Bell & Vosikovsky	Kawahara & Kurihara
25,00	50,87	2,035E+00	2,45E+07	3,42E+07
50,00	101,73	2,035E+00	2,21E+06	4,27E+06
120,00	244,16	2,035E+00	7,77E+04	3,09E+05
Nominal tensile stress	Max principal stress	SCF tension	Kawahara & Kurihara	Shang Xian
25,00	44,67	1,787E+00	1,42E+07	1,51E+07
50,00	89,33	1,787E+00	1,77E+06	1,89E+06
120,00	214,40	1,787E+00	1,28E+05	1,36E+05
Geometry 5				
Nominal bending stress	Max principal stress	SCF bending	Bell & Vosikovsky	Kawahara & Kurihara
25,00	62,72	2,509E+00	1,45E+07	2,56E+07
50,00	125,45	2,509E+00	1,23E+06	3,20E+06
120,00	301,07	2,509E+00	3,78E+04	2,31E+05

Nominal tensile stress	Max principal stress	SCF tension	Kawahara & Kurihara	Shang Xian
25,00	55,77	2,231E+00	1,18E+07	1,26E+07
50,00	111,54	2,231E+00	1,48E+06	1,57E+06
120,00	267,70	2,231E+00	1,07E+05	1,14E+05
Geometry 6				
Nominal bending stress	Max principal stress	SCF bending	Bell & Vosikovsky	Kawahara & Kurihara
25,00	54,14	2,165E+00	1,61E+07	2,60E+07
50,00	108,27	2,165E+00	1,36E+06	3,25E+06
120,00	259,85	2,165E+00	4,76E+04	2,35E+05
Nominal tensile stress	Max principal stress	SCF tension	Kawahara & Kurihara	Shang Xian
25,00	50,04	2,002E+00	1,22E+07	1,30E+07
50,00	100,08	2,002E+00	1,53E+06	1,63E+06
120,00	240,20	2,002E+00	1,11E+05	1,18E+05
Geometry 7				
Nominal bending stress	Max principal stress	SCF bending	Bell & Vosikovsky	Kawahara & Kurihara
25,00	58,23	2,329E+00	1,52E+07	2,56E+07
50,00	116,47	2,329E+00	1,26E+06	3,20E+06
120,00	279,52	2,329E+00	4,15E+04	2,31E+05
Nominal tensile stress	Max principal stress	SCF tension	Kawahara & Kurihara	Shang Xian
25,00	52,00	2,080E+00	1,18E+07	1,26E+07
50,00	104,00	2,080E+00	1,48E+06	1,68E+06
120,00	249,60	2,080E+00	1,07E+05	1,14E+05
Geometry 8				
Nominal bending stress	Max principal stress	SCF bending	Bell & Vosikovsky	Kawahara & Kurihara
25,00	65,73	2,629E+00	1,03E+07	2,12E+07
50,00	131,45	2,629E+00	8,18E+05	2,65E+06
120,00	315,48	2,629E+00	2,57E+04	1,92E+05
Nominal tensile stress	Max principal stress	SCF tension	Kawahara & Kurihara	Shang Xian
25,00	56,20	2,248E+00	1,03E+07	1,10E+07
50,00	112,40	2,248E+00	1,29E+06	1,37E+06
120,00	269,76	2,248E+00	9,35E+04	9,94E+04
Geometry 9				
Nominal bendingstress	Max principal stress	SCF bending	Bell & Vosikovsky	Kawahara & Kurihara
25,00	62,36	2,494E+00	1,05E+07	2,11E+07
50,00	124,71	2,494E+00	8,46E+05	2,63E+06
120,00	299,31	2,494E+00	2,72E+04	1,91E+05
Nominal tensile stress	Max principal stress	SCF tension	Kawahara & Kurihara	Shang Xian
25,00	53,56	2,143E+00	1,04E+07	1,10E+07
50,00	107,13	2,143E+00	1,30E+06	1,38E+06
120,00	257,10	2,143E+00	9,38E+04	9,97E+04

Table D 1 Fatigue life calculations

Appendix E MATLAB code

SIF CALCULATIONS

```
tic
close all
clear all
clc
format short G
nsamp=10000;
Ds=25;
Sp=65.73;

i=1;

A=5.36*10^(-12);
m=3;
k=2.09*(1E-6)*(Sp^1.95);

for j=1:1:nsamp

Nt=0;

   %GEOMETRY VARIATIONS%

thita=normrnd(1,5)*0.03486+1.02974;
rovert=normrnd(1,2)*0.02+0.056;
lovert=normrnd(1,1)*0.3+1.35;

toverr=1/rovert;
double(thita);
double(lovert);
double(rovert);

%standard deviations: thita=9deg, r=2.2mm, l=6mm


ainit=0.5;
double(ainit);
afin=1;
double(afin);
aovert=0.025 ;
double(aovert);

for i=1:1:19
```

```
aoverc=exp(-k*exp(ainit));
aoverc_value=double(aoverc);

Ma=0.597-0.649*thita-0.0028*toverr;
Mo=1.282-1.325*thita-0.0077*toverr;
M1=-2.222+2.154*thita+0.017*toverr;
M2=0.789-0.621*thita-0.0097*toverr;
P=-0.686+0.31*(aoverc^0.5)+0.0622*aoverc+Ma;
Co=-0.645+1.111*(aoverc^0.5)-0.648*aoverc+Mo;
C1=3.86-6.128*(aoverc^0.5)+2.876*aoverc+M1;
C2=-1.648+0.926*(aoverc^0.5)+0.00393* aoverc+M2;

if aovert<0.25
C3=-0.25*((0.25-aovert)^0.5)*((1.1-aoverc)^0.16)*(thita^2)*(rovert^(-
0.16))*(lovert^(-0.37))*(1-exp(-(((0.25-aovert)/0.15)^2)));
else
C3=0;
end

if aovert<0.05
C4=0.5*((0.05-aovert)^1.1)*((1.1-aoverc)^(-0.486))*(thita^(-
2.66))*(rovert^0.11)*((lovert-0.455)^(-0.0384))*(1-exp(-(((0.05-
aovert)/0.015)^2)));
else
C4=0;
end

if aovert>0.35
C5=-0.14*((aovert-0.35)^0.098)*((1.1-aoverc)^0.862)*(thita^0.675)*(rovert^(-
0.077))*(lovert^0.148)* (1-exp(-(((aovert -0.35)/0.2)^2)));
else
C5=0;
end

Y=0.96*P*log(aovert)+Co+C1*aovert+C2*(aovert^2)+C3+C4+C5;
Yvalue=double(Y);
Nom=2*(afin^(1-(m/2)))-2*(ainit^(1-(m/2)));
Den=((2-m)*A*((Y*Ds)^m)*(pi^(m/2)));
N=Nom/Den;
Nvalue=double(N);
Nt=Nt+N;
Ntvalue=double(Nt);

%TenRes(i,:)=[1 2 3 4 5 6 7 8 9 10 11 12];
TenRes(i,:)=[j i thita rovert lovert aovert ainit afin aoverc_value Yvalue Nvalue
Ntvalue];
fid = fopen('twoangle.txt', 'a');
```

```
fprintf(fid, '%i %i %10.3e %10.3e %10.3e %10.3e %10.3e %10.3e %10.3e %10.3e %10.3e %10.3e\n', TenRes(i,1), TenRes(i,2), TenRes(i,3), TenRes(i,4), TenRes(i,5), TenRes(i,6), TenRes(i,7), TenRes(i,8), TenRes(i,9), TenRes(i,10), TenRes(i,11), TenRes(i,12));
fclose(fid);

i=i+1;
ainit=ainit+0.5;
double(ainit);
afin=afin+0.5;
double(afin);
aovert=aovert+0.025;
double(aovert);

end

end
save twoangle.dat
toc
```

Monte Carlo Simulations

```
% nsamp=10000;

%NN=N;

 load twoangle.txt

%  nsampALL=size(twoangle,1);

 j=1;
 for i=31:31:31000
Nt(j,1)=twoangle(i,12);

j=j+1;
 end
 nsamp=size(Nt,1);

for j=1:nsamp
NN(j,1)=Nt(j,1);
end
%%
IndT=0;
for i=1:nsamp
    if NN(i,1)<1000000
        Ind_currT = IndT;
        IndT = Ind_currT+1;
```

```
   end
end
%%
% Probability of failure equals the fraction between the sum of 1s in the
% indicator vector fot the sum of the cases over the total sample size.
NomT=sum(IndT);
PfT=(NomT)/nsamp
RelT=1-PfT

% Reliability Index is calculated as the inverse normal cumulative
% distribution function of the Pf value.
betaT = (norminv(RelT))
%%
figure(1)
hist(NN,1000)
title('Nt distribution')
xlabel('Ntotal'), ylabel('frequency')

 %%
[y2,j2] = sort(NN);
  NN( j2(1:(size(NN,1) - 10)) ) = 0*j2(1:(size(NN,1) - 10));

n95= round(nsamp/95)

% 95% highest value
NN95=y2(nsamp-n95)
```